



Linking gas, particulate, and toxic endpoints to air emissions in the Community Regional Atmospheric Chemistry Multiphase Mechanism (CRACMM) version 1.0

Havala O. T. Pye¹, Bryan K. Place², Benjamin N. Murphy¹, Karl M. Seltzer^{2,3}, Emma L. D'Ambro¹,
5 Christine Allen⁴, Ivan R. Piletic¹, Sara Farrell², Rebecca H. Schwantes⁵, Matthew M. Coggon⁵, Emily
Saunders⁷, Lu Xu^{5,6}, Golam Sarwar¹, William T. Hutzell¹, Kristen M. Foley¹, George Pouliot¹, Jesse
Bash¹, and William R. Stockwell⁸

¹Office of Research and Development, US Environmental Protection Agency, Research Triangle Park, North Carolina, USA

10 ²Oak Ridge Institute for Science and Engineering (ORISE) Postdoctoral Program at the Office of Research and Development,
US Environmental Protection Agency, Research Triangle Park, North Carolina, USA

³Office of Air and Radiation, US Environmental Protection Agency, Research Triangle Park, North Carolina, USA

⁴General Dynamics Information Technology, Research Triangle Park, North Carolina, USA

⁵NOAA Chemical Science Laboratory (CSL), Boulder, Colorado, USA

15 ⁶Cooperative Institute for Research in Environmental Science (CIRES), University of Colorado, Boulder, Colorado, USA

⁷Office of Chemical Safety and Pollution Prevention, US Environmental Protection Agency, Washington D.C, USA

⁸University of Texas at El Paso, El Paso, Texas, USA

Correspondence to: Havala O. T. Pye (pye.havala@epa.gov)

Abstract. Chemical mechanisms describe the atmospheric transformations of organic and inorganic species and connect air
20 emissions to secondary species such as ozone, fine particles, and hazardous air pollutants (HAPs) like formaldehyde. Recent
advances in our understanding of several chemical systems and shifts in the drivers of atmospheric chemistry warrant updates
to mechanisms used in chemical transport models such as the Community Multiscale Air Quality (CMAQ) modeling system.
This work builds on the Regional Atmospheric Chemistry Mechanism version 2 (RACM2) and develops the Community
Regional Atmospheric Chemistry Multiphase Mechanism (CRACMM) version 1.0, which fully couples the chemistry leading
25 to ozone and secondary organic aerosol (SOA) with consideration of HAPs. CRACMM v1.0 includes 178 gas-phase species,
51 particulate species, and 508 reactions spanning gas-phase and heterogeneous pathways. To support estimation of health
risks associated with HAPs, nine species in CRACMM cover 50% of the total cancer and 60% of the total noncancer health
risk estimated for primary HAPs from anthropogenic and biomass burning sources in the U.S., with the coverage of risk higher
(>80%) when secondary formaldehyde and acrolein are considered. In addition, new mechanism species were added based on
30 the importance of their emissions for ozone, organic aerosol, or atmospheric burden of total reactive organic carbon (ROC):
sesquiterpenes, furans, propylene glycol, alkane-like low to intermediate volatility organic compounds (9 species), low to
intermediate volatility oxygenated species (16 species), intermediate volatility aromatic hydrocarbons (2 species), and slowly
reacting organic carbon. Intermediate and lower volatility organic compounds were estimated to increase the coverage of
anthropogenic and biomass burning ROC emissions by 40% compared to current operational mechanisms. Autoxidation, a



35 gas-phase reaction particularly effective in producing SOA, was added for C₁₀ and larger alkanes, aromatic hydrocarbons,
sesquiterpenes, and monoterpene systems including second generation aldehydes. Integrating the radical and SOA chemistry
put additional constraints on both systems and enabled the implementation of previously unconsidered SOA pathways from
phenolic and furanone compounds, which were predicted to account for ~30% of total aromatic hydrocarbon SOA under
typical atmospheric conditions. CRACMM organic aerosol species were found to span the atmospherically relevant range of
40 carbon number, number of oxygens per carbon, and oxidation state with a slight high bias in number of hydrogens per carbon.
In total, eleven new emitted species were implemented as precursors to SOA compared to current CMAQv5.3.3 representations
resulting in a bottom-up prediction of SOA, which is required for accurate source attribution and design of control strategies.
CRACMMv1.0 will be available in CMAQv5.4.

1 Introduction

45 Reactive organic carbon (ROC) (Safieddine et al., 2017) includes all atmospheric organic species excluding methane and is
abundant throughout the troposphere. Particulate forms of ROC are found in fine particles (PM_{2.5}) and gaseous ROC is a major
precursor to ozone (O₃) and secondary organic aerosol (SOA) (Heald and Kroll, 2020). Recent work indicates that
preferentially controlling emissions of ROC could yield significant health benefits by mitigating the mortality associated with
ambient air pollution in the U.S. (Pye et al., 2022). These benefits come primarily from reductions in SOA which is strongly
50 associated with cardiorespiratory mortality (Pye et al., 2021; Pond et al., 2022). ROC also includes hazardous air pollutants
(HAPs) such as benzene and formaldehyde that result in cancer and noncancer risks to health (Scheffe et al., 2016).

Atmospheric chemical mechanisms connect ROC emissions to endpoints like SOA, O₃, and secondary HAPs and are used to
inform air quality management strategies to mitigate the impacts of air pollution. Chemical mechanisms were traditionally
55 designed for estimating ambient O₃ although not necessarily the lower levels of O₃ observed today in the U.S. (Kaduwela et
al., 2015) or sources of growing importance like volatile chemical products (VCPs) (Coggon et al., 2021) and biomass burning
(Jaffe and Wigder, 2012). Controls on combustion emissions are shifting cities in the U.S. towards increasingly oxygenated
ROC (Venecek et al., 2018) compared to the alkane-dominated conditions of the 1990s (Middleton et al., 1990). While
mechanisms may predict O₃ reasonably well on broad spatial and temporal scales (fractional biases in O₃ are typically much
60 less than 20% for models examined by Simon et al. (2012)), model-predicted O₃ can be biased low by 5 to 10 ppb (>20%) in
wintertime western U.S. conditions and biased high by more than 5 ppb across the U.S. south in summer compared to
observations (Appel et al., 2021). In addition, mechanisms can differ substantially in terms of predicted intermediates like the
hydroxyl radical (HO) and nitrate radical (NO₃) as well as products like formaldehyde and SOA even if they are relatively
similar in their O₃ predictions (Knote et al., 2015). Given parts of 22 different states are in marginal attainment to extreme
65 nonattainment for the current U.S. 8-hour (2012) O₃ standard (as of August 2022) (U.S. Environmental Protection Agency,
2022e) as well as recent work demonstrating health effects below the current fine particle standards (Makar et al., 2017),



70 increasingly accurate representations of emissions and how they connect to chemistry will be needed to inform air quality management strategies going forward. In addition, future implementation of global air quality guidelines, such as those from the World Health Organization, may need to account for the speciation of ambient aerosol since different species have different anthropogenic contributions (Pai et al., 2022).

75 In most chemical transport models used for air quality prediction, SOA algorithms are disconnected from the gas-phase radical chemistry leading to O₃ formation (Pye et al., 2010; Ahmadov et al., 2012; Koo et al., 2014; Tilmes et al., 2015) leading to duplication of mass in the O₃ and SOA representations. Gas-phase chemical mechanisms also typically exclude non-traditional species with saturation concentrations, C_i^* , in the low volatility organic compound (LVOC, $10^{-2.5} \leq C_i^* < 10^{-0.5} \mu\text{g m}^{-3}$) and semivolatile organic compound (SVOC, $10^{-0.5} \leq C_i^* < 10^{2.5} \mu\text{g m}^{-3}$) range. In addition, some gas-phase mechanisms also exclude intermediate volatility organic compounds (IVOCs, $10^{2.5} \leq C_i^* < 10^{6.5} \mu\text{g m}^{-3}$) (Shah et al., 2020) which are potent SOA precursors but are somewhat less important for O₃ formation than volatile organic compounds (VOCs, $C_i^* \geq 10^{6.5} \mu\text{g m}^{-3}$). Recent studies (Qin et al., 2021; Zhu et al., 2019) have noted that the magnitude of VCP emissions exerts significant impact on model-predicted O₃ but predicted SOA mass is relatively insensitive to VCP emissions due to a lack of suitable SOA precursors in standard mechanisms (Qin et al., 2021; Pennington et al., 2021). This conclusion is consistent with ROC budget analysis for Pasadena, California by Heald et al. (2020) that suggests SOA formation requires consideration of precursors beyond traditional, non-oxygenated volatile hydrocarbons represented in most current SOA treatments.

85 Due to the challenges in representing SOA chemistry in mechanisms, some chemical transport models have opted to use empirical representations of anthropogenic SOA. These parameterizations are not tied to the behavior of specific parent hydrocarbon compounds or emissions sources and fall into two classes: multigenerational and simplified. Multigenerational anthropogenic SOA treatments (Robinson et al., 2007) generally leverage the volatility basis set (VBS) framework and add IVOC and SVOC emissions thought to be missed by current measurement techniques (Koo et al., 2014; Ahmadov et al., 2012). Species throughout the $C_i^* < 10^{6.5} \mu\text{g m}^{-3}$ volatility range are chemically processed over multiple HO reactions leading to production of lower volatility species and SOA mass. Simplified representations use CO (Hodzic and Jimenez, 2011; Kim et al., 2015), primary organic aerosol (Murphy et al., 2017), or C₄H₁₀ (Dunne et al., 2020) as a surrogate for anthropogenic activity and precursor emissions that oxidize in one step to SOA. Since the SOA predicted from traditional anthropogenic hydrocarbon precursors has typically been small compared to observed SOA in urban locations (Woody et al., 2016), these schemes can be implemented in parallel to, or as a replacement for, explicit SOA precursor schemes based on traditional VOC precursors. The simplified surrogate approaches are fit to ambient data and thus have the advantage of reproducing observed levels of SOA (Qin et al., 2021; Nault et al., 2018; Murphy et al., 2017). For applications like calculation of present-day aerosol optical depth or PM_{2.5} mass (e.g., Pye et al. (2021)), empirical representations of anthropogenic SOA may be sufficient. However, the policy applications of empirical approaches are limited because they add emissions external to the regulatory reporting and model platform framework, do not allow for the separation of individual anthropogenic source contributions, and do not consider the

95
100



representativeness of the emitted proxy in the context of changing emissions or chemical regime, all of which are needed for design of regulatory control strategies.

In this work, the first version of the Community Regional Atmospheric Chemistry Multiphase Mechanism (CRACMM) is developed and presented. CRACMM v1.0 builds off the history of the Regional Atmospheric Chemistry Mechanism (RACM) development (Stockwell et al., 1997). RACM version 2 (Goliff et al., 2013) was chosen as a framework since it is implemented in regional models such as the Community Multiscale Air Quality (CMAQ) modeling system (Sarwar et al., 2013), provides competitive computational speed with mechanisms used in regulatory applications (Sarwar et al., 2013), retains the carbon backbone of emitted species, represents individual peroxy radicals, and relies minimally on aggregated species for radical cycling (operators). Because of these features, RACM2 facilitates comparison with observations, provides transparency in emissions mapping, and is relatively easy to modify and expand.

The CRACMM effort includes development of rules for mapping emitted ROC to mechanism species and aims to improve representation of atmospheric chemistry by closely coupling the pathways to O₃ and SOA as well as representing several HAPs explicitly. While the mechanism is presented here in the context of U.S. conditions, it is informed by conditions outside the U.S. (e.g., the work of Zhao et al. (2016) for China) and is meant to be generally relevant for tropospheric chemistry. CRACMM will be available in the public release of CMAQv5.4 (expected in 2022) and is distributed as a stand-alone mechanism. In this work, the aggregation of individual organic species to mechanism species (Sect. 2), the chemistry (Sect. 3), and representation of HAPs (Sect. 4) are described for atmospheric ROC. The manuscript continues with a characterization of ROC in terms of oxidation state and van Krevelen space as well as estimated implications for O₃ and fine particle mass (Sect. 5). The manuscript concludes with a discussion of the importance of mechanism development with recommendations for future work (Sect. 6).

2 ROC Emissions

Various aspects of the development of CRACMM are related to the identity of ROC emissions. The methods behind characterizing emitted ROC and how it maps to mechanism species are described in the following section.

2.1 Individual emitted species

To inform the aggregation of individual species to mechanism species as well as estimate the contributions of mechanism species to endpoints like O₃ and SOA, an emission inventory of individual ROC species was created for 2017 U.S. conditions. Total ROC emissions from wildland fires, oil and gas extraction, vehicles, volatile chemical products (solvents), residential wood combustion, and other non-biogenic sectors were obtained following the EPA's Air Quality TimE Series (EQUATES) methods (Foley et al., 2022) based on the U.S. National Emissions Inventory (NEI). The HAPs naphthalene, benzene,



acetaldehyde, formaldehyde, and methanol (NBAFM) were included as specific species when available in the NEI. In the case of mobile emissions estimated with the MOVES model (U.S. Environmental Protection Agency, 2020) and solvents estimated with the Volatile Chemical Products in python (VCPy) model (Seltzer et al., 2021), total ROC and individual HAPs (e.g., ethyl benzene, acrolein, styrene, and others in addition to NBAFM) were estimated consistently. For the remaining sectors, HAP species were estimated as a fraction of total ROC based on speciation profiles for different sources. In addition to the base EQUATES emissions, L/S/IVOC emissions missing from the mobile-sector inventoried ROC mass, estimated at 4.6% of non-methane organic gases (NMOG) for gasoline vehicles and 55% of NMOG from diesel vehicles, were added using the volatility distribution from the work of Lu et al. (2020). An additional 20% of NMOG from wood burning sources (wildland, prescribed, and residential) was estimated to be an IVOC (assigned a C_i^* of $10^4 \mu\text{g m}^{-3}$) following the estimates of Jathar et al. (2014).

The identity of the individual species within inventoried ROC as well as the L/S/IVOCs (Jathar et al., 2014; Lu et al., 2020) were characterized using the EPA SPECIATE Database (Simon et al., 2010) version 5.2 (release expected in 2022). To provide chemical structure information and facilitate automated property estimation, compounds in the SPECIATE database were assigned a unique Distributed Structure-Searchable Toxicity Database Substance Identifier (DTXSID) (Grulke et al., 2019) using U.S. EPA's CompTox Chemicals Dashboard (the Dashboard, U.S. Environmental Protection Agency (2021c)) (Williams et al., 2017). DTXSIDs allowed for each emitted species to be associated with structural identifiers like Simplified Molecular Input Line Entry System (SMILES) and IUPAC (International Union of Pure and Applied Chemistry) International Chemical Identifier (InChI) representations. In about two-thirds of cases, the emitted SPECIATE species could be exactly matched to a representative compound with a DTXSID in the Dashboard. In the other cases, an isomer or generally representative compound with similar functionality (e.g., presence of aromaticity or other functional groups) and carbon number (e.g., undecane for "isomers of undecane") was manually selected. For the small number of cases in which the SPECIATE species was indicated as "unknown," "unidentified", or similarly undefined, n-decane was assigned as the representative compound. If the unidentified compound was also indicated as exempt from the regulatory definition of VOC (Code of Federal Regulations, 1986) (e.g., "Aggregated exempt compounds", "other, lumped, exempts, individually <2% of category"), acetone was used as the representative compound. The representative compound's preferred name from the Dashboard, DTXSID identifier, and a degree of assignment confidence score (1: species not well defined, 2: species manually mapped, 3: species automatically matched in Dashboard but some properties inconsistent, 4: exact match in Dashboard) were added to SPECIATEv5.2 (U.S. Environmental Protection Agency, 2022a). A logical (true/false) field in the SPECIATE database was also used to identify individual compounds classified as HAPs (see Sect. 4).

By mapping each emitted species, i , to a unique structural identifier, properties of the emissions could be estimated in a traceable manner. The batch feature of the Dashboard (Lowe and Williams, 2021) was used to obtain molecular weights, SMILES strings, and molecular formulas as well as perform OPEn structure-activity/property Relationship App (OPERA) (Mansouri et al., 2018) calculations for the Henry's Law coefficient, rate constant for atmospheric reaction with HO, and vapor



pressure of each ROC species. Vapor pressures (P_i^{vap}) and molecular weights (M_i) were used to calculate pure-species saturation concentrations (Donahue et al., 2006) at a temperature (T) of 298 K ($C_i^* = P_i^{vap} M_i / (RT)$, where R is the gas constant and C_i^* is reported in $\mu\text{g m}^{-3}$).

170 While actual mechanism calculations are required to estimate the contribution of any species to O_3 and SOA in a specific location, two simple structure activity relationships (SARs) were created for screening level analysis of organic aerosol (OA) and O_3 formation potentials of individual ROC species. In the case of OA potential, several sources, largely following what is outlined in the work of Seltzer et al. (2021), were aggregated to estimate the SOA yield of individual species. In this work, exponential or quadratic polynomial fits depending on what was most applicable were applied to data on the yield of SOA vs
175 $\log_{10}(C_i^*)$ by chemical class for oxygenated hydrocarbons, polycyclic aromatic hydrocarbons (PAHs), substituted aromatics, and alkenes, and to the yield of SOA vs. number of carbons for normal, branched, and cyclic alkanes. Most systems showed a good correlation between predicted and expected SOA yield with coefficient of determination (r^2) of 0.67 in the case of oxygenated hydrocarbons and greater for the other species types. Explicit yield assignments were made based on published data in the case of sesquiterpenes, monoterpenes, benzene, toluene, and xylene (Pye et al., 2010; Ng et al., 2007). Published
180 single-ring aromatic yields were scaled up by the vapor wall loss factor (Zhang et al., 2014). An OA concentration of $10 \mu\text{g m}^{-3}$ and equal RO_2 (organic peroxy) reaction rates with HO_2 (hydroperoxyl radical) (“low- NO_x ”) and NO (nitric oxide) (“high- NO_x ”), typical of northern hemisphere July conditions (Porter et al., 2021), were assumed for these explicit yield assignments. While this OA concentration is on the high end of the atmospherically relevant range, it is on the low end of concentrations probed in laboratory studies (Porter et al., 2021) thus providing a bridge between observations and ambient conditions.

185 A second simple SAR was created to estimate the role of individual ROC species in O_3 formation as indicated by maximum incremental reactivity (MIR). Input data for regression fits were obtained from the SAPRC database (Carter, 2019) which contains MIR data for over 1000 compounds. In the case of ill-defined compounds in the SAPRC database, representative compound structures with DTXSIDs were assigned. Compounds were filtered into various chemical classes (halocarbons, oxygenated, aromatic, alkenes, etc.). Within a given class, the MIR was fit via multiple linear regression, an
190 exponential/logarithmic equation, or through averaging as a function of number of carbons per molecule, HO rate constant (from OPERA), number of oxygens, number of double bonds, number of ring structures, number of double bonded oxygen, and/or number of branches depending on the chemical class. The overall r^2 between SAPRC-estimated and simple-SAR predicted MIRs (Fig. S8) was 0.72. The MIRs are most appropriate for comparing species under a given set of conditions as
195 changes in chemical (or meteorological) regime, such as those in the U.S. between 1988 and 2010, have been found to decrease species MIRs by about 20% on average (Venecek et al., 2018). The SARs were used to estimate average SOA yields and MIR for all ROC species in the SPECIATE database.



2.2 Mechanism species

CRACMM species were designed to leverage the original RACM2 chemistry while also considering the properties of present-day emitted species, including properties indicative of SOA formation potential, with a goal of maintaining a reasonable mechanism size (by species count) for computational efficiency. New explicit species were added for multiple reasons. First, certain species are known to contribute significantly to cancer and noncancer health risk (Scheffe et al., 2016). Second, recent advances in measurement techniques, particularly for VOCs, have increased the number of measured species available, which motivates adding these newly measured species explicitly into models for direct comparison. Third, some individual species are emitted in significant quantities and explicit representation facilitates better conservation of mass and representation of product distributions. New lumped species were also added when existing RACM2 species did not provide a good fit in terms of molecular properties, SOA yields, or O₃ formation potential for emissions.

A python mapper (see Code Availability) was developed to automate mapping of individual, emitted ROC species to mechanism species. Once initial rules were created with the intent of following RACM2, properties of the mechanism species were visualized, and mapping rules were manually adjusted to better preserve mass (minimize the spread in number of carbon per molecule, molecular weight, and molar oxygen to carbon ratio within the model species), estimate SOA (minimized spread in saturation concentration, SOA yield, and Henry's law coefficient within the model species), and predict O₃ (minimize spread in HO rate constant and O₃ formation potential within each model species). A decision tree summarizing the final mapper is provided schematically in Supplement Fig. S1-S4. The mapper uses as input the SMILES string for the ROC species, HO rate constant (k_{OH}), and pure component C_i^* . Both k_{OH} and C_i^* can be estimated from a SMILES string prior to mapper input using OPERA algorithms (Mansouri et al., 2018) available for any organic species through the EPA Chemical Transformation Simulator (U.S. Environmental Protection Agency, 2022b). This emission mapping follows a hierarchy of rules in which explicit species are mapped first followed by lumped biogenic VOCs (α -pinene and other monoterpenes with one double bond, API; limonene and other monoterpenes with two or more double bonds, LIM; and sesquiterpenes, SESQ). Other lumped species and mapping rules were created to consider volatility, functional groups (parsed in python using the work of RDKit (2022)), and k_{OH} . For L/SVOCs, mechanism assignment was based purely on volatility except in the case of PAHs (more than one aromatic ring) which were grouped with naphthalenes (NAPH, Sect. 3.5). For IVOCs, assignments considered volatility and presence of specific functional groups (aromatic, oxygenated, alkane). For VOCs, mapping considered only functional groups and k_{OH} .

Figures 1-3 (and Supplementary Fig. S5-S6) show the final U.S. 2017 emission-weighted distributions of compound properties for all emitted ROC species in CRACMMv1.0. Looking across multiple properties illustrates the hierarchy of emission mapping rules. For example, three classes of alkane-like species (discussed in Sect. 3.1) were inherited from RACM2: HC3, HC5, and HC10 (formerly HC8). In carbon-number space (Fig. 1), these species overlap in their coverage of individual



compounds with all three classes including species with 2 to 8 carbons per molecule. Their saturation concentration distributions (Fig. 2) also show overlap. The $\log_{10}(k_{OH})$ (Fig. 3) highlights that HC3, HC5, and HC10 are defined by distinct and mutually exclusive ranges of the HO rate constant. Indeed, the HO rate constant is the classifying property for the HC3, HC5, and HC10 species and is implemented after volatility, functional group identity, and other features of the species have
235 been considered. As another example, SLOWROC is multimodal in number of carbons per molecule (n_C) and C_i^* (Fig. 1-2) which could necessitate separation into more species. However, SLOWROC reacts so slowly (Fig. 3) that additional speciation is not warranted. The systems in Fig. 1-3 indicated by color coding will be further discussed in the next section.

3 ROC Chemistry

Multiple data sources were used to build the chemistry of CRACMM. As CRACMM will be a community mechanism in which
240 different chemical systems are developed by different investigators, individual systems are expected to evolve at different rates and will be informed by different sources of data. Development of CRACMM v1.0 leveraged existing chemical mechanisms including the Generator for Explicit Chemistry and Kinetics of Organics in the Atmosphere (GECKO-A, Aumont et al. (2005)), Master Chemical Mechanism (MCM, Jenkin et al. (1997)), SAPRC-18 Mechanism Generation System (Carter, 2020b), and RACM2, as well as literature. ROC systems not previously represented in RACM2 (such as furans and L/S/IVOCs), precursors
245 to SOA, and systems with new kinetic data (Sect. 3.10) were targeted for development in this initial CRACMM version.

CRACMM v1.0 includes 178 gas-phase species (ROC species in Appendix A) and 508 reactions spanning gas-phase and heterogeneous pathways (Appendix B). In the CMAQv5.4 modal aerosol implementation, CRACMM includes 51 different chemical species in the particulate phase (81 model species across Aitken, accumulation, and coarse modes). CRACMM
250 specifically builds on the implementation of RACM2 chemistry coupled with aerosol chemistry of AERO6 (411 reactions) in the CMAQ v5.3.3 model which differs slightly from the original RACM2 implementation (Goliff et al., 2013) (363 reactions) due to SOA pathways and other minor updates (see the work of Sarwar et al. (2013) and Code Availability section for the CMAQ implementation of RACM2).

255 In contrast to almost all SOA representations in current chemical transport models, SOA systems in CRACMM are integrated with the gas-phase radical chemistry. Specifically, all condensible or soluble precursors to SOA are formed directly as gas-phase products with the ability to condense (systems in Sect. 3.1-3.7) or react heterogeneously (Sect. 3.8) and form SOA. Formation of SOA thus removes mass from the gas phase, sequestering RO_2 , NO, and/or hydrogen oxide (HO_x) radicals with implications for ozone and species modulated by oxidant abundance such as sulfate.

260

All CRACMM species (both primary and secondary) have a representative structure (ROC species in Appendix A) based on the most abundantly emitted species or likely oxidation product. Representative structures were used to obtain properties such



as the molecular weight, rate coefficient, solubility, and/or volatility of species except in 2 cases (SLOWROC in Sect. 3.1, ROICIOXY in Sect. 3.3). These representative structures can enable future prediction of other properties such as aerosol
265 viscosity and propensity to phase separate as well as deviations from ideal partitioning. They can also be used to synthesize CRACMM chemistry as demonstrated in Sect. 5. The species and chemistry of the major ROC systems updated compared to RACM2, reactions for two additional new HAPs, as well as rate constant updates (including many for inorganic reactions) are described in this section. Table 1 summarizes the SOA pathways.

3.1 Alkane-like ROC

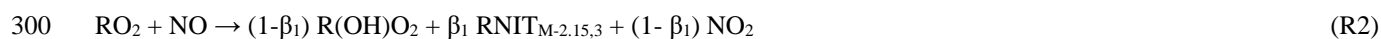
270 CRACMM includes 14 classes of alkane-like species ranging from low-volatility compounds to ethane (Fig. 1-3 red series). Methane reaction with HO is from RACM2 and assumes a fixed background concentration (1.85 ppm for the late 2010s, Dlugokencky (2022)). After remapping all ROC species, the RACM2 alkane class HC8 (alkanes and other species with $k_{OH} > 6.8 \times 10^{-12} \text{ cm}^3 \text{ molec}^{-1} \text{ s}^{-1}$) was renamed to HC10 based on the n_C (Fig. 1) and is consistent with a $C_i^* \sim 10^7 \mu\text{g m}^{-3}$ (Fig. 2). Nine new alkane-like mechanism species with high OA formation potential span the L/S/IVOC range and are grouped by $\log_{10}(C_i^*)$
275 into ROCN2ALK, ROCN1ALK, ROCP0ALK, ROCP1ALK, ROCP2ALK, ROCP3ALK, ROCP4ALK, ROCP5ALK, and ROCP6ALK, where the numbers indicate the negative (N) or positive (P) $\log_{10}(C_i^* [\mu\text{g m}^{-3}])$ value (Fig. 2). When the species reside in the gas-phase as a vapor, it is prepended with a “V” (as in Appendix B) and when in the particulate aerosol phase, an “A.” For example, VROCN2ALK is an alkane-like vapor species with C_i^* of $10^{-2} \mu\text{g m}^{-3}$, and AROCN2ALK is a particulate species of the same volatility.

280

The 9 new alkane-like model species roughly correspond to carbon numbers of 30, 29, 28, 27, 24, 21, 18, 14, and 12 (Fig. 1) and are not represented in traditional atmospheric chemical mechanisms due to low ozone formation potential per unit mass (Fig. S5). For example, $\sim\text{C}_8$ is the largest alkane category in RACM2 and SAPRC18, and n-dodecane (C_{12}) is the largest alkane in MCM (Jenkin et al., 1997). Conceptually, for deposition and other processes, the gas-phase paraffinic species in Carbon
285 Bond (CB6r3) is equivalent to a C_4 species. Regardless of the chemical mechanism, regional modeling emission infrastructure previously used by CMAQ did not classify species with ~ 20 or more carbons (Pye and Pouliot, 2012), and S/IVOC emissions were not propagated to model-ready species for CMAQ mechanisms (Shah et al., 2020). The CRACMM species with $\log_{10}(C_i^*) \leq 3$ can exist in the gas or particle phase based on the local organic aerosol loading and absorptive partitioning theory (Pankow, 1994) while ROCP4ALK-ROCP6ALK exist meaningfully in the gas-phase only (Appendix A). The low
290 volatility alkanes, $C_i^* \leq 1 \mu\text{g m}^{-3}$, are assumed to be primarily in the particulate phase and have a minor potential to react and contribute to O_3 formation (Fig. S5) so do not participate in gas-phase radical chemistry (Appendix B). Most of the L/S/IVOC emissions are expected to be unresolved at the individual species level (Robinson et al., 2007) and are characterized through other means such as volatility analysis (e.g., Lu et al., 2018).



295 Gas-phase chemistry for the alkane species with $10 \mu\text{g m}^{-3} \leq C_i^* \leq 10^7 \mu\text{g m}^{-3}$ (ROCP1ALK-ROCP6ALK and HC10) is based on GECKO-A predictions for C_{10} - C_{26} n-alkanes (Lannuque et al., 2018) and known H-shift pathways (Praske et al., 2018). The chemical reactions representing the major product channels and types of functionalities added to the parent hydrocarbon (RH) are:



where stable products are subscripted with their saturation concentration in $\log_{10}(C_i^*)$ (relative to a parent hydrocarbon with $\log_{10}(C_i^*) = M$) and the number of oxygens per molecule (n_O). The initial product, RO_2 , is the prompt peroxy radical resulting from hydrogen abstraction followed by O_2 addition (R1). RO_2 reactions lead to stable products like organic nitrates (RNIT) and peroxides (ROOH) (R2, R4) that can further react (following Sect. 3.2 for S/IVOCs and RACM2 for VOCs). The alkoxy radical generated from the prompt RO_2 can also undergo a 1,5 H-shift followed by addition of O_2 leading to a new hydroxy-peroxy radical, R(OH)O_2 (R2, R3). The R(OH)O_2 can undergo standard bimolecular peroxy radical fates leading to multifunctional nitrates (R(OH)NIT), ketones (R(OH)KET), and peroxides (R(OH)OOH) or a 1,6 H-shift at a rate of 0.188 s^{-1} (Vereecken and Nozière, 2020) producing a ketohydroperoxide (R(O)OOH) and HO_2 (R5) as described by Praske et al. (2018). Following GECKO-A (Lannuque et al., 2018), the yield of organic nitrates in reaction R2, β_1 , is 0.28 for S/IVOC alkanes and 0.26 for HC10, consistent with the plateau at ~ 0.3 observed for C_{13} and larger alkanes (Yeh and Ziemann, 2014). The yield of organic nitrates for the hydroxy-peroxy radical, β_2 , is 0.14 for S/IVOC alkanes and 0.12 for HC10 (Lannuque et al., 2018). Rate constants are provided in Appendix B.

320 Products are often 2-3 orders of magnitude lower in C_i^* than their parent and can be 4-5 orders of magnitude lower in the case of the multifunctional nitrates and peroxides. For the alkane systems, product C_i^* are based on vapor pressures obtained from GECKO-A output using the Nannoolal method (Nannoolal et al., 2008; Nannoolal et al., 2004). With one exception, all stable products from the VOC, HC10 ($M=7$), are expected to remain in the gas phase and thus map to the standard gas-phase species ONIT (organic nitrates), OP2 (organic peroxides), and KET (ketones) inherited from RACM2. The hydroxyhydroperoxide from HC10 oxidation is predicted to be sufficiently functionalized to be semivolatile. That C_{10} multifunctional peroxide along with all the stable products from alkane-like S/IVOCs are mapped to new CRACMM species of matching C_i^* and molar oxygen to carbon ($n_O:n_C$) ratio (secondary, oxygenated L/S/IVOC species, Sect. 3.2).



According to the SOA SAR (Fig. S5) as well as the prompt (one HO reaction) mechanism predictions (Table 1), SVOCs of
330 ROCP2ALK and lower volatility have SOA yields that are near 100% by mole (up to 150% by mass), and the atmospherically
relevant SOA yields will depend on competition between phase partitioning, reaction, and deposition. Much of the alkane-like
L/SVOC contribution to ambient OA will be in the form of direct emission of the lower volatility species as primary organic
aerosol (POA). The mechanism-predicted prompt SOA yields for ROC3PALK and ROCP4ALK by mass (Table 1) are very
similar to the emission-weighted SAR-based prediction of 0.83 and 0.55 by mass (Fig. S5). The mechanism-based prompt
335 SOA yields for the more volatile alkane-like ROC species (ROCP5ALK, ROCP6ALK, and HC10) are lower than those
predicted by the SOA SAR (28%, 18%, and 6% by mass). Note that the HC10 class is estimated to contain substantial emissions
(Shown in Sect. 4 and accompanying Fig. 6b), some of which are poorly identified in SPECIATE (representative compound
score of 1, Section 2.1).

340 The alkane-like ROC species differ from the previous CMAQ S/IVOC species implemented in AERO6/7 (\times symbols Fig. 1,
3) in terms of the trend in n_c with volatility as they are all conceptualized as alkane-like structures because those are the
representative structures currently populated with emissions in the S/IVOC range. SVOCs with $\log_{10}(C_i^*[\mu\text{g m}^{-3}]) < 2.5$ are
lumped into ROCN2ALK-ROCP2ALK species based on volatility regardless of their functionality resulting in some higher
 $n_o:n_c$ species being included (Fig. S6). CMAQ AERO6/7 previously assumed a slight increase in $n_o:n_c$ and corresponding
345 decrease in n_c as volatility decreased (Fig. 1, Fig. S6). CRACMM alkane-like SVOCs with k_{OH} from OPERA are also less
reactive than AERO6/7 SVOCs (Fig. 3).

The reaction products of ethane (ETH), C3 alkanes and other slowly-reacting species ($3.5 \times 10^{-13} \leq k_{OH} < 3.4 \times 10^{-12} \text{ cm}^3 \text{ molec}^{-1} \text{ s}^{-1}$, HC3), and C5 alkanes and other moderately reacting species ($3.4 \times 10^{-12} \leq k_{OH} \leq 6.8 \times 10^{-12} \text{ cm}^3 \text{ molec}^{-1} \text{ s}^{-1}$, HC5) (Fig. 3)
350 are obtained directly from RACM2 with the addition of a very small yield of SOA from HC3 (2.8×10^{-5} by mole) and HC5 (1.3×10^{-3} by mole) (Table 1). Ethane is the only explicit alkane in CRACMM its rate constant with the hydroxyl radical is
updated to follow recent recommendations (Burkholder et al., 2019). In addition, CRACMM includes a new species called
SLOWROC with a lifetime of about one month ($k_{OH} < 3.5 \times 10^{-13} \text{ cm}^3 \text{ molec}^{-1} \text{ s}^{-1}$) to prevent loss of emitted carbon that may
contribute to the ambient atmospheric ROC burden (effective carbons per molecule of 2.1). SLOWROC also contains many
355 HAPs (Sect. 4). Due to the highly empirical nature of SLOWROC, the molecular weight is based on an emission-weighted
value rather than a representative compound. Oxidation of SLOWROC produces the ethylperoxy radical (ETHP) and a small
yield of SOA (0.10% by mole).

Effective SOA yields for the alkane-like VOC systems except HC10 use the simple SAR for SOA and are driven by isopropyl
360 acetate and methyl butanoate (estimated SOA yields of 2.8 and 2.2% by mass) in the case of HC3, by isopentane (estimated
SOA yield of 1.9% by mass) in the case of HC5, and by two long-lived aromatic species in the case of SLOWROC. HC3,
HC5, and SLOWROC SOA is mapped to species ASOAT, a general, nonvolatile SOA species with molecular weight of 200



g mol⁻¹ (Table 1). HC3, HC5, and SLOWROC are estimated to contribute 0.003%, 0.062%, and 0.0002% by mass, respectively of the total OA potential for anthropogenic and biomass burning emissions in the U.S. for 2017 conditions.

365 3.2 Secondary oxygenated L/S/IVOCs

Gas-phase oxidation of S/IVOC alkanes readily leads to oxygenated L/S/IVOC products with $n_o:n_c$ ratios up to 0.3 (Reactions R1-R8). The products of these prompt reactions continue to be processed in the atmosphere, resulting in further functionalization as well as fragmentation (cleaving of the carbon backbone) with implications for increasing or decreasing SOA, respectively. Functionalization products of the secondary oxygenated L/S/IVOC chemistry can sequester radicals, but
370 fragmentation products, like formaldehyde, can eventually release radicals via photolysis (Edwards et al., 2014).

The chemistry of secondary oxygenated L/S/IVOCs is parameterized using the 2-D VBS framework (Donahue et al., 2012) with some modifications. The decrease in $\log_{10}(C_i^*)$ per oxygen in the 2-D VBS box model was set at -2.3, roughly equivalent to the magnitude expected for an alcohol (Pankow and Asher, 2008). The decrease in $\log_{10}(C_i^*)$ per carbon was set to 0.475
375 with a carbon-oxygen interaction parameter (-0.3) to correct for the behavior of diacids (Donahue et al., 2011). Homogeneous, gas-phase HO reaction rate constants were specified based on the parameterization proposed by Donahue et al. (2013):
 $k_{OH}(cm^3 molec^{-1} s^{-1}) \approx 1.2 \times 10^{-12}(n_c + 9n_o - 10(n_o:n_c)^2)$. Following the reaction with HO, the probability of functionalization was parameterized as $f^{func} = 1 - (n_o:n_c)^{0.4}$, with subsequent probabilities of adding one, two, or three
380 oxygens set at 30%, 50%, and 20%, respectively, following the 2-D VBS functionalization kernel derived for photo-oxidation of POA and IVOCs (Zhao et al., 2016). The sensitivity of yields to NO_x and formation of organic nitrates were not explicitly addressed in the 2-D VBS-based aging mechanism, although both are addressed by CRACMM more broadly and some products mapped to secondary L/S/IVOCs contain nitrate functionality. Rather than recycling hydroxyl radicals as is standard practice for VBS-style reactions that are only meant to capture SOA, CRACMM sequesters HO_x in oxygenated L/S/IVOC products as might be expected when peroxides form. For example, reactions of type R1 followed by type R4 sequester two
385 HO_x for each initiating reaction.

L/S/IVOC products predicted by the 2-D VBS were lumped into a reduced series of fifteen mechanism species spanning C_i^* of 10⁻² through 10⁶ μg m⁻³ and $n_o:n_c$ of 0.1 through 0.8 for use in CRACMM: ROCN2OXY2, ROCN2OXY4, ROCN2OXY8, ROCN1OXY1, ROCN1OXY3, ROCN1OXY6, ROCP0OXY2, ROCP0OXY4, ROCP1OXY1, ROCP1OXY3, ROCP2OXY2,
390 ROCP3OXY2, ROCP4OXY2, ROCP5OXY1, and ROCP6XY1. These species follow a similar naming convention as the S/IVOC alkanes, where numbers after N and P indicate the negative or positive $\log_{10}(C_i^*)$ value and the name ends in 10× $n_o:n_c$ (e.g., ROCN2OXY2 is $C_i^* = 10^{-2}$ μg m⁻³ with $n_o:n_c = 0.2$). VBS products of known n_c and n_o were mapped to the available CRACMM model species, first by interpolating to the two nearest $\log_{10}(C_i^*)$ points, and then to the two nearest



species in $n_O:n_C$ space. The number of $n_O:n_C$ levels represented at a given volatility in CRACMM increases with decreasing
395 C_i^* to reflect increasing diversity in chemical functionality and size of products with lower saturation concentrations.

The portion of reacted mass following the fragmentation pathway, $f^{frag} = (n_O:n_C)^{0.4}$, was assumed to form fragments of
sizes varying from one up to n_C carbons. The distribution of fragments was estimated assuming the probability of attack on
any carbon as $1/n_C$. Fragments with greater than seven carbons were functionalized using the same oxygen addition
400 probabilities and remapping to lumped model species as above. Stable fragmentation products with six or fewer carbons were
mapped back to active gas-phase species from RACM2 based on their carbon number as follows: C_1 to formaldehyde (HCHO),
 C_2 to acetaldehyde (ACD), C_3 to higher aldehydes (ALD), C_4 to methyl ethyl ketone (MEK), C_5 to dicarbonyls (DCB1), C_6
from low $n_O:n_C$ reactants to hydroxy ketones (HKET), and C_6 from high $n_O:n_C$ reactants to higher ketones (KET). A new
semivolatile peroxide (OP3), equivalent to a $C_8H_{16}O_4$ species with C_i^* of $\sim 10 \mu\text{g m}^{-3}$, in CRACMM provides an oxygenated
405 peroxide species between the L/S/IVOC oxygenated series and RACM2's higher organic peroxides (OP2). In addition, radical
products are mapped to RACM2 peroxy radical species as follows: C_1 to methyl peroxy radical (MO2), C_2 to ethyl peroxy
radicals (ETHP), C_3 to isopropylperoxy radicals (HC3P), C_4 to peroxy radicals from methyl ethyl ketone (MEKP), C_5 to
pentan-3-ylperoxy (HC5P) radicals, and C_6 to ketone-derived peroxy radicals (KETP). OP3 can photolyze or react with HO.

410 Overall, the CRACMM scheme performs similarly to the medium-yield 2D-VBS scheme optimized for S/IVOCs by Zhao et
al. (2016) (Fig. 4). For precursors with $n_O:n_C > 0.05$ and 12 hours of chemical processing, the 2-D VBS and CRACMM aging
schemes are almost the same in terms of OA yield (Fig. 4a-c) with values ranging from near 0.1 to above 1 as a function of
volatility (Table 1). Some deviations occur between the schemes for the most oxygenated and volatile precursors ($n_O:n_C >$
 0.45 and $\log_{10}(C_{OA}/C_i^*) \leq 0$, where C_{OA} is the mass-based concentration of the condensed-phase partitioning medium) for
415 which CRACMM predicts a stronger dependence of yield on precursor volatility and also predicts less OA formation. Both
CRACMM and the 2-D VBS predict consistent trends in OA yield as a function of precursor properties with more oxygenated
and volatile precursors having lower yields due to an increased likelihood of fragmentation. At very long processing times
CRACMM predicts OA yields will decrease (which has been observed in experimental systems in the work by He et al. (2022))
while the 2-D VBS indicates yields continue to increase from 2.5 days (Fig. 4) to 5.5 days (Fig. S7). In CRACMM $n_O:n_C$
420 ratios are predicted to increase with time, which can be due to both functionalization (Heald et al., 2010) and fragmentation
(Kroll et al., 2009) reactions. CRACMM generally predicts lower $n_O:n_C$ ratios in OA products from oxygenated ROC (0.1 to
0.5 for least oxygenated and 0.6 to 0.7 for most oxygenated precursors) than the 2-D VBS (Fig. 4d-f).

3.3 Primary oxygenated IVOCs

425 Volatile chemical products emit significant amounts of oxygenated IVOCs (Seltzer et al., 2021; McDonald et al., 2018). Many
of these oxygenated species are structurally different than what is conceptualized in the secondary oxygenated L/S/IVOCs



(Section 3.2) since they include siloxanes and ethers, while secondary oxygenated species are primarily alcohols, peroxides, nitrates, and ketones. Emitted oxygenated IVOCs have a significantly lower potential to form SOA than hydrocarbon IVOCs of similar volatility (Pennington et al., 2021). In addition, oxygenated species generally differ from hydrocarbon-like emissions in their ability to form O₃, peroxyacetyl nitrate (PAN), and formaldehyde (Coggon et al., 2021) and should be represented
430 separately from hydrocarbon-like species.

Two new types of oxygenated IVOCs with direct emissions are included as distinct species in CRACMM (Fig. 1-3 purple): propylene glycol (PROG) and oxygenated IVOCs (ROCIOXY). 1,2-propylene glycol is one of the most prevalent species in consumer product purchases (Stanfield et al., 2021) and is associated with increased allergic symptoms when inhaled (Choi et al., 2010). Propylene glycol is represented in CRACMM with chemistry based on MCM following the work of Coggon et al. (2021). The ROCIOXY class includes non-aromatic, saturated IVOCs with $n_o:n_c > 0.1$ and all species containing silicon. Decamethylcyclopentasiloxane is the most abundant individual species in ROCIOXY, and ROCIOXY has an emission-weighted effective carbon number of 9.5. Due to the highly aggregated nature of ROCIOXY, the k_{OH} and molecular weight are emission-weighted properties rather than based on a representative compound. ROCIOXY produces the ethylperoxy radical
440 with an 85.2% molar yield and SOA with a 14.9% molar yield (Table 1) upon reaction with HO in CRACMM. While the SOA yield may appear high, the lifetime of ROCIOXY is 40 hours at typical daytime HO concentrations which should limit the amount of SOA in urban source regions, similar to siloxane behavior in the work of Pennington et al. (2021). Future versions of CRACMM emission processing could redirect alcohols, carbonyls, and other oxygenated S/IVOCs from ROCIOXY to the secondary oxygenated L/S/IVOC series (Sect. 3.2) and readjust the effective ROCIOXY SOA yield.

445 3.4 Furans

FURAN is a new lumped ROC species introduced in CRACMM with the most abundant individual species in the category being furfural followed by furan. Furans were not previously an independent category in RACM2, and Carter (2020a) recommended mapping 2-furfural to ~C8 hydrocarbons (now HC10) and furan to the lumped o-xylene (XYO in RACM2). Given the abundance of furans (140 Gg yr⁻¹ of emission, primarily from wood burning for 2017 U.S. conditions), unique
450 functional group structure, OH reactivity (Koss et al., 2018), and O₃ formation potential (Coggon et al., 2019), FURAN was implemented in CRACMM as a new species (Fig. 1-3 blue). Furans have been shown to form SOA with yields between 1.85% to 8.5% by mass depending on the structure (Gómez Alvarez et al., 2009) and the simple SAR predicts a yield of 2.6% by mass (Fig. S5). The furan SOA yield is about a factor of 4 lower than that of xylenes but products such as furanone (FURANONE, a new species in CRACMM) are also formed in aromatic systems like benzene (Section 3.5). The CRACMM
455 species, FURAN, includes small amounts of other species with 2 double bonds (Fig. S3) including 2.4 Gg yr⁻¹ of anthropogenic dienes.

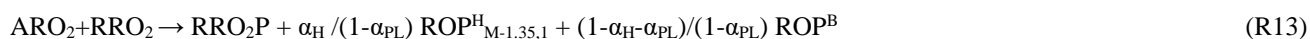
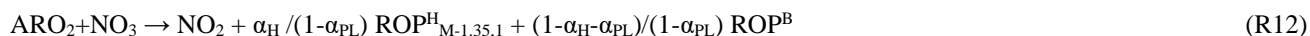
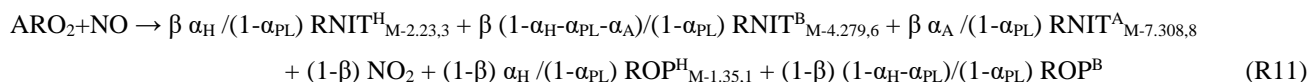
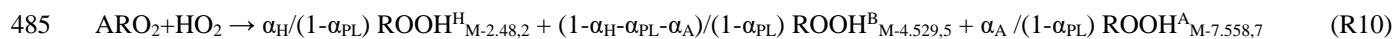
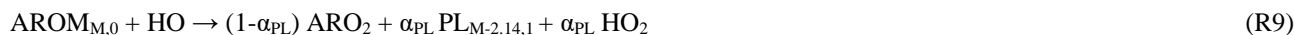


The FURAN chemistry in CRACMM is based on a 5-species weighted average using furan emission factors reported by Koss et al. (2018) and the furan chemistry outlined by Wang et al. (2021) and Coggon et al. (2019). FURAN will predominantly react with hydroxyl radicals leading to gas-phase products including dicarbonyls (DCB1, DCB3), organic nitrates (ONIT), peroxides (OP2), furanone (FURANONE), and aldehydes (ALD) in addition to radicals (Appendix B). CRACMM assigns SOA from FURAN to further reactions in the ring-retaining product channel, FURANONE, which reacts to form ketones, glyoxal, and SOA. The effective SOA yield from FURAN is approximately 5% by mass (Bruns et al., 2016) when branching between high- and low-NO_x reactions is equal. The yield of SOA from FURANONE in CRACMM is set to 4% by mole or 8% by mass (Table 1).

3.5 Aromatics

Aromatic hydrocarbons (Fig. 1-3 blue) were reorganized in CRACMM to reduce the number of aromatic VOC model species and increase the number of aromatic IVOC species. Instead of 4 aromatic VOC categories based on reactivity (k_{OH}), CRACMM uses two categories of xylene-like hydrocarbon species based on reactivity: m-xylene and more reactive aromatics (XYM) and aromatics less reactive than m-xylene (XYE). Toluene (TOL), a HAP (Sect. 4), is now explicit in CRACMM, and benzene (BEN) was already explicit in RACM2. The three new IVOC aromatic hydrocarbons ($n_o:n_c = 0$) are: naphthalene and other polycyclic aromatic hydrocarbons (NAPH), single-ring aromatics of $\log_{10}(C_i^*) \approx 5$ (ROCP5ARO), and single-ring aromatics of $\log_{10}(C_i^*) \approx 6$ (ROCP6ARO). The ROCP5ARO and ROCP6ARO categories were previously found to be important for representing SOA from vehicle combustion sources (Lu et al., 2020), and the emissions for 2017 indicated insufficient mass and SOA formation potential to warrant another aromatic species at $\log_{10}(C_i^*) \approx 4$.

MCM v3.3.1 chemistry (Bloss et al., 2005; Jenkin et al., 2003) was used to obtain a basic mechanism for aromatic reaction for seven hydrocarbon-like aromatics in CRACMM (BEN, TOL, XYE, XYM, NAPH, ROCP6ARO and ROCP5ARO). The MCM epoxide yield (which includes unidentified species mass, Birdsall and Elrod (2011)) was set to zero and product mass redirected to the bicyclic peroxy channel following Xu et al. (2020). In addition, the organic nitrate yield (β , Reaction R11) from RO₂+NO is 0.2% in CRACMM (Xu et al., 2020). A fraction of the bicyclic peroxy radical channel is assumed to undergo autoxidation (Wang et al., 2017; Molteni et al., 2018; Xu et al., 2020). The following reactions describe this chemistry for a parent aromatic species, AROM:





490 Stable, individual species are subscripted with their $\log_{10}(C_i^*)$ relative to the parent volatility of M (estimated with SIMPOL
(Pankow and Asher, 2008) based on expected functionality) and number of oxygens per molecule. The phenolic product (PL)
yield (α_{PL} , 53% for benzene and 16-18% otherwise) is from MCM (o-xylene if a species was not available) and independent
of NO level, in good agreement with experimental data for conditions below a few hundred ppb NO (Bates et al., 2021). The
PL product is mapped to phenol (for benzene), cresols (for toluene and xylenes), or a lumped secondary oxygenated product
495 (described in Sect. 3.2) based on volatility and $n_o:n_c$ (for all other aromatics). Aromatic peroxy radical (ARO₂) products
included peroxides, organic nitrates, and alkoxy radical decomposition products (ROP). ROP products are produced by H-
abstraction (H), traditional OH addition resulting in bicyclic peroxy radicals (B), and/or autoxidation (A). The fraction of all
AROM + HO through the H-abstraction route (α_H) is from MCM with the product mapped to benzaldehyde in the case of
toluene and xylenes or a product based on expected volatility and $n_o:n_c$ (H-abstraction not applicable for benzene). ROP^B
500 products from the bicyclic peroxy radical alkoxy radical decomposition channel follow MCM and include glyoxal and/or
methylglyoxal, furanones, dicarbonyl(s), and HO₂. α_A is the fraction of products undergoing autoxidation and is a subset of
the bicyclic RO₂ products. Coefficients in Reactions R9-R13 (α_H , α_{PL} , α_A) are relative to total AROM + HO except the fraction
of RO₂ + NO branching to organic nitrates (β) in Reaction R11.

505 Aromatic peroxy radicals can react with other organic peroxy radicals (RRO₂) with methyl peroxy radicals and acetylperoxy
radicals being the most abundant and always represented in RACM2 (Stockwell et al., 1990). The RRO₂ products (RRO₂P)
are based on MCM at yields specified independently of the ARO₂ product channels. Specifically, methyl peroxy radicals
(RRO₂ as RACM2 species MO₂), result in 0.68 formaldehyde, 0.37 HO₂, and 0.32 higher alcohols (RRO₂P = 0.68 HCHO +
0.37 HO₂ + 0.32 MOH). Acetylperoxy radicals (RRO₂ as RACM2 species ACO₃) result in 0.7 methyl peroxy radicals and 0.3
510 acetic acid (RRO₂P = MO₂ + ORA₂).

Reactions R9-R13 produce condensible gases and SOA precursors. In the case of volatile aromatics like benzene, toluene, and
xylenes, further reaction of the phenolic product along with autoxidation are proposed as the major SOA channels in
CRACMM since traditional bimolecular RO₂ products are generally not of sufficiently low volatility. For aromatic IVOCs,
515 peroxides, nitrates, and aldehydes from bimolecular RO₂ reactions can be semivolatile and partition based on their saturation
concentration. Further oxidation of furanone produced from aromatic oxidation also results in small amounts of SOA (Sect.
3.4). For products in Reactions R9-R13 that are mapped to a corresponding surrogate of matching volatility and $n_o:n_c$, further
chemical processing follows the secondary oxygenated S/IVOC chemistry in Sect. 3.2.

520 CRACMM retains the three phenolic species of RACM2 (hydroxy substituted benzenes like phenol and benzene diols, PHEN;
cresols, CSL; and methylcatechols, MCT) with the same gas-phase chemistry as RACM2 except for the addition of one,
nonvolatile SOA product for PHEN and CSL. The yield of SOA from phenols and cresols is set to reproduce the high-NO_x
SOA yields from benzene and toluene oxidation observed in chamber experiments by Ng et al. (2007) with wall loss corrections



525 based on Zhang et al. (2014) (see the supplement information for a detailed derivation). The molar SOA yield using this method
is estimated as 15% by mole for phenols and 20% by mole for cresols (Table 1), within the range of 24-52% by mass for
phenols and 27-49% by mass for cresols as summarized by Bruns et al. (2016). Future work should expand upon this phenolic
SOA treatment as improvements in the phenoxy-phenylperoxy radical chemistry have been shown to modulate O₃ formation
and could improve predictions for laboratory conditions over MCM, RACM2, and SAPRC by breaking the catalytic radical
cycles (Bates et al., 2021). Products like methylcatechols could also lead to SOA with implications for O₃ and HO production
530 in aromatic systems.

The bicyclic peroxy radical fate in aromatic hydrocarbon systems is not well characterized but includes autoxidation. Molteni
et al. (2018) estimate molar yields of autoxidation products from aromatic oxidation of just under 3% by mole and that value
is used for the aromatic IVOC systems in CRACMM ($\alpha_A=0.03$). Higher values are not needed to produce significant SOA in
535 IVOCs systems since traditional bimolecular RO₂ fates result in sufficiently functionalized products to contribute to SOA.
Specifically, with $\alpha_A=0.03$, CRACMM predicts SOA yields for ROCP5ARO, ROCP6ARO, and NAPH of 37%, 21% and 21%
by mole respectively (Table 1). However, such low levels of autoxidation, even when combined with phenolic (PHEN and
CSL) SOA, are insufficient to explain observed SOA production for the more volatile aromatics, particularly in RO₂ + HO₂
dominant conditions where SOA yields are around 27% by mole based on chamber experiments. Xu et al. (2020) indicate
540 bicyclic peroxy radicals in the benzene system may predominantly form alkoxy radicals (even in RO₂ + HO₂ conditions) that
continue to highly oxygenated organic molecules (HOM) in addition to other products. Given the current lack of carbon closure
for gas-phase aromatic chemistry (Xu et al., 2020) and low-volatility of laboratory generated RO₂ + HO₂ aromatic SOA (Ng
et al., 2007), the amount of autoxidation in the benzene, toluene, and xylene aromatic systems is set in CRACMM to reproduce
observed RO₂ + HO₂ chamber SOA yields when combined with the phenolic channel (see supplementary information for molar
545 yield derivation). The resulting estimates for the fraction of AROM + HO reaction leading to autoxidation (α_A) are estimated
as 19% by mole for benzene and 23% by mole for toluene and xylenes. This results in the phenolic channel contributing 30%
of the SOA in the benzene system and 13% in the toluene systems for RO₂ + HO₂ conditions, similar to the previously published
estimate of 20% for low-NO_x conditions for benzene, toluene, and m-xylene (Nakao et al., 2011) and 20-40% for toluene
(Schwantes et al., 2017) as well as the relative abundance of phenolic products in benzene versus toluene systems.

550

In general, autoxidation of the bicyclic RO₂ in the aromatic systems is assumed to involve one H-shift followed by O₂ addition
and result in peroxides and nitrates about seven $\log_{10}(C_i^*)$ values lower in volatility than the parent aromatic (products in
Reactions R10-R11). The autoxidation product in benzene and toluene systems with only one H-shift would have a C_i^* of 10
 $\mu\text{g m}^{-3}$, making it semivolatile according to SIMPOL (Pankow and Asher, 2008). To improve consistency with Ng et al. yields
555 and nonvolatile partitioning behaviors under low-NO_x conditions at low organic aerosol concentrations (<10 $\mu\text{g m}^{-3}$), the
products from autoxidation in the toluene and benzene systems are assumed to result from two H-shifts followed by O₂ addition
leading to two additional hydroperoxide functional groups and autoxidation products with $C_i^* = 0.01 \mu\text{g m}^{-3}$. Xylene-like



(XYM and XYE) autoxidation products assume one H-shift with O₂ addition resulting in autoxidation products with C_i^{*} = 1 μg m⁻³. ROOH^B products from XYM and XYE are slightly lower in volatility than those from benzene and toluene and mapped to the new multifunctional C₈ peroxide (OP3, see Sect. 3.2 and Table 1) resulting in SOA from channels other than autoxidation and phenolic routes for xylenes. SOA yields for benzene, toluene, and xylenes summarized in Table 1 generally reproduce wall-loss corrected laboratory values (Ng et al., 2007; Zhang et al., 2014) due to the imposed autoxidation channel. Benzene and toluene are predicted to have lower SOA yields than the IVOC aromatics NAPH, ROCP5ARO, and ROCP6ARO. However, the amount of autoxidation for aromatic IVOCs was not adjusted to match literature SOA yields since many traditional bimolecular products were already in the S/IVOC range and thus SOA for aromatic IVOCs could be underestimated compared to laboratory work (Srivastava et al., 2022).

Figure 5 shows the molar flows to organic aerosol in the combined aromatic, phenolic, and furan systems based on anthropogenic and biomass burning emissions in the U.S. for 2017 and equal RO₂ + HO₂ vs RO₂ + NO branching. Most (69%) phenol mass is directly emitted with the balance from benzene oxidation. In contrast, cresols are predominantly chemically produced (80% of source) rather than directly emitted. Approximately 22% of furanone is produced directly from furan oxidation but most furanone is predicted to be from oxidation of aromatic hydrocarbons like toluene and xylenes with smaller contributions from IVOC aromatics. About 32% of the aromatic system SOA is predicted to come from phenols, cresols, and furanone through the ASOATJ species. Peroxides (OP3) may be a substantial contributor to SOA mass. Autoxidation, leading to species such as ROCN1OXY6, also make meaningful contributions to the predicted SOA mass. By acknowledging further oxidation of phenolic species as contributors to overall aromatic hydrocarbon SOA, all phenolic emissions can now be considered SOA precursors. In addition, adding phenolic sources of SOA increases the overall amount of SOA from ROC emissions compared to previous CMAQ aerosol representations that did not include phenols or cresols as SOA precursors.

3.6 Sesquiterpenes

Sesquiterpenes (C₁₅H₂₄) are a new radical system in CRACMM (previously only considered for SOA formation in CMAQ, Fig. 1-3 green) with chemistry built using β-caryophyllene from MCM (Jenkin et al., 2012) and autoxidation based on literature. β-caryophyllene is an IVOC (log₁₀(C_i^{*}) of 5.05 μg m⁻³) and MCM chemistry readily predicts sesquiterpene products that are S/IVOCs, consistent with the semivolatile nature of observed SOA (Griffin et al., 1999). Sesquiterpenes, SESQ, react with NO₃, O₃, and HO:





Where α_A is the fraction of ozonolysis products undergoing autoxidation and β is the fraction of $\text{RO}_2 + \text{NO}$ products resulting
595 in organic nitrates ($\beta = 0.25$). The ozonolysis reaction (R18) is highly simplified and predicted to result in a ketone and
autoxidation product, PA, of specified volatility and degree of oxygenation. Autoxidation is based on Richters et al. (2016)
and α_A set to 1.8% by mole. Observations indicate sesquiterpenes are not major contributors by mass to ambient SOA in the
Amazon (Yee et al., 2018), southeastern U.S., or boreal forest (Lee et al., 2020). As a result, CRACMM does not retain the
unique identity of sesquiterpene products and all stable products in reactions R14-R22 are mapped to the corresponding
600 secondary oxygenated S/IVOC of corresponding volatility and degree of oxygenation with further chemistry specified in Sect.
3.2.

CRACMM predicts prompt (first generation) sesquiterpene SOA that is less volatile than previous CMAQ work (Carlton et
al., 2010; Griffin et al., 1999), is NO_x and oxidant dependent, and has the potential for higher yields through multigenerational
605 chemistry. The yield of prompt SOA under $\text{RO}_2 + \text{HO}_2$ dominant conditions is predicted to be 50% ($\text{OA} = 1 \mu\text{g m}^{-3}$) to 91%
($\text{OA} = 10 \mu\text{g m}^{-3}$) by mole for HO and NO_3 oxidation. These low- NO NO_3 yields are within the range of those observed in
 NO_3 oxidation experiments (SOA yields of 56-109% by mole of C, Jaoui et al. (2013)) albeit laboratory values corresponded
to a higher concentration of organic aerosol ($60\text{-}110 \mu\text{g m}^{-3}$) and the RO_2 fate was not characterized. Under higher NO_x
conditions ($\text{RO}_2 + \text{NO}$ dominant) and moderate organic aerosol loading ($\text{OA} = 10 \mu\text{g m}^{-3}$), prompt SOA yields are expected to
610 be ~12% by mole from HO oxidation similar to the carbon-based yields of aerosol from laboratory work (19% by mole for β -
caryophyllene, Jaoui et al. (2013)). Nitrate oxidation is not expected to produce significant SOA when RO_2 react with NO or
 NO_3 (Reaction R16-R17), and prompt SOA yields from ozonolysis are 2.7% by mole, lower than the observed yield of 28%
by mole C for ozonolysis (Jaoui et al., 2013). Thus, further chemical processing of first-generation sesquiterpene-derived
ketones (mapped to CRACMM species ROCP3OXY2, chemistry in Sect. 3.2) likely results in lower volatility species that
615 increase SOA yields beyond the prompt values, especially under high- NO_x and ozonolysis conditions.

3.7 Monoterpenes

CRACMM retains the two monoterpene categories of RACM2 with α -pinene and Δ -limonene as the major representative
compounds in each class (API and LIM, respectively, Fig. 1-3 green). The two classes differ in the number of double bonds
per species which is expected to influence reactivity and SOA formation potential (Hoffmann et al., 1997). In addition, species
620 with two double bonds in their initial structure likely experience faster autoxidation (Møller et al., 2020). The two classes of
monoterpenes (API vs LIM) have different sources of emissions with α -pinene being predominantly from vegetation but
limonene having the potential for significant anthropogenic emissions from volatile chemical products (Coggon et al., 2021)
in addition to biogenic sources. A new representation of API and LIM reaction with OH, NO_3 , and O_3 was created to account



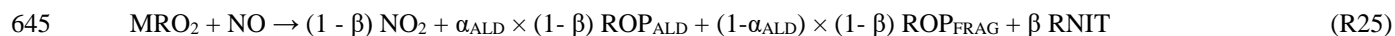
for autoxidation leading to HOM and SOA. In addition, bimolecular peroxy radical reactions leading to dimers of extremely
625 low volatility (CRACMM species ELHOM) with the potential to contribute to new particle formation via nucleation (Bianchi
et al., 2019) were added.

When a monoterpene species, MT, reacts with an oxidant like HO (or NO₃), it directly forms a collection of peroxy radicals
(MRO₂ and MRO₂^A), a fraction of which (α_A) can undergo autoxidation and form HOM:



Autoxidation is implemented as a fixed yield rather than competitive fate since autoxidation in monoterpene + HO systems
proceeds rapidly (rates of 3 to >10 s⁻¹) and only via specific peroxy radical isomers (Piletic and Kleindienst, 2022; Zhao et al.,
2018; Berndt et al., 2016; Xu et al., 2019). This assumption of a fixed yield is valid for bimolecular RO₂ lifetimes (time scale
for RO₂ reaction with NO or HO₂) greater than ~1 second (NO < ~1 ppb) which is consistent with most current conditions near
635 earth's surface except for select urban locations, more often in winter, (Porter et al., 2021) and episodically near sources. The
fraction of prompt API + HO peroxy radicals undergoing autoxidation and forming monoterpene-derived HOM (tracked as
CRACMM species, HOM) (α_A) is set to 2.5% by mole (Berndt et al., 2016; Piletic and Kleindienst, 2022) with the uncertainty
in the yield around a factor of two. Limonene is expected to have rapid H-shift reactions (Møller et al., 2020) and higher
amounts of autoxidation products than α-pinene (Jokinen et al., 2015), and α_A is 5.5% for LIM + HO (Piletic and Kleindienst,
640 2022) (Table S7).

The peroxy radicals from monoterpene (API and LIM) reactions with HO undergo traditional bimolecular RO₂ fates leading
to peroxides, alkoxy radical products, and nitrates:



MRO₂ also reacts with MO₂ and ACO₃ (See Sect. 3.5) (Appendix B). Peroxides from MRO₂ reaction with HO₂ (Reaction
R24) map to a new organic peroxide, OPB, added specifically to represent the C₁₀ hydroperoxides from monoterpene oxidation.
Further reaction or photolysis of OPB is assumed to produce products like existing organic peroxide reactions in RACM2 with
products fed back to the lumped aldehydes (ALD), ketones (KET), and a saturated C₁₀ RO₂ (HC10P). To better conserve
650 carbon and track the identity of monoterpene-derived nitrates CRACMM includes a new C₁₀ organic nitrate, TRPN (Reaction
R25, RNIT product). The OPB peroxides and TRPN nitrates are assumed to remain in the gas phase (see representative
structures in Appendix A).

The yield of organic nitrates (β, R25) is 18% for API (Nozière et al., 1999) and 23% for LIM based on MCM v3.3.1. (Saunders
655 et al., 2003). Further reaction of the terpene nitrates produces LVOCs with a 100% molar yield (Zare et al., 2019; Browne et
al., 2014) with products mapped to then new lumped CRACMM species for monoterpene HOM. While the yield of SOA from



TRPN reaction is 100% by mole, chemical sinks will compete with deposition resulting in less than 100% of TRPN converted to SOA in chemical transport models.

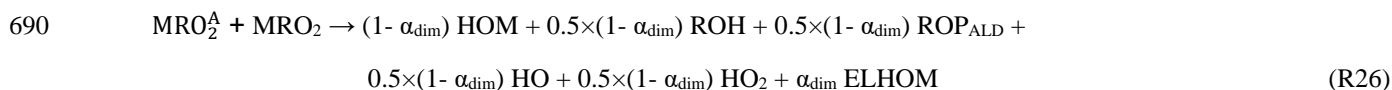
- 660 In addition to terpene nitrates, major organic products from $\text{RO}_2 + \text{NO}$ (Reaction R25) are alkoxy radicals which decompose to either aldehydes and HO_2 (ROP_{ALD}) with a yield of α_{ALD} or other smaller carbon number fragmentation products and HO_2 (ROP_{FRAG}). In the case of LIM ($\alpha_{\text{ALD}} = 64\%$), the alkoxy radical decomposition products are assumed to be smaller fragments (HCHO and UALD), but $\alpha_{\text{ALD}} = 1$ for α -pinene according to MCM. Since the aldehydes from API and LIM could undergo autoxidation as hinted by Rolletter et al. (2020), new aldehydes, PINAL and LIMAL, were added for the monoterpene systems.
- 665 Autoxidation for PINAL and LIMAL is added as competitive fate with plausible autoxidation rate constant for terpene systems ($k = 1 \text{ s}^{-1}$) for OH-initiated peroxy radicals formed at a yield of 23% (PINALP) or 70% (LIMALP) based on MCM v3.3.1. LIMAL and PINAL can also be lost via photolysis, and LIMAL can react with O_3 . In general, rate constants in monoterpene systems (Appendix B) are from RACM2.
- 670 In the case of API and LIM reaction with nitrate radicals, Reactions analogous to R23-R25 generally apply but products are multifunctional and can release NO_2 . Nitrate radical reactions are assumed to behave similarly in terms of autoxidation and use the same α_A as HO reactions which is likely in the case of limonene (Chen et al., 2021a) but an overestimate in the case of α -pinene (Kurtén et al., 2017). For reactions where multifunctional peroxy nitrates (or other multifunctional nitrates) are expected, the nitrate identity is prioritized for tracking and the product mapped to TRPN. Reaction of nitrate-derived MRO_2
- 675 with NO is expected to predominantly release all the nitrate as NO_2 ($\beta = 0$) and convert NO to NO_2 (additional NO_2 product alongside aldehyde production) while yielding a terpene aldehyde (PINAL or LIMAL) ($\alpha_{\text{ALD}} = 1$).

MRO_2^{A} from autoxidation in monoterpene + HO systems is implemented using two new peroxy radicals (labeled APIP2 and LIMP2) that are assumed to result in C_{10}O_7 radicals (Berndt et al., 2016) that can undergo traditional bimolecular fates. For all

680 API and LIM reactions with HO and NO_3 , the $\text{MRO}_2^{\text{A}} + \text{HO}_2$ product is mapped to HOM. In the case of $\text{MRO}_2^{\text{A}} + \text{NO}$, all products that release NO_2 ($1-\beta$) are also assumed to re-release HO via different fragmentation routes and the highly oxidized terpene nitrate as well as other carbon-containing products were mapped to HOM. $\text{MRO}_2^{\text{A}} + \text{MO}_2$ and $\text{MRO}_2^{\text{A}} + \text{ACO}_3$ aldehydes, ketones, and alcohols are also mapped to HOM. As a result, under all conditions, the yield of HOM from initial API or LIM reaction with HO or NO_3 is α_A .

685

The speciation of HOM changes slightly when MRO_2^{A} cross react with other monoterpene or isoprene RO_2 . In addition to the traditional peroxy radical cross reactions with other organic peroxy radicals (MO_2 and ACO_3), the monoterpene-derived peroxy radicals undergoing autoxidation, MRO_2^{A} , react with the most abundant MRO_2 from α -pinene and limonene + HO to produce C_{20} dimers. These reactions followed the basic form:



where α_{dim} is the fraction of MRO_2^A incorporated in dimers and set to 4% based on the work of Zhao et al. (2018). Other products include highly oxygenated monomers (mapped to HOM), aldehydes (mapped to PINAL or LIMAL), and alcohols with branching between those products also as specified by Zhao et al. (2018). In the case of nitrate-initiated MRO_2^A , NO_2 rather than HO is released. The same approach is used for monoterpene MRO_2^A + isoprene RO_2 with HCHO and MVK produced rather than PINAL or LIMAL. Dimer reactions are assumed to proceed quickly, and the rate constant was set to $1 \times 10^{-10} \text{ cm}^3 \text{ molecule}^{-1} \text{ s}^{-1}$ based on the work of Molteni et al. (2019). In both the monoterpene and isoprene cross reactions, the dimer products are predicted to have a $\log_{10}(C_i^*) < -3$ and are mapped to ELHOM.

700 The ozonolysis of monoterpenes in CRACMM also mimics reaction R23 where the oxidant in these reactions is O_3 . Initially, the ozonolysis reaction will break a monoterpene double bond and yield Criegee intermediates that self-react to release hydroxyl radicals and produce peroxy radicals which were classified into the same two types of peroxy radical categories as with HO reactions: either autoxidizable or non-autoxidizable. The yield of peroxy radicals able to undergo autoxidation (MRO_2^A) for ozonolysis is set to 5% and 11% respectively in the API and LIM systems. These yields are doubled compared to
705 HO to fall within the uncertainty of laboratory and computational studies that indicated autoxidation yields from O_3 -initiated reactions are universally higher than autoxidation from OH-initiated chemistry (Jokinen et al., 2015; Ehn et al., 2014; Chen et al., 2021a). The formation of OH, H_2O_2 , CO and aldehyde products from the ozonolysis reactions alongside MRO_2^A were prescribed following MCM and RACM2 and further reaction of the MRO_2 and MRO_2^A peroxy radicals is the same as in the HO system.

710 Predicted SOA in the monoterpene systems comes from HOM and ELHOM products that are either promptly produced or from further reaction of terpene nitrates or terpene aldehydes. The yield of SOA from API reaction with HO or NO_3 is expected to be 2.5% by mole (4.6% by mass) from the initial autoxidation HOM but is further increased to 11% by mole (21% by mass) when the terpene nitrates further react under typical ambient conditions (Table 1). Under high- NO_x conditions ($\text{RO}_2 + \text{NO}$ as the dominant bimolecular fate), the yield of SOA from API + HO approaches 37% by mass with most of the mass from terpene nitrate products highlighting the importance of the terpene nitrate fate which is currently assumed to be reaction with HO and functionalization. LIM SOA yields from HO and NO_3 are similar with values of 16% by mole or 30% by mass for typical conditions but as much as 50% by mass if $\text{RO}_2 + \text{NO}$ dominates and terpene nitrates react further. Yields also increase compared to the typical values if the terpene aldehydes react with HO which is estimated to yield SOA at 21% by mole (31% by mass)
715 or 64% by mole (95% y mass) for PINAL and LIMAL, respectively. Terpene aldehyde photolysis, OPB (and OP3) reaction with OH, or LIMAL reaction with O_3 can also lead to trace amounts of SOA via a $\text{C}_{10} \text{RO}_2$ product (<1% molar yield, chemistry of Sect. 3.1 for HC_{10} peroxy radical).



725 The autoxidation derived HOM yield for α -pinene from CRACMM is similar to the computed yield predicted by Weber et al. (2020) using a more detailed CRI-HOM mechanism that invoked multi-generational peroxy radical chemistry in a global atmospheric chemistry model. Other models have applied numerous autoxidation mechanisms of varying complexity including a steady state HOM yield assumption similar to CRACMM (Gordon et al., 2016), a volatility basis set model (Schervish and Donahue, 2020), and a near explicit autoxidation mechanism involving 1773 reactions (Roldin et al., 2019). While the fixed HOM yields implemented in CRACMM consolidate the mechanism, additional species and reactions are considered here
730 including NO_3 oxidation chemistry, the chemistry of reactive monoterpenes like limonene, and many accretion reactions that may produce ELHOM. Further refinements to the autoxidation mechanism will be considered in future CRACMM versions including an implementation of the temperature dependence of H-shift reactions, potentially revised volatilities for HOM and ELHOM, and fragmentation reactions of highly oxidized peroxy radicals that may limit HOM production.

735 The CRACMM approach to monoterpene organic nitrates differs from previous CMAQ approaches where organic nitrates were incorporated into the particle via heterogenous uptake driven by hydrolysis reactions (Pye et al., 2015; Zare et al., 2019). CRACMM indicates a potentially significant role for TRPN in forming SOA but via a different mechanism than previous work which assumed a 3-hour lifetime against condensed phase hydrolysis (k_{HET} (defined in footnote of Appendix B) of $1.13 \times 10^{-7} \text{ s}^{-1}$). TRPN could also release NO_x upon chemical reaction (Saunders et al., 2003) and fragment into smaller molecules (Weber
740 et al., 2020) which are not considered here. Future versions of CRACMM should incorporate monoterpene nitrate hydrolysis and release NO_x upon reaction where appropriate.

Note that the identity of terpene nitrates when they are lumped into HOM or ELHOM is not retained. Lower volatility nitrates, peroxides, ketones, and alcohols from terpene oxidation are lumped together based on volatility with HOM having an effective
745 $\log_{10}(C_i^*)$ of 0 to -3 and a representative structure with $\log_{10}(C_i^*)$ of -2.2. ELHOM are nominally highly oxygenated C_{20} dimers with an effective $\log_{10}(C_i^*)$ of -5 but species with C_{15} structures are also mapped to ELHOM based on their volatility (estimated as $\log_{10}(C_i^*) < -3$). Given the importance of volatility as a driver of new particle formation events (McFiggans et al., 2019), the resolution in volatility for highly oxidized products should be investigated in future work in the context of predicting new particle formation events.

750 3.8 Isoprene and aqueous aerosol pathways

The treatment of isoprene chemistry in CRACMM version 1.0 is the same as in RACM2-AERO6 as implemented in CMAQ v5.3.3. Notably, the CMAQ implementation includes formation of isoprene epoxydiols (IEPOX) as a tracer. An investigation of isoprene chemistry in CRACMM using the Automated Model Reduction (AMORE) condensation of a detailed isoprene mechanism (Wennberg et al., 2018) with isoprene nitrate hydrolysis (Vasquez et al., 2020), is available in the work of Wiser
755 et al. (in prep.) and as CRACMM1AMORE in CMAQv5.4.



Precursors to SOA from aqueous reactions include IEPOX, glyoxal (GLY), and methylglyoxal (MGLY) and follow CMAQ AERO7. GLY is a lumped species and emissions include glycolaldehyde (total U.S. 2017 GLY emissions: 418 Gg yr⁻¹). MGLY is also lumped and includes 2-oxobutanal and other carbonyl aldehydes (total U.S. 2017 MGLY emissions: 1129 Gg yr⁻¹) (cite). SOA from IEPOX uptake follows the reactive uptake formulation of Pye et al. (2013) with the Henry's law coefficient for IEPOX ($3.0 \times 10^7 \text{ M atm}^{-1}$) and organosulfate condensed-phase formation rate constant ($8.83 \times 10^{-3} \text{ M}^{-2} \text{ s}^{-1}$) from the work of Pye et al. (2017). New in CRACMM compared to standard AERO7 in CMAQ are separate species for the organosulfate (AISO3OS) vs. non-sulfated (2-methyltetrol, AISO3NOS) IEPOX-derived SOA to facilitate tracking of sulfur. Reactive uptake of GLY and MGLY on aqueous particles uses a fixed uptake coefficient (2.9×10^{-3}) (Liggio et al., 2005) as in CMAQ version 5.2-5.3.3 (Pye et al., 2015). Cloud-processed SOA from GLY and MGLY is based on the reaction with aqueous HO and the work of Carlton et al. (Carlton et al., 2008). Glyoxal SOA may include formation of salt-like structures in the aerosol phase, but for simplicity, the oligomeric structure of Loeffler et al. (2006) is used as the representative structure of all glyoxal and methylglyoxal SOA. Note that the molecular weight of GLY and MGLY SOA specified in CRACMM differs from the representative structure. Aqueous reaction products leading to SOA in CRACMM, as implemented in CMAQ, are not currently allowed to volatilize to the gas phase which likely occurs for a subset of IEPOX products (Riedel et al., 2015; D'ambro et al., 2019).

3.9 Acrolein and 1,3-butadiene

Acrolein (ACRO) is a major oxidation product of 1,3-butadiene (BDE13) and both species were added explicitly in CRACMM due to their importance for health (Scheffe et al., 2016) (see Sect. 4). For BDE13 reaction with OH, which is likely its dominant removal pathway (Agency for Toxic Substances and Disease Registry, 2012; Tuazon et al., 1999), the SAPRC18 Mechgen utility (Carter, 2020b) was used to generate products that are mapped to the analogous CRACMM species. SAPRC18 Mechgen is convenient since the products are already aggregated to a similar degree as RACM2 and CRACMM. A peroxy radical specific to BDE13 reaction with HO (BDE13P) is used so that formation of acrolein (from all channels except BDE13P+HO₂) could be explicitly predicted. For BDE13 + O₃, a Criegee biradical is predicted to be a significant product in SAPRC18 and MCMv3.3.1. Criegee biradicals are not implemented in CRACMM due to their short lifetime, so MCMv3.3.1 was used to determine the likely products from Criegee decomposition. For simplicity, BDE13 reaction with nitrate follows the diene + NO₃ products from RACM2 with acrolein instead of MACR specified as the product. Products from reaction of ACRO with HO and NO₃ are taken from RACM2's lumped MACR species. In the case of ACRO ozonolysis, prompt products as well as the expected Criegee biradical products are from MCM. ACRO photolysis products are from SPARC18 Mechgen.

3.10 Additional rate constant updates

The inorganic chemistry of RACM2 is retained in CRACMM with updated rate constants for some reactions. In CRACMM, rate expressions for 26 inorganic reactions and 2 organic reactions (carbon monoxide and methane with OH, ethane was also



updated as mentioned in Sect. 3.1) were updated compared to RACM2 values (IUPAC, 2010; Sander et al., 2011; Goliff et al., 2013) to follow the NASA/JPL evaluation number 19 (Burkholder et al., 2019) and IUPAC recommendations (Atkinson et al., 2004). Photolysis rate coefficients were updated for 5 chemical species: C3 and higher aldehydes (ALD), acetone (ACT), methyl ethyl ketone (MEK), higher ketones (KET), and formaldehyde (HCHO). The photolysis rate coefficient for ALD is set to that of propionaldehyde from the NASA/JPL evaluation number 19 (Burkholder et al., 2019). CRACMM adds the acetone photolysis pathway producing methyl peroxy radical and carbon monoxide in addition to the existing RACM2 pathway that produces methyl peroxy and acetyl peroxy radicals. Quantum yields of ACT are updated following the NASA/JPL evaluation number 19 (Burkholder et al., 2019). In addition, the temperature and pressure effects on ACT photolysis rate coefficients now follow Blitz et al. (2004). Photolysis rate coefficients and products of MEK and KET use quantum yield from Raber and Moortgat (1996) and absorption cross sections from Brewer et al. (2019). The photolysis pathway for formaldehyde in RACM2 contained an error in quantum yield data resulting in overestimated photolysis rate coefficients, which are now corrected in CRACMM using data from the NASA/JPL evaluation number 19. These general kinetic updates are expected to lead to minor decreases in O₃ formation compared to RACM2-AERO6.

4 ROC Hazardous Air Pollutants

Hazardous air pollutants are known or suspected to cause serious adverse health or environmental effects and are therefore a priority to represent in chemical mechanisms. However, the number of HAPs routinely considered should be moderated for computational efficiency. While 189 substances are designated as HAPs by the U.S. EPA, HAP species such as polycyclic organic matter (POM) and glycol ethers contain many individual compounds such that the actual number of individual species meeting the definition of a HAP is well over 3,000 (U.S. Environmental Protection Agency, 2022d). The SPECIATE database, which includes a HAP identifier, was used as the initial source of identification for the species-level emission inventory and supplemented with additional data sources. POM was identified based on species with more than 1 benzene ring and $n_o:n_c = 0$ in their representative structure (an additional 56 species to the HAP category in SPECIATE). The POM requirement of a boiling point above 100° C was found to be duplicative with the aromaticity criteria based on the work of Achten and Andersson (2015). The identifier of 1-bromopropane, a newly designated HAP (U.S. Environmental Protection Agency, 2022c), was updated. SPECIATE was also cross referenced with individual glycol ethers (U.S. Environmental Protection Agency, 2022d) (4 additional HAPs). CAS numbers of individual species and their representative structures were cross-referenced with the toxicity value file input to the Human Exposure Model (U.S. Environmental Protection Agency, 2021a) identifying an additional 39 HAPs. Overall, 491 HAPs were identified in SPECIATE of which 188 had nonzero ROC emissions in the 2017 inventory used here.

To assess the coverage of HAPs and their risk in CRACMM, toxicity risk potentials were estimated using chronic inhalation metrics from the U.S. Environmental Protection Agency (2021b). EPA's process for estimating a cancer risk is based on the



820 unit risk estimate (URE) which is the estimated number of excess tumors per person due to inhalation of $1 \mu\text{g m}^{-3}$ of the
pollutant over a lifetime. Non-cancer (mutagenicity, developmental toxicity, neurotoxicity, and/or reproductive toxicity) risk
uses a reference concentration (RfC) which is an estimate of the concentration that could be inhaled over a lifetime without an
appreciable risk. Species in SPECIATE were matched to the inhalation RfC and URE values (U.S. Environmental Protection
Agency, 2021a) by CAS number. A few SPECIATE species (2,4-toluene diisocyanate, an m & p-xylene mixture, an m & p-
825 cresol mixture, and a chrysene mixture) were manually mapped to relevant exposure risk values. In cases where a species in
SPECIATE did not have a CAS or unique structure, a representative structure was used for mapping. A relative non-cancer
toxicity potential was estimated based on the emitted mass of a species divided by the RfC, and a relative cancer toxicity
potential was estimated as the product of the emissions and URE (Simon et al., 2010). For species designated as HAPs but not
included in the toxicity value table (U.S. Environmental Protection Agency, 2021a), a RfC of 20 mg m^{-3} and URE of 1×10^{-8}
830 $\mu\text{g}^{-1} \text{ m}^3$, corresponding to the maximum RfC and minimum URE values for known HAPs, were used to provide what is
potentially a conservative underestimate of risk.

Nine species in CRACMM cover 50% of the total cancer and 60% of the total noncancer health risk estimated for the
anthropogenic and biomass burning emissions for 2017 U.S. conditions (Fig. 6a: ACD, ETEG, ACRO, TOL, NAPH, MOH,
835 HCHO, BDE13, and BEN). Toluene (chemistry in Sect. 3.5) is now separated from other aromatics and explicit due to its role
as a HAP and significant emissions on an individual basis (430 Gg yr^{-1} in 2017, Fig. 6b) as well as to facilitate comparison
with routine measurements. Ethylene glycol, toluene, and methanol are, however, not particularly strong drivers of cancer and
noncancer inhalation risk (Fig. 6b). NAPH (chemistry in Sect. 3.5), ACRO (chemistry in Sect. 3.9), and BDE13 (chemistry in
Sect.3.9) are new mechanism species and are estimated to carry significant risk (Scheffe et al., 2016) (Fig. 6b). NAPH
840 emissions are dominated by naphthalene (74%) but include POM as well, making it an aggregate of HAPs. Naphthalene alone
accounts for 70% of the cancer and 98% of the non-cancer risk of NAPH. In the case of ACRO, significant secondary
production (not shown in Fig. 6b) is expected, and acrolein has been previously shown to be the largest contributor to noncancer
inhalation risk in the U.S. (Scheffe et al., 2016). Given acetaldehyde and formaldehyde are also produced by oxidation of
biogenic and anthropogenic emissions, the actual coverage of risk by the 9 major HAP species is likely much higher than
845 estimated based on the emissions alone. Previous work including secondary production estimated that acetaldehyde, benzene,
formaldehyde, methanol, acrolein, 1,3-butadiene, and naphthalene represented over 84% of the cancer risk and 93% of the
non-cancer respiratory risk effects in the U.S. in 2011 (Scheffe et al., 2016).

The lumped, slowly reacting ROC (SLOWROC, Sect. 3.1) is 61% HAP by mass with enough inhalation risk to make it the
850 second leading contributor to cancer and noncancer health risk out of all CRACMM species (Fig. 6b). Species within
SLOWROC have a lifetime against chemical reaction of about 1 month and are typically discarded from chemical transport
model calculations for that reason. SLOWROC includes ethylene oxide and 1,2-dibromoethane, among many other species,
that individually contribute to high levels of cancer risk (2^{nd} and 10^{th} highest out of all 188 individual HAPs in this work).



Hydrogen cyanide is the most abundant individual species in SLOWROC and is the second largest contributor to noncancer
855 health risk for all HAPs considered. In standard CRACMM applications, SLOWROC concentrations could be used to indicate
areas warranting additional investigation, but individual compound tracers would be required for studies specifically
addressing the health impacts of these longer-lived pollutants. In CMAQv5.4, additional individual HAPs needed for air toxic
assessments (e.g., Scheffe et al., 2016), can be added to a chemical mechanism as tracers with reactive decay.

860 In total, twenty-nine ROC species in CRACMM contain some amount of HAP emissions (Fig. 6a). In terms of species with
significant HAP emissions by mass, the two lumped, single-ring aromatic hydrocarbon categories (XYE and XYM) are 61 and
67% HAP by mass with ethylbenzene (in XYE) and indene (in XYM) being the largest contributors to cancer risk and m-
xylene (in XYM) and o-xylene (in XYE) being the largest contributors to noncancer health risk. The gas-phase chemistry of
XYE is based on ethylbenzene (Sect. 3.5), so XYE could become an explicit HAP in CRACMM with changes only to emission
865 mapping (redirecting single-ring species in XYE other than ethylbenzene to XYM). The two aromatic IVOCs are about 10%
HAP by emitted mass with 2,4-toluene diisocyanate (ROCP5ARO) and aniline (ROCP6ARO) being the largest HAP
contributors by mass as well as in terms of noncancer health risk (#5 and #10 out of 188 species). ALD (35% HAP) includes
the HAP propionaldehyde. OLT (5% HAP by mass) includes acrylonitrile resulting in moderate cancer and noncancer health
risk. Despite the low contributions by mass of HAPs to FURAN, FURAN shows moderate contributions to cancer risk due to
870 the inclusion of chloroprene.

HAPs added in CRACMM provide greater explicit coverage of species contributing to chronic inhalation health risks, and
many of the species classified as HAPs also contribute substantially to criteria pollutant formation. In total, HAPs are estimated
to account for about 8% of the total OA formation potential for 2017 U.S. anthropogenic and biomass burning emissions (using
875 SAR methods from Sect. 2.1). HAPs, with major contributors being formaldehyde, toluene, acetaldehyde, m-xylene, 1,3-
butadiene, ethylbenzene, o-xylene, acrolein, ethylene glycol, and phenol, are predicted to contribute 31% of the O₃ formation
potential for 2017 U.S. anthropogenic and biomass burning emissions. Based on their potential for cancer risk (C), noncancer
health risk (N), and O₃ formation potential (O), priority HAPs to consider for purposes of protecting public health are:
formaldehyde (CNO), ethylene oxide (C), naphthalene (C), 1,3-butadiene (CN), benzene (C), acrolein (N), hydrogen cyanide
880 (N), toluene 2,4-diisocyanate (N), acetaldehyde (O), toluene (O), m-xylene (O), and methanol (O).

5 Implications for the Chemical Evolution of ROC

In this section, CRACMM ROC species are visualized in terms of the carbon oxidation state and degree of oxygenation to
understand if there are critical gaps in the atmospheric representation of ROC. The mean carbon oxidation state (OS_C) of a
species increases upon oxidation and compounds generally move towards lower n_C and higher OS_C as they are chemically
885 processed in the atmosphere (Kroll et al., 2011). This view emphasizes SOA as a chemical intermediate on the path toward



smaller and more functionalized compounds with carbon dioxide ($OS_C = 4$) as the ultimate endpoint. Using the CRACMM representative structures (Appendix A), each stable ROC species was plotted in the OS_C vs n_C space (Fig. 7) using the OS_C definition of Kroll et al. (2011) considering the number of carbon, hydrogen (n_H), and oxygen (n_O) per molecule and expanded to include nitrogen (n_N) and sulfur (n_S) (assuming sulfate and nitrate functionality) as follows:

$$890 \quad OS_C = 2 \times n_O : n_C - n_H : n_C - 5 \times n_N : n_C - 6 \times n_S : n_C \quad (1).$$

CRACMM species cover the atmospherically relevant range of ROC oxidation state and n_C (Fig. 7). The largest n_C species in CRACMM are alkane-like with 20 to 30 carbons and a low oxidation state consistent with observations of particulate vehicle exhaust and ambient hydrocarbon-like organic aerosol (Kroll et al., 2011). Other OA species in CRACMM generally fall in
895 the range of n_C and OS_C reported for ambient observations of biomass burning organic aerosol, fresh ambient (less oxygenated) SOA, and aged (more oxygenated) ambient SOA. These ambient observations are based on bulk analysis (Kroll et al., 2011), and thus the observed ranges shown do not identify each possible SOA contributor at the molecular level. Monoterpene SOA, specifically C_{10} HOM monomers and C_{20} HOM dimers, have an oxidation state of -0.4 and -0.9, respectively, similar to laboratory data (Kroll et al., 2011). Monoterpene SOA has also been linked with the less oxidized (fresh ambient SOA) aerosol
900 mass spectrometer (AMS) surrogate (Xu et al., 2018).

Two species in CRACMM, the glyoxal and methylglyoxal SOA from uptake in aqueous particles (AGLYJ) and clouds (AORGC), have overlap with the observed ambient aged SOA which is often identified via positive matrix factorization analysis as a more oxidized oxygenated organic aerosol (MO-OOA) (Zhang et al., 2011). The MO-OOA factor has been linked
905 to SOA from aqueous processing (Xu et al., 2017), and 10% by mass of the MO-OOA in the southeast U.S. has been attributed to low molecular weight carboxylic acids, of which dicarboxylic acids are primarily from aqueous processing (Chen et al., 2021b). Aqueous isoprene SOA species such as isoprene-derived organosulfates and 2-methyltetrols ($n_C = 5$) match properties of known major isoprene SOA constituents (Kroll et al., 2011; Surratt et al., 2010), and aqueous isoprene SOA (not shown in Fig. 7) is often resolved separately from MO-OOA. If the aged SOA region described by MO-OOA does represent an
910 intermediate through which significant amounts of carbon should pass, additional chemical pathways beyond those from glyoxal and methylglyoxal may be needed.

Other mechanisms besides CRACMM (top of Fig. 7) focus on the more volatile range of ROC. MCM and SAPRC18 include a sesquiterpene species with 15 carbons, but otherwise focus on smaller carbon number species. The range in n_C for alkane-
915 like species in current mechanisms was highlighted in Section 3.1 and never exceeds 12. In terms of aromatics, the largest aromatic in MCM is a C_{11} diethyltoluene. SAPRC18 includes some naphthalene-like species with 12 carbons, and RACM2 represents single ring aromatics with ~9 carbon (Fig. 1, XYM). CB6 has a xylene species with 8 carbons, and RACM2 and CB6 both include monoterpenes as their largest species by n_C . CRACMM S/IVOCs with alkane, aromatic, and oxygenated



structures populate the higher carbon number ($n_C > 10$) space that includes known organic aerosol species as well as precursors
920 with high SOA yields and is not covered by current mechanisms due to their focus on gas-phase endpoints.

As a complement to OS_C , van Krevelen diagrams of $n_H:n_C$ versus $n_O:n_C$ for individual and bulk species have been used to
provide insight into the evolution of ambient organic aerosol (Heald et al., 2010). Since hydrogen and oxygen are generally
the most abundant non-carbon elements in organic aerosol, these diagrams can help identify types of chemical
925 functionalization. Primary emissions, particularly for alkane-like sources like vehicles tend to reside near an $n_H:n_C$ of two and
 $n_O:n_C$ of zero. Atmospheric processing generally moves OA towards higher $n_O:n_C$ and lower $n_H:n_C$ with the trajectory
determined by the abundance of alcohol and peroxide (slope of zero) vs ketone and aldehyde (slope of -2) groups (Heald et
al., 2010). Mean atmospheric transformation of OA has been observed to occur along a slope of -0.5 (Ng et al., 2011) to -0.6
(Chen et al., 2015) which reflects either carboxylic acids or a combination of alcohols, peroxides, ketones, and aldehydes.
930 Figure 8 (black line) shows the observed trend and range in $n_O:n_C$ from the ambient atmosphere from multiple field campaigns
extended to $n_O:n_C$ of zero for primary source measurements.

The 26 individual particulate organic species in CRACMM span the full range of observed $n_O:n_C$ in bulk OA with excellent
coverage for $n_O:n_C < 0.5$ (Fig. 8). The highest observed $n_O:n_C$ conditions (~ 1.2) were only present in remote regions sampled
935 by aircraft as described in the work by Chen et al. (2015). While CRACMM includes species with high $n_O:n_C$, those species
(glyoxal SOA, isoprene organosulfate SOA, and non-sulfated isoprene SOA) tend to have much higher $n_H:n_C$ than the ambient
trend suggests. Note that $n_O:n_C$ based on measurement techniques may not include all the oxygen in organosulfate compounds
and oxidation state is likely a more robust way to measure degree of oxidation than $n_O:n_C$ based on techniques like an AMS
(Canagaratna et al., 2015). Particularly for the $n_O:n_C > 0.5$ OA species, CRACMM indicates more hydrogen than ambient
940 observations suggest. If the ambient observations are correct, future versions of CRACMM could resolve the overestimate in
 $n_H:n_C$ by: (1) shifting the representative compound structures (for species like ROCN2OXY8) to reflect more ketones, (2)
adjusting the assumed change in volatility per oxygen in the secondary oxygenated chemistry (Sect. 3.2), and/or (3) adding
more chemical channels resulting in condensible ketones, carboxylic acids, or other high $n_O:n_C$, low $n_H:n_C$ products (e.g.,
photolysis of SOA, Baboomian et al. (2020)). Chen et al. (2015) noted that SOA produced in laboratory experiments was
945 generally too low in $n_H:n_C$ at a given $n_O:n_C$ and tended to reside below the black ambient line in Fig. 8. Combined with the
information from the oxidation state plot (Fig. 7), CRACMM may need SOA species that are both lower in H and higher in O
and at smaller carbon numbers with implications for aerosol hygroscopicity and mass (Pye et al., 2017). CRACMM species,
informed by known gas-phase chemistry and 2-D VBS approaches, being above the ambient trendline suggests that our
conceptual picture of atmospheric processing to SOA does not match what is observed in laboratory experiments. One possible
950 reason is the preferential sampling of certain chemical space in laboratory experiments (Porter et al., 2021).



Figures 7 and 8 suggest that chemistry leading to OA needs to be considered in mechanism development to obtain an accurate representation of gas and particulate ROC including the correct properties of OA. Accurate properties of OA are critical for estimating hygroscopicity with implications for climate (Haywood and Boucher, 2000) as well as fine particle mass (Pye et al., 2017). The linkages between gas and particulate endpoints are further emphasized by examining emissions from anthropogenic and biomass burning sources of ROC by volatility class and their propagation to endpoints (Fig. 9). Total emissions of ROC in 2017 (excluding biogenic VOCs) are estimated at 21 Tg yr⁻¹ with VOCs as the most abundantly emitted volatility class of compounds. VOCs dominate ROC HO reactivity accounting for 81% of the total. In addition, the total U.S. O₃ formation potential is estimated as 47 Tg yr⁻¹ with VOCs accounting for 90% of it (based on the MIR SAR, Fig. 9). Thus, across all anthropogenic and biomass burning sources and locations for 2017, VOCs are the dominant contributors to gas-phase endpoints such as HO reactivity and O₃; however, emitted IVOCs (generally excluded from mechanism development) make appreciable contributions to estimated gas-phase endpoints (18% of HO reactivity and 10% of the O₃ formation potential). As a class, the O₃ from IVOCs (about 4.5 Tg yr⁻¹) exceeds the O₃ estimated for any individual CRACMM species in Figure 1. In terms of effective MIR, IVOCs (effective MIR of 1.1 g O₃ g⁻¹ ROC) are comparable to HC10 and exceed that of BEN, HC3, and ETH. L/SVOCs are not substantial contributors to HO reactivity or O₃ formation (~1%) due to slower reaction rates (k_{OH}, Fig. 3) and alkane-like structures with less potential for O₃ formation (effective MIR 0.14 to 0.27 g O₃ g⁻¹ ROC). The OA potential from ROC emissions in the U.S. (excluding biogenic emissions) is estimated as 5 Tg yr⁻¹ and emphasizes the need to consider L/S/IVOCs. Traditional VOCs (effective SOA yield of 5%), are important (14% of total) contributors to OA potential, but OA potential is dominated by IVOCs (38%) and S/IVOCs (48%) due to their initially lower volatility and ability to become condensible with only small additions in functionality.

6 Discussion

CRACMM provides an integrated approach to the representation of O₃, organic aerosol, and many HAPs in air. These endpoints are linked as O₃, SOA, and secondary HAPs such as formaldehyde and acrolein are products of gas-phase precursor emissions including primary HAPs. This section highlights reasons why mechanism development remains important and provides specific recommendations for future work based on lessons from CRACMM development.

First, the magnitude and compound identity of ROC emissions is an active area of research and mechanisms need to interface with this emerging information. Improving emissions characterization without the accompanying mechanism linkages hinders accurate source apportionment and effective air quality management decisions. Much of the work on emissions speciation is identifying new species in the IVOC range which has been historically neglected by gas-phase mechanisms but is necessary for both O₃ and SOA prediction. Emissions speciation work should continue to characterize source profiles in databases and other forums at the highest level of individual compound detail available using representative structures when necessary so compounds can be easily mapped to mechanisms. In addition, efforts to accurately determine the emissions of individual



985 HAPs, especially formaldehyde, acetaldehyde, toluene, m-xylene, and methanol which are important for O₃, should be leveraged in the preparation of emission inputs for regional chemical transport models even when HAPs are not the primary objective. Development of emissions and mechanisms should continue to be an iterative process in which new measurement techniques better quantify and identify emissions resulting in new or refined mechanism species. Simultaneously, mechanisms can indicate which emitted species are high priority to constrain due to their role in secondary pollutant formation or health impacts.

990

Second, current chemical transport model mechanisms do not characterize the full range of atmospheric ROC and such analysis could help identify missing sources of SOA, HO reactivity, formaldehyde, and other secondary HAPs. The ability to account for all reactive tropospheric carbon and perform a ROC budget analysis in current mechanisms is limited due to the focus on the more volatile range of ROC which excludes lower volatility primary ROC. In addition, some carbon in secondary ROC, including species in the volatile range, is discarded in mechanisms like SAPRC07 and RACM2 because of product lumping for computational efficiency. For example, the largest organic peroxide in RACM2 is OP2 with two carbons. So, peroxides formed from RO₂+HO₂ reactions for xylene-like aromatics ($n_C = 9$) result in a loss of seven carbon per reaction. In the RACM2 monoterpene system, eight carbons or 80% of the parent carbon is lost each time a peroxide is formed; and SAPRC07 loses 4 carbon for each monoterpene peroxide formed. While conservation of emitted mass was a priority for the design of CRACMM and more secondary mechanism species were added at the higher carbon numbers (e.g., a C₈ and C₁₀ peroxide), the chemical scheme in CRACMM is like RACM2 and SAPRC07 in that it does not conserve mass upon reaction for all chemical systems. However, by curating structural identifiers (SMILES) for all species in CRACMM, conservation of carbon can now be calculated and the importance of lost (or gained) carbon can be examined. The CMAQv5.4 implementation of CRACMM includes an updated chemical mechanism processor that creates an optional diagnostic file containing the elemental balance for each CRACMM reaction. Future work will aim to calculate mass balance across the mechanism and use it as a diagnostic tool to guide development.

1000
995
1005

Third, current gas-phase mechanisms do not couple radical chemistry with SOA formation and linking the development provides additional constraints for ozone-forming reactions as well as secondary inorganic aerosol production. Particles and ozone are inherently linked systems (Ivatt et al., 2022; Womack et al., 2019). Molar yields for SOA are often comparable to molar yields of existing gas-phase product channels, and SOA mass should be removed from volatile gas-phase products. Properly sequestering products like peroxides in the particle will remove them as a potential photolytic source of radicals that release HO_x back to the atmosphere. Similarly, sequestering one organic nitrate in the particle-phase could remove one HO_x and one NO from the gas-phase system. Autoxidation, implemented in CRACMM primarily to produce SOA, effectively sequesters radicals since they are generally of sufficiently low volatility to condense. CRACMMv1.0 targeted SOA systems for development, but CRACMM updates impact O₃ as will be demonstrated for the Northeast U.S. in future companion work.

1010
1015



Future versions of CRACMM should continue to consider chemical channels that lead to both gas-phase and particulate products to better constrain O_3 .

1020 Fourth, linking gas-phase chemistry with SOA formation for the first time enabled the treatment of new SOA precursors with implications for the magnitude and source attribution of OA. Organic aerosol is dynamic with properties that evolve as a function of precursor and chemical regime and thus need to be considered as part of a holistic treatment of atmospheric chemistry. The interconnected nature of aromatic, phenolic, and furan systems highlights why mechanism development should consider SOA production alongside gas-phase chemistry. Developing phenolic and furanone gas-phase chemistry without
1025 consideration of SOA (as in CMAQv5.3.3) neglects a significant SOA source. Specifying SOA yields for phenolic and aromatic hydrocarbon precursors without recognizing they are also secondary would duplicate SOA mass. As a result, both phenolic and non-phenolic routes to SOA need to be specified consistently. The attribution of aromatic SOA to these two routes will affect how much SOA is predicted overall and how it is attributed to various sources. In the case of benzene SOA, the more SOA comes from phenol vs non-phenol channels, the higher the total SOA potential of U.S. emissions (as phenol >
1030 benzene emissions) and larger attribution to sources with high phenol to benzene ratios such as wildland fires and residential wood combustion. Previous work estimated oxidation of phenol, naphthalene, and benzene alone can account for 80% of the SOA from residential wood combustion (Bruns et al., 2016). The importance of connecting SOA with multigenerational gas-phase chemistry also applies to the monoterpene system where the fate of terpene nitrates and aldehydes will significantly modulate SOA formation. In the case of monoterpene SOA, the allocation of SOA between initial autoxidation, terpene nitrate,
1035 and aldehyde channels will affect the NO_x dependence of total monoterpene SOA and therefore how much is considered controllable vs. noncontrollable. The allocation of SOA among different later generation species should continue to be evaluated and revised as new information becomes available which will improve source apportionment of fine particle mass.

Fifth, new measurement techniques, observational studies, and computational methods are continually improving the
1040 characterization of many chemical systems, and their results need to be translated to model mechanisms. Autoxidation, a novel, atmospherically relevant chemical pathway discovered just under a decade ago (Crouse et al., 2013), will be considered in CMAQ for the first time in CRACMMv1.0. Just this year, a new class of atmospherically relevant compounds, hydrotrioxides were identified (Berndt et al., 2022). Even for traditional systems, information continues to emerge. For example, benzene mechanisms have been historically built on data that characterized about half of the product mass with recent work used to
1045 inform CRACMMv1.0 reaching ~80% carbon closure (Xu et al., 2020). Measurement techniques and the availability of observational data will only further improve, providing more complete data to design and evaluate mechanisms going forward.

Finally, the chemistry of the atmosphere in the U.S. and elsewhere is changing, and previously acceptable representations of chemistry may need modification. Autoxidation is one example of a pathway likely to grow in importance, but indications of
1050 change can be seen in multiple systems. Deposition of nitrogen has shifted from primarily oxidized nitrogen (nitrate) to reduced



nitrogen (ammonia) (Li et al., 2016). Fine particle mass is no longer dominated by summertime sulfate (Chan et al., 2018), and the temperature dependence of summertime urban Northeast U.S. $PM_{2.5}$ is now being modulated by organic aerosol (Vannucci and Cohen, 2022). Particulate sulfur is also becoming increasingly recognized as organic (Riva et al., 2019; Moch et al., 2018). At the same time sulfate and nitrate in cloud water have been decreasing at a mountaintop site in the Northeast U.S., total organic carbon in cloud water may be increasing (Lawrence et al., 2022). Organic compounds in air are changing with total U.S. emissions of anthropogenic ROC going from ~30% lower than NO_x in 2002 to exceeding NO_x by ~40% in 2019 (Pye et al., 2022). The composition of ROC is also changing to more oxygenated forms resulting in an average reduction in the O_3 formation potential of an individual VOC of about 20% due to mixture effects (Venecek et al., 2018). Questions chemical transport modeling and mechanisms are being asked to answer are also changing with increasing interest in wildland fires (McClure and Jaffe, 2018), volatile chemical products (Seltzer et al., 2022), and per- and poly-fluoroalkyl substances (D'ambro et al., 2021) among them. Changes in air pollution sources and questions of interest as well as chemical regimes over time require continued mechanism development, and CRACMM is now available as a community framework for further development.

Code and data availability

EPA's CompTox Chemicals Dashboard is available at: <https://comptox.epa.gov/dashboard> (U.S. Environmental Protection Agency, 2021c). OPERA predictions of species properties can be obtained from the Chemicals Dashboard or for any species with a SMILES using the EPA's Chemical Transformation Simulator at <https://qed.epa.gov/cts/> (U.S. Environmental Protection Agency, 2022b). SPECIATE is distributed at <https://www.epa.gov/air-emissions-modeling/speciate>. RDKit version 2020.09.01 was used in python (RDKit, 2020). The implementation of RACM2-AERO6 is available in CMAQ v5.3.3 (U.S. Environmental Protection Agency Office of Research and Development, 2019). RACM2 and CRACMMv1 in CMAQ v5.4 will be available on github (<https://github.com/USEPA/CMAQ>) and zenodo. Supporting data for CRACMM, including the SPECIATE database mapped to CRACMM, input to the Speciation Tool, profile files output from Speciation Tool for input to SMOKE, python code for mapping species to CRACMM, chemical mechanism, and mechanism metadata is available at <https://github.com/USEPA/CRACMM>. Specific analyses and scripts used in this manuscript such as the 2017 U.S. species-level inventory and code for figures are archived on data.gov and will be available at <https://doi.org/10.23719/1527956>.

Author contributions

HOTP designed the overall scope and drafted the initial document with input from coauthors. Main text figures were prepared by BNM (Fig. 4) and HOTP (all others). HOTP, BNM, and KMS prepared supplement figures. Chemistry of various ROC systems was designed by HOTP (aromatics, sesquiterpenes, primary oxygenated IVOCs, and other miscellaneous SOA systems), BKP (monoterpenes), BNM (secondary oxygenated ROC), KMS (S/IVOC alkanes), ELD (1,3 butadiene and



acrolein), IRP (monoterpenes), RHS (S/IVOC alkanes, furans), MMC (furans, propylene glycol), and LX (aromatics). HOTP, BKP, BNM, KMS, ELD, SF, GS, BH, and JB coded the CMAQ implementation of CRACMM. HOTP, KMS, ELD, IRP, and SF determined representative compound structures for SPECIATE. HOTP, KMS, CA, KMF, and GP developed the 2017 emissions inventory and resulting SOA and ozone analysis. ES, GS, BH, and WRS updated rate constants and photolysis reactions in reactions ported from RACM2. HOTP performed the HAP analysis. All coauthors contributed to developing the mechanism and editing the manuscript.

Competing interests

The authors declare that they have no conflict of interest.

Disclaimer

The views expressed in this article are those of the authors and do not necessarily represent the views or policies of the U.S. Environmental Protection Agency, Department of Energy (DOE), or Oak Ridge Institute of Science and Education (ORISE).

Acknowledgements

This work was supported by the U.S. Environmental Protection Agency Office of Research and Development. This research was supported in part by an appointment to the U.S. Environmental Protection Agency (EPA) Research Participation Program administered by the ORISE through an interagency agreement between the U.S. DOE and the U.S. Environmental Protection Agency. ORISE is managed by ORAU under DOE contract number DE-SC0014664. We thank internal reviewers at EPA for providing comments on a draft of this manuscript. We thank Kelley Barsanti for useful discussion about emissions and mechanism development and Chris Nolte for perspectives on model development. We thank Rohit Mathur and Sergey Napelenok for comments on a draft version of the manuscript. MMC, RHS, and LX acknowledge support through the EPA-STAR program, Grant # 84001001 and the CIRES cooperative agreement NA17OAR4320101. LX also acknowledges NASA grant 80NSSC21K1704.



Tables

1105 **Table 1: Pathways to SOA in CRACMM by system. Some systems include a representation of autoxidation (Auto? = Yes). Actual**
SOA formation in CRACMM is modulated by oxidant concentration (OH, NO₃, O₃), RO₂ bimolecular fate (NO/HO₂), bimolecular
RO₂ lifetime (τ_{RO2}), abundance of the partitioning medium (OA), photolysis (hv), and/or aqueous environment (see heterogeneous
reactions in Appendix B). When autoxidation is represented but τ_{RO2} is not listed here, autoxidation is assumed to be sufficiently
 1110 **fast that it is not modulated by ambient conditions. All SOA is modulated by temperature through gas-phase reaction rates and**
effect of temperature on volatility (not explicitly listed). For estimated yield calculations, typical population-weighted values (Porter
et al., 2021) of the bimolecular RO₂ fate (equal RO₂+HO₂ and RO₂+NO), the bimolecular lifetime (10s), and the amount of organic
partitioning medium (10 μg m⁻³) are assumed (if applicable). Estimated yields exclude multigenerational oxidation of secondary
oxygenated ROC species unless explicitly mentioned.

System	Precursor	Main SOA Species	Scientific Basis	Auto?	Factors affecting SOA	Est. Yield (Mole Frac.)	Est. Yield (Mass Frac.)
Alkane-like systems (Sect. 3.1)							
~C27 SVOCs ^{a,b}	ROCP1ALK	secondary oxygenated L/S/IVOCs	GECKO (Lannuque et al., 2018) + literature (Praske et al., 2018; Vereecken and Nozière, 2020)	Yes	OH, HO ₂ /NO, τ _{RO2} , OA	1.0	0.75
~C24 SVOCs ^{a,b}	ROCP2ALK	secondary oxygenated L/S/IVOCs	GECKO (Lannuque et al., 2018) + literature (Praske et al., 2018; Vereecken and Nozière, 2020)	Yes	OH, HO ₂ /NO, τ _{RO2} , OA	0.98	0.87
~C21 IVOCs ^{a,b}	ROCP3ALK	secondary oxygenated L/S/IVOCs	GECKO (Lannuque et al., 2018) + literature (Praske et al., 2018; Vereecken and Nozière, 2020)	Yes	OH, HO ₂ /NO, τ _{RO2} , OA	0.86	0.72
~C18 IVOCs ^a	ROCP4ALK	secondary oxygenated L/S/IVOCs	GECKO (Lannuque et al., 2018) + literature (Praske et al., 2018; Vereecken and Nozière, 2020)	Yes	OH, HO ₂ /NO, τ _{RO2} , OA	0.48	0.51
~C14 IVOCs ^a	ROCP5ALK	secondary oxygenated L/S/IVOCs	GECKO (Lannuque et al., 2018) + literature (Praske et al., 2018; Vereecken and Nozière, 2020)	Yes	OH, HO ₂ /NO, τ _{RO2} , OA	0.13	0.15
~C12 IVOCs ^a	ROCP6ALK	secondary oxygenated L/S/IVOCs	GECKO (Lannuque et al., 2018) + literature (Praske et al., 2018; Vereecken and Nozière, 2020)	Yes	OH, HO ₂ /NO, τ _{RO2} , OA	0.040	0.043
~C10 VOCs	HC10	secondary oxygenated L/S/IVOCs	GECKO (Lannuque et al., 2018) + literature (Praske et al., 2018; Vereecken and Nozière, 2020)	Yes	OH, HO ₂ /NO, τ _{RO2} , OA	0.0059	0.0083
~C ₅ VOCs	HC5	ASOAT	Emission-based SAR	No	OH	0.0013	0.0037
~C ₃ VOCs	HC3	ASOAT	Emission-based SAR	No	OH	2.8×10 ⁻⁵	0.00013
Long-lived species ^a	SLOWROC	ASOAT	Emission-based SAR	No	OH	0.0010	0.0027
Oxygenated L/S/IVOCs (Sect. 3.2-3.3)							



Secondary oxygenated L/SVOCs ^c	ROCP0OXY02 ROCN1OXY06 ROCN1OXY03 ROCN1OXY01	secondary oxygenated L/S/IVOCs	Multigeneration 2-D VBS	No	OH, OA	^d	1.02-1.16 ^d
Secondary oxygenated SVOCs ^c	ROCP1OXY01 ROCP0OXY04	secondary oxygenated L/S/IVOCs	Multigeneration 2-D VBS	No	OH, OA	^d	0.85-0.89 ^d
Secondary oxygenated SVOCs ^c	ROCP2OXY02 ROCP1OXY03	secondary oxygenated L/S/IVOCs	Multigeneration 2-D VBS	No	OH, OA	^d	0.63-0.64 ^d
Secondary oxygenated IVOCs ^c	ROCP3OXY02	secondary oxygenated L/S/IVOCs	Multigeneration 2-D VBS	No	OH, OA	^d	0.52 ^d
Secondary oxygenated IVOCs ^c	ROCP4OXY02	secondary oxygenated L/S/IVOCs	Multigeneration 2-D VBS	No	OH, OA	^d	0.37 ^d
Secondary oxygenated IVOCs ^c	ROCP5OXY01	secondary oxygenated L/S/IVOCs	Multigeneration 2-D VBS	No	OH, OA	^d	0.36 ^d
Secondary oxygenated IVOCs ^c	ROCP6OXY01	secondary oxygenated L/S/IVOCs	Multigeneration 2-D VBS	No	OH, OA	^d	0.23 ^d
Multi-functional ~C8 peroxides	OP3	AOP3	New lumped, semivolatile species; Chemistry like RACM OP2	No	OA, hv, OH	0.50 ^e	0.50 ^e
Emitted oxygenated IVOCs ^a	ROCIOXY	ASOAT	Emission-based SAR	No	OH	0.15	0.12
Aromatics and furans (Sect. 3.4-3.5)							
Furanone ^a	FURANONE	ASOAT	Literature on furans (Bruns et al., 2016)	No	OH	0.040	0.080
Less volatile aromatic IVOCs ^a	ROCP5ARO	secondary oxygenated L/S/IVOCs ASOAT	MCM (Bloss et al., 2005) + literature (Xu et al., 2020; Molteni et al., 2018)	Yes	OH, HO ₂ , NO, OA	0.37 ^f	0.47 ^f
More volatile aromatic IVOCs ^a	ROCP6ARO	secondary oxygenated L/S/IVOCs, ASOAT	MCM (Bloss et al., 2005) + literature (Xu et al., 2020; Molteni et al., 2018)	Yes	OH, HO ₂ , NO, OA	0.21 ^f	0.25 ^f
Naphthalene and PAHs	NAPH	secondary oxygenated L/S/IVOCs ASOAT	MCM (Bloss et al., 2005) + literature (Xu et al., 2020; Molteni et al., 2018)	Yes	OH, HO ₂ , NO, OA	0.21 ^f	0.34 ^f



Benzene	BEN	AROCN10 XY6, ASOAT	MCM (Bloss et al., 2005) + literature (Xu et al., 2020; Molteni et al., 2018; Ng et al., 2007)	Yes	OH, HO ₂ , NO, OA	0.18 ^{f,g}	0.44 ^{f,g}
Toluene	TOL	AROCN10 XY6, ASOAT	MCM (Bloss et al., 2005) + literature (Xu et al., 2020; Molteni et al., 2018; Ng et al., 2007)	Yes	OH, HO ₂ , NO, OA	0.15 ^{f,g}	0.33 ^{f,g}
More reactive aromatic VOCs	XYM	AROCN10 XY4, ASOAT, AOP3	MCM (Bloss et al., 2005) + literature (Xu et al., 2020; Molteni et al., 2018; Ng et al., 2007)	Yes	OH, HO ₂ , NO, OA	0.28 ^{f,g}	0.54 ^{f,g}
Less reactive aromatic VOCs	XYE	AROCN10 XY4, ASOAT, AOP3	MCM (Bloss et al., 2005) + literature (Xu et al., 2020; Molteni et al., 2018; Ng et al., 2007)	Yes	OH, HO ₂ , NO, OA	0.28 ^{f,g}	0.50 ^{f,g}
Phenol and aromatic diols ^a	PHEN	ASOAT	Literature including benzene constraints (Bruns et al., 2016; Ng et al., 2007; Zhang et al., 2014)	No	OH	0.15	0.28
Cresols ^a	CSL	ASOAT	Literature including xylene+toluene constraints (Bruns et al., 2016; Ng et al., 2007; Zhang et al., 2014)	No	OH	0.20	0.29
Sesquiterpenes (Sect. 3.6) + Monoterpenes (Sect. 3.7)							
Sesquiterpenes	SESQ	secondary oxygenated L/S/IVOCs	MCM (Jenkin et al., 2012) + literature (Richters et al., 2016)	Yes	OH, NO ₃ , O ₃ , HO ₂ , NO, OA	OH: 0.52, O ₃ : 0.028, NO ₃ : 0.46	OH: 0.60, O ₃ : 0.034, NO ₃ : 0.45
α-pinene and similar	API	AHOM, AELHOM	Literature (Nozière et al., 1999; Berndt et al., 2016; Piletic and Kleindienst, 2022; Zhao et al., 2018; Jokinen et al., 2015)	Yes	OH, NO ₃ , O ₃ , HO ₂ , NO	OH, NO ₃ : 0.11, ^h O ₃ : 0.13 ^h	OH, NO ₃ : 0.21, ^h O ₃ : 0.24 ^h
limonene and similar	LIM	AHOM, AELHOM	Literature (Piletic and Kleindienst, 2022; Zhao et al., 2018; Jokinen et al., 2015)	Yes	OH, NO ₃ , O ₃ , HO ₂ , NO	OH, NO ₃ : 0.16, ^h O ₃ : 0.21 ^h	OH, NO ₃ : 0.30, ^h O ₃ : 0.38 ^h
Pinonaldehyde ^a	PINAL	AHOM	MCM (Saunders et al., 2003) + RACM2 photolysis + assumed autoxidation	Yes	OH, τ _{RO2}	Phot: see HC10 OH: 0.21	OH: 0.31
Limonene-like aldehydes ^a	LIMAL	AHOM	MCM (Saunders et al., 2003) + RACM2 photolysis + assumed autoxidation	Yes	OH, O ₃ , τ _{RO2}	Phot: See HC10 OH: 0.64, O ₃ : <1%	OH: 0.95
Terpene peroxides	OPB	see HC10	New volatile biogenic peroxide, Chemistry like RACM2 OP2	No	OH, OH, hv	OH: <1%	--
Terpene nitrates	TRPN	AHOM	Literature (Zare et al., 2019)	No	OH, NO ₃ , O ₃	1.0	1.16
Aqueous Systems (Sect. 3.8)							



Isoprene epoxydiols	IEPOX	AISO3NOS, AISO3OS	CMAQ AERO6-7 (Pye et al., 2017; Pye et al., 2013)	No	Particle pH, liquid water, sulfate, size distribution	Variable	Variable
Glyoxal + methylglyoxal uptake to particles	GLY, MGLY	AGLY	CMAQ AERO6-7 (Pye et al., 2015)	No	Particle size distribution	Variable	Variable
Glyoxal + methylglyoxal uptake in clouds	GLY, MGLY	AORGC	CMAQ AERO5-7 (Carlton et al., 2008)	No	OH	Variable	Variable

^aNew SOA precursor system compared to CMAQ AERO6-7 (Appel et al., 2021).

1115 ^bROCN2ALK, ROCN1ALK, ROCP0ALK, ROCP1ALK, ROCP2ALK, and ROCP3ALK can partition directly to particles and form POA (See Sect. 3.1). Yields here are for chemical reaction.

^cWhile these species are envisioned as secondary, oxygenated semivolatile emissions from sources such as biomass burning could be mapped to this system based on volatility.

^dCalculated for 12 hours of reaction time across multiple generations. Only mass-based yields are provided. See Fig. 4.

1120 ^eBased on semivolatile partitioning of OP3. Further reaction of OP3 with HO produces <1% molar yield of SOA.

^fSOA yield includes furanone route contributions.

^gSOA yield includes phenolic (PHEN or CSL) route contributions.

^hSOA yield includes complete further reaction of TRPN but not aldehydes (PINAL or LIMAL).

1125



Figures

1130

Figure 1: Emission-weighted number of carbon per molecule of individual ROC species grouped by CRACMM species. Violin plots (with shaded colors for families of species in Sect. 3) are weighted by the magnitude of U.S. anthropogenic and biomass burning emissions in 2017. Overlaid boxplots indicate the 25th percentile, median, and 75th percentile values. Whiskers extend from the minimum to maximum properties for species with emissions >100 Mg yr⁻¹. CMAQ v5.3.3 values are for RACM2 with the aerosol module AERO6 or represent an individual HAP from CMAQ. In some cases, the CMAQv5.3.3 values represent similar species from RACM2 (e.g., HC8 values at CRACMM HC10). Emission magnitudes by species are available in supporting data Table D2.

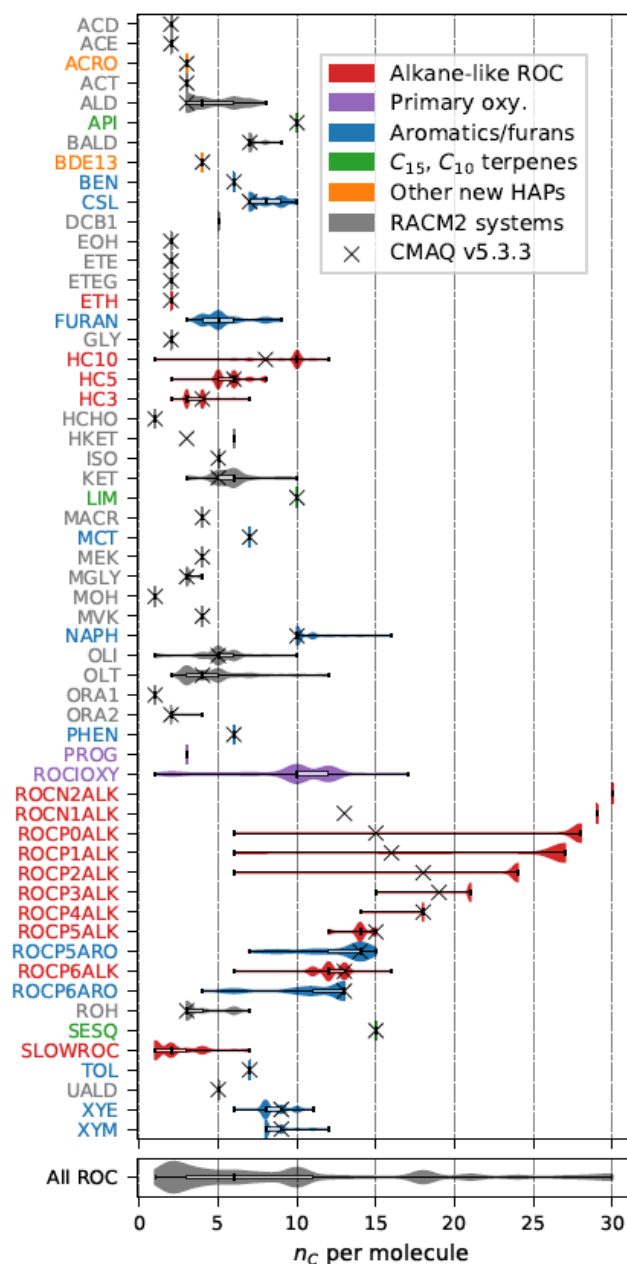




Figure 2: Same as Fig. 1 except the property displayed is the saturation concentration in $\log_{10}(C_i^*)$.

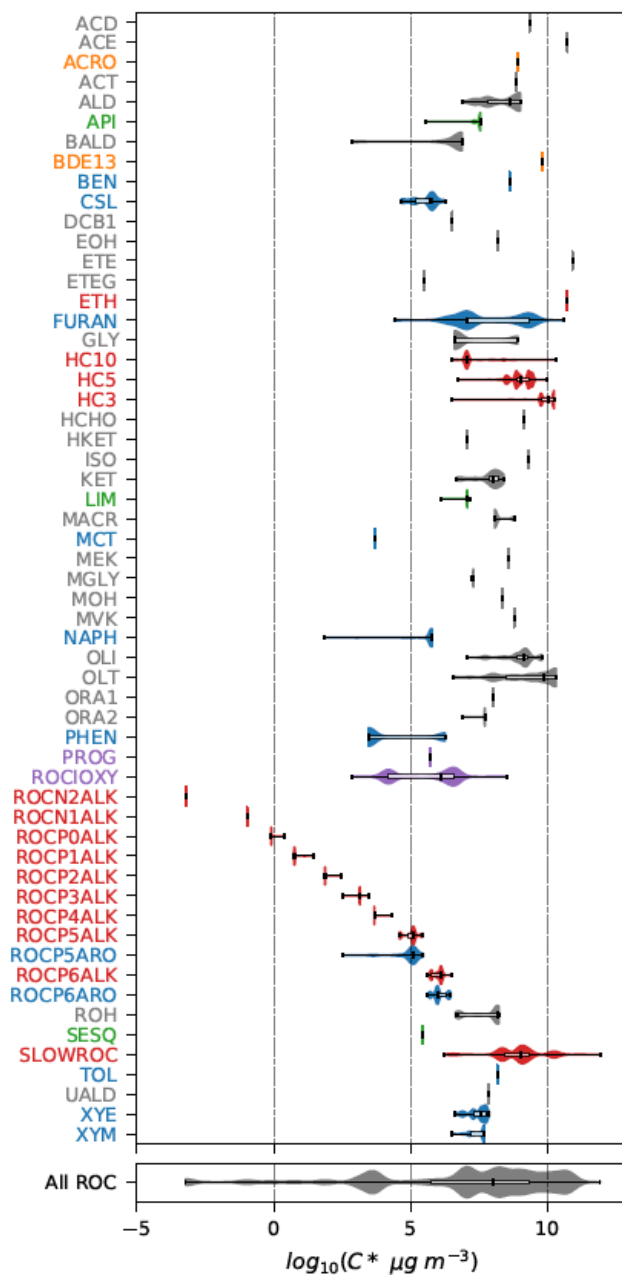
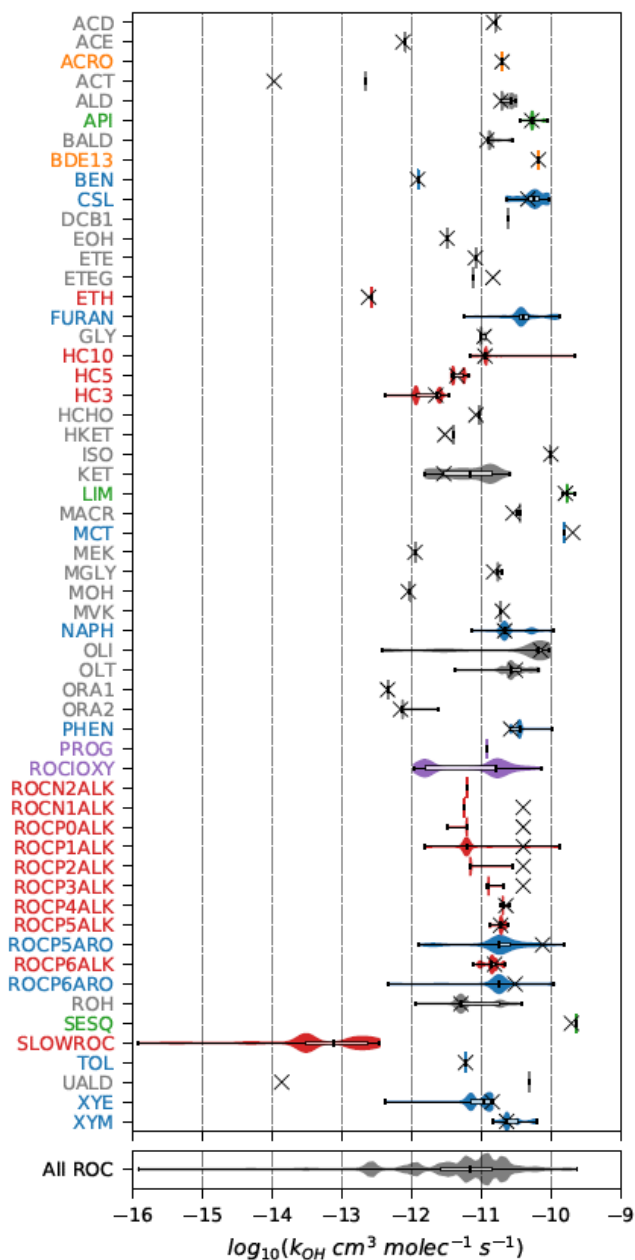


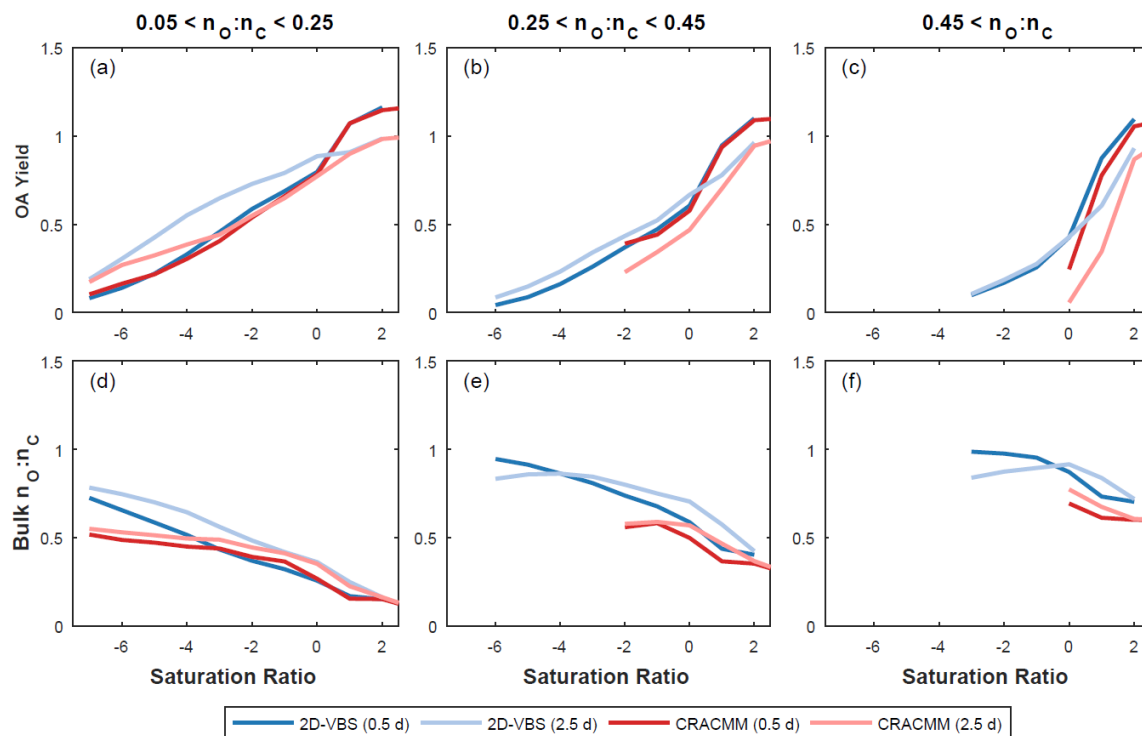


Figure 3: Same as Fig. 1 except the property displayed is the HO rate constant estimated by OPERA.



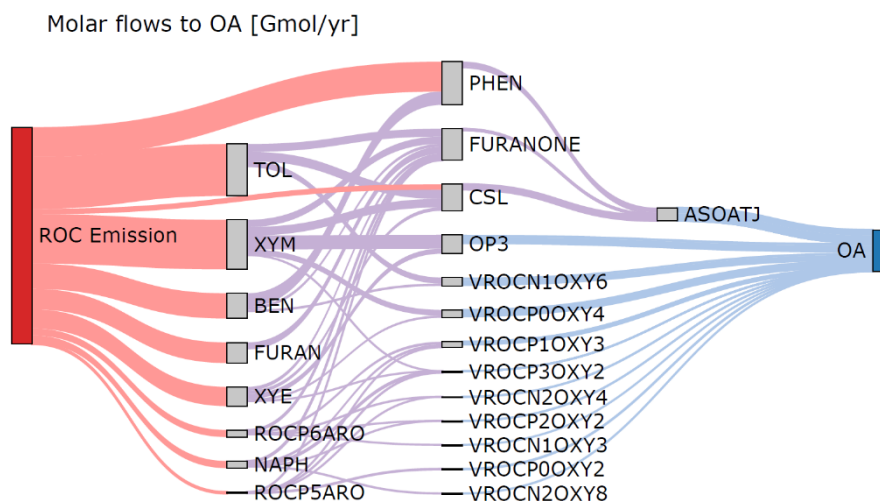


1140 **Figure 4: Organic aerosol yield and bulk $n_o:n_c$ predicted by the CRACMM oxygenated ROC aging mechanism (Sect. 3.2) and the**
2D-VBS configuration reported by Zhao et al. (2016). The saturation ratio is defined as $\log_{10}(C_{OA}/C_i^*)$ where C_{OA} is the
background OA concentration and C_i^* is the saturation concentration of the precursor. The aging of each species is simulated at a
constant HO concentration of 10^6 molec cm^{-3} for 12 hours (darker colors) and 2.5 days (lighter colors) at four different C_{OA}
 1145 **conditions (0.1, 1, 10, and $100 \mu\text{g m}^{-3}$). In cases where multiple predictions are present for the same saturation ratio, values are**
averaged.



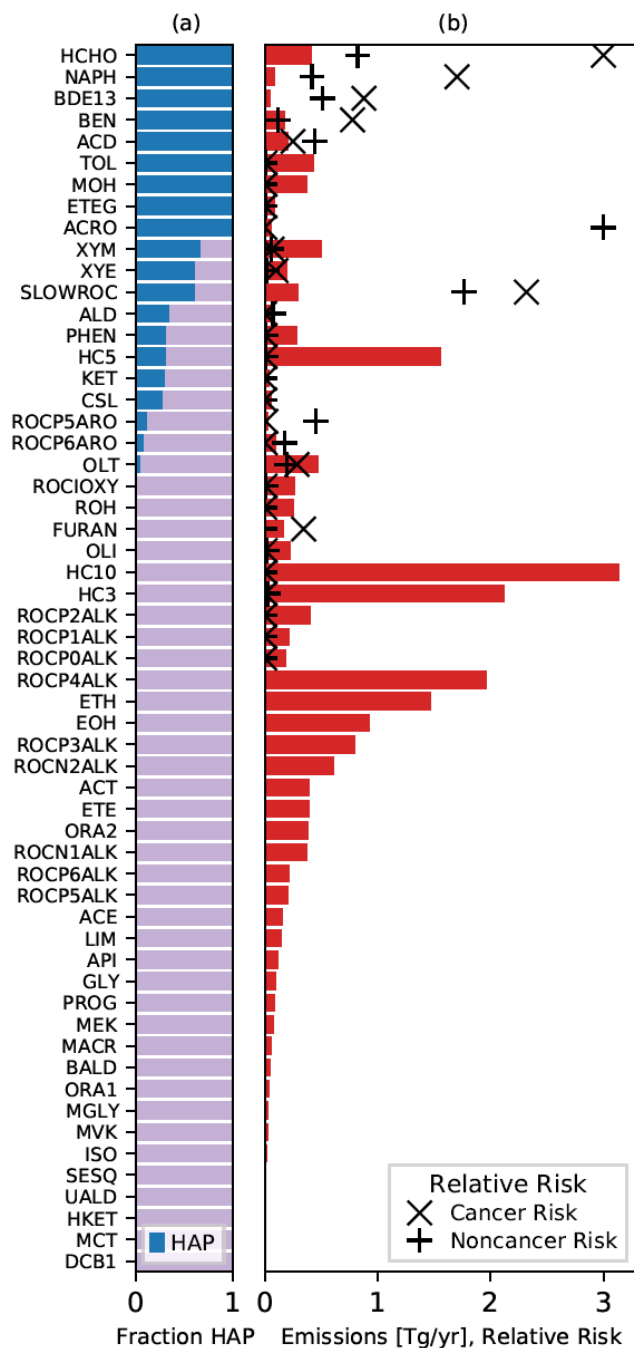


- 1150 **Figure 5: Molar flows to organic aerosol in the aromatic + phenolic + furan systems for 2017 U.S. emissions. Bimolecular RO₂**
reactions are split equally between RO₂+NO and RO₂+HO₂ with the fraction of products undergoing autoxidation as specified in
CRACMM. Partitioning of semivolatile species is calculated for 10 µg m⁻³ of organic aerosol. Precursor species include: toluene
(TOL), m-xylene and more reactive aromatic VOCs (XYM), benzene (BEN), ethylbenzene and less reactive aromatic VOCs (XYE),
phenolic species (PHEN), cresols (CSL), naphthalene and PAHs (NAPH), and other IVOC aromatics of higher (ROCP6ARO) and
1155 **lower (ROCP5ARO) volatility. Aqueous pathways to SOA from glyoxal and methylglyoxal are not shown. Products that do not lead**
to OA are not shown but are indicated by the outflow from a species being smaller than the inflow. Red flows indicate emissions.
Purple flows indicate hydroxyl radical oxidation chemistry. Blue flows indicate partitioning to the condensed phase.



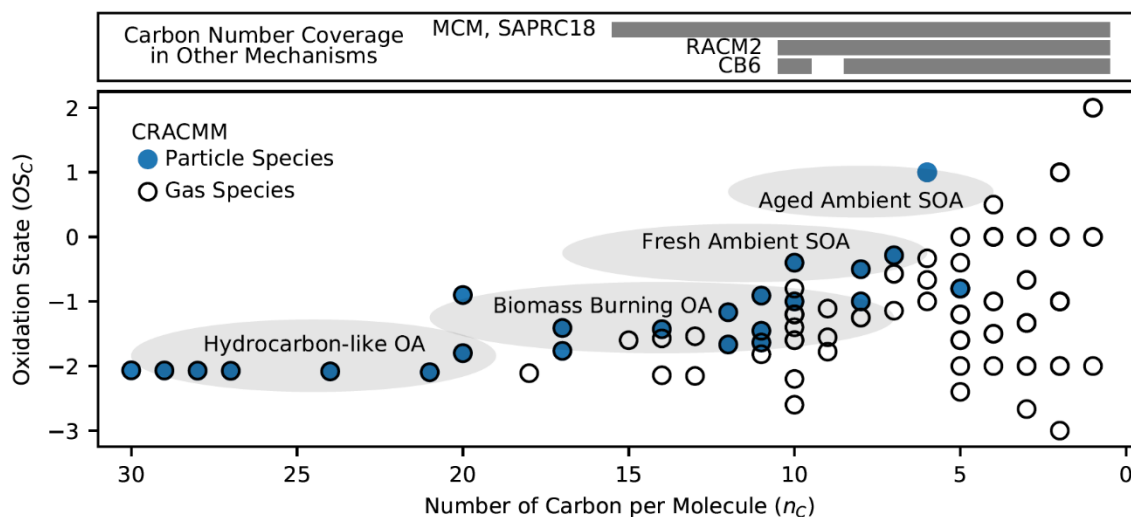


1160 **Figure 6: Distribution of hazardous air pollutants (HAPs) across CRACMM emitted species. Panel (a) indicates the mass fraction of 2017 U.S. anthropogenic and biomass burning ROC emissions by CRACMM species that are HAPs (blue). Panel (b) indicates the magnitude of emissions in Tg yr^{-1} by CRACMM species (bars) and the relative potential for cancer (x) or noncancer (+) risks to health. Cancer and noncancer health risks are normalized such that the species with the maximum relative risk in each category is 3. Health risks are only shown for CRACMM species that contain non-zero amounts of HAPs. This data is available in the**
 1165 **supplementary archive as Table D3.**





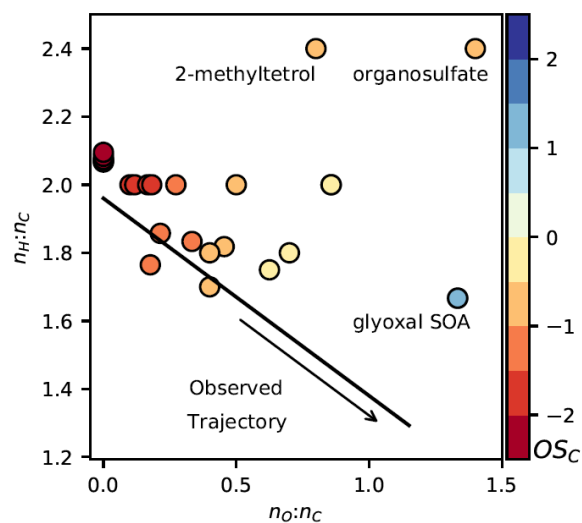
1170 **Figure 7: Mean carbon oxidation state (OS_C) and number of carbon atoms per molecule (n_C) for all stable ROC species. Filled circles indicate at least one particulate species present in CRACMM. Black circles indicate the presence of at least one gas species in CRACMM. Grey ellipses indicate approximate ranges of observation-based bulk OS_C and n_C from the work by Kroll et al. (2011) for hydrocarbon-like OA (vehicle emissions and ambient hydrocarbon-like organic aerosol), biomass burning OA, fresh ambient SOA, and aged ambient SOA. Grey bars indicate n_C coverage in mechanisms other than CRACMM.**



1175



1180 **Figure 8: Molar hydrogen to carbon ($n_H:n_C$) and oxygen to carbon ($n_O:n_C$) ratios of CRACMM particulate ROC species. Color indicates the mean carbon oxidation state (OS_C). The observed trajectory trendline with slope of -0.6 is based on ambient measurements assembled by Chen et al. (2015) and extended to laboratory systems with $n_O:n_C$ near zero. Three CRACMM species are labeled: glyoxal SOA (AGLY), isoprene-derived organosulfates (AISO3OS), and non-sulfated isoprene SOA represented as 2-methyltetrols (AISO3NOS).**

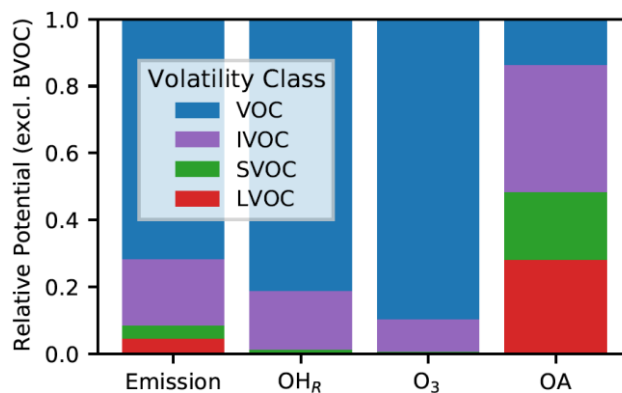


1185



1190

Figure 9: Anthropogenic and wood-burning ROC emissions and their relative potential HO reactivity (OH_R), ozone (O_3) formation, and OA for 2017 U.S. conditions by volatility class. Biogenic VOCs (BVOC) are not considered here. Ozone and OA formation potentials are calculated using the MIR and OA simple SAR approaches from Sect. 2.1. Metrics are aggregated from the individual species level to volatility classes: low volatility organic compounds (LVOC), semivolatile organic compounds (SVOC), intermediate volatility organic compounds (IVOC), and volatile organic compounds (VOC).



1195



1200

Appendix A: ROC Species in CRACMM and their description, phase (Phs) in which they can exist (G=gas, P=particle), and SMILES for representative compound structure. Appendix A along with additional ROC species information is also available in csv format in the data archive associated with this work (Table D1). Species properties such as molecular weights are determined from the representative structure except in the case of highly empirical species (SLOWROC, ROCIOXY, ASOAT). In CMAQ, aerosol species reside in Aitken, accumulation, and/or coarse modes and are appended with the letter to indicate the size mode. Prepending of species with a V or A (e.g., in Appendix B) indicates gas or particulate phase.

Species	Description	Phs	Representative Compound
ACD	Acetaldehyde	G	CC=O
ACE	Acetylene	G	C#C
ACO3	Acetyl peroxy radicals	G	CC(=O)O[O]
ACRO	Acrolein	G	C=CC=O
ACT	Acetone	G	CC(C)=O
ACTP	Peroxy radicals formed from ACT	G	CC(=O)CO[O]
ADCN	Aromatic-NO ₃ adduct from PHEN	G	OC1=C[C]C(O[N+])([O-])=O)C=C1
ADDC	Aromatic-HO adduct from CSL	G	CC1=CC(O)=CC([O])C1
AGLY	SOA from reactive uptake of glyoxal on particles	P	OC2OC(C1OC(O)C(O)O1)OC2O
AISO3NOS	Non-sulfated SOA from IEPOX uptake	P	C(O)C(O)(C)C(O)CO
AISO3OS	Organosulfate SOA from IEPOX uptake	P	C(O)C(OS(O)(=O)(=O))(C)C(O)CO
ALD	C3 and higher aldehydes	G	CCC=O
AORGC	SOA from cloud processing of GLY and MGLY	P	OC2OC(C1OC(O)C(O)O1)OC2O
API	Alpha-pinenes and cyclic terpenes with one double bond	G	CC1=CCC2CC1C2(C)C
APINP1	Peroxy radicals from API+NO ₃ that do not undergo autoxidation	G	[O]OC1(C)C(ON(=O)=O)CC2CC1C2(C)C
APINP2	Peroxy radicals from API+NO ₃ that undergo autoxidation	G	[O]OC1(C)C(ON(=O)=O)CC2CC1C2(C)C
APIP1	Peroxy radicals from API+HO that do not undergo autoxidation	G	[O]OC1(C)C(O)CC2CC1C2(C)C
APIP2	Peroxy radicals from API+HO that undergo autoxidation	G	[O]OC1(C)C(O)CC2CC1C2(C)C
ASOAT	An empirical SOA	P	CC(=O)C(C(C(C(O)O)O)O)O
BAL1	Peroxy radicals formed from BALD	G	[O]OC1=CC=C(C)C=C1
BAL2	Peroxy radicals formed from BALD	G	[O]OC1=CC=CC=C1
BALD	Benzaldehyde and other aromatic aldehydes	G	O=CC1=CC=CC=C1
BALP	Peroxy radicals formed from BALD	G	O=C(O[O])C1=CC=CC=C1
BDE13	1,3-butadiene	G	C=CC=C
BDE13P	Peroxy radicals from BDE13	G	C=CC(O[O])CO
BEN	Benzene	G	C1=CC=CC=C1
BENP	Peroxy radicals formed from benzene	G	[O]OC1C=CC2OOC1C2O
CHO	Phenoxy radical formed from CSL	G	[O]C1C=C(C)C(O)C(=C1)C
CO	Carbon monoxide	G	[C-]#[O+]
CSL	Cresol and other hydroxy substituted aromatics	G	CC(C)(O)C1=CC=CC=C1
DCB1	Unsaturated dicarbonyls	G	O=CC=C(C)C=O
DCB2	Unsaturated dicarbonyls	G	O=CC(=CC(=O)C)C
DCB3	Unsaturated dicarbonyls	G	O=CC=CC=O
ELHOM	Extremely-low volatility highly oxygenated molecules from terpenes	GP	OC1CC2C(OOC2(C)C)C(OOC3(C)C4C(C)(C)C(C4)CC3O)C1(C)OO
EOH	Ethanol	G	CCO
ETE	Ethene	G	C=C
ETEG	Ethylene glycol	G	OCCO
ETEP	Peroxy radicals formed from ETE	G	OCCO[O]
ETH	Ethane	G	CC
ETHP	Peroxy radicals formed from ethane and other species	G	CCO[O]



FURAN	Furans and other dienes	G	O=CC1=CC=CO1
FURANO2	Peroxy radicals from FURAN oxidation	G	OC1C=CC(O1)(O[O])(C=O)
FURANONE	Ring-retaining ketone product from FURAN oxidation	G	C1=CC(=O)OC1O
GLY	Glyoxal and glycoaldehydes	G	O=CC=O
HC10	Alkanes and other species with HO rate constant greater than 6.8×10^{-12} molec $\text{cm}^{-3} \text{sec}^{-1}$	G	CCCCCCCCC
HC10P	Peroxy radicals formed from HC10	G	CCCCCCCC(CC)O[O]
HC10P2	Hydroxy peroxy radicals from HC10P alkoxy product	G	CCCC(O[O])CCC(O)CC
HC3	Alkanes and other species with HO rate constant less than 3.4×10^{-12} molec $\text{cm}^{-3} \text{sec}^{-1}$	G	CCC
HC3P	Peroxy radicals formed from HC3	G	CC(C)O[O]
HC5	Alkanes and other species with HO rate constant between 3.4×10^{-12} and 6.8×10^{-12} molec $\text{cm}^{-3} \text{sec}^{-1}$	G	CCCCC
HC5P	Peroxy radicals formed from HC5	G	CCC(O[O])CC
HCHO	Formaldehyde	G	C=O
HKET	Hydroxy ketone	G	CC(=O)CO
HOM	Highly oxygenated molecules from terpenes	GP	OC1CC2C(OOC2(C)C)C(OO)C1(C)OO
IEPOX	Isoprene epoxydiols	G	OCC1OC1(C)CO
ISHP	Beta-hydroxy hydroperoxides from ISOP+HO ₂	G	C=CC(OO)(CO)C
ISO	Isoprene	G	CC(=C)C=C
ISON	Beta-hydroxyalkylnitrates from ISOP+NO alkylnitrates from ISO+NO ₃	G	OCC(C)(C=C)ON(=O)=O
ISOP	Peroxy radicals formed from ISO+HO	G	OCC(O[O])C(C)=C
KET	Ketones	G	CCC(=O)CC
KETP	Peroxy radicals formed from KET	G	CCC(C(C)O[O])=O
LIM	Δ -limonene and other cyclic diene-terpenes	G	CC(=C)[C@@H]1CCCC(C)=CC1
LIMAL	Limonene aldehyde and similar LIM-derived aldehydes	G	O=CCC(CCC(=O)C)C(=C)C
LIMALP	Peroxy radicals from LIMAL	G	O=CCC(CCC(=O)C)C(C)(CO)O[O]
LIMNP1	Peroxy radicals from LIM+NO ₃ that do not undergo autoxidation	G	[O-][N+](=O)OC1CC(CCC1(C)O[O])C(=C)C
LIMNP2	Peroxy radicals from LIM+NO ₃ that undergo autoxidation	G	[O-][N+](=O)OC1CC(CCC1(C)O[O])C(=C)C
LIMP1	Peroxy radicals from LIM+HO that do not undergo autoxidation	G	[O]OC1(C)CCC(CC1O)C(=C)C
LIMP2	Peroxy radicals from LIM+HO that undergo autoxidation	G	[O]OC1(C)CCC(CC1O)C(=C)C
MACP	Peroxy radicals formed from MACR+HO	G	CC(=C)C(=O)O[O]
MACR	Methacrolein and other C ₄ aldehydes	G	CC(=C)C=O
MAHP	Hydroperoxides from MACP+HO ₂	G	C=C(C)C(OO)=O
MCP	Peroxy radical formed from MACR+HO which does not form MPAN	G	OCC(C)(O[O])C=O
MCT	Methyl catechol	G	CC1=CC(O)=C(O)C=C1
MCTO	Alkoxy radical formed from MCT+HO and MCT+NO ₃	G	CC1=CC(O)=CC([O])=C1
MCTP	Radical formed from MCT+O ₃ reaction	G	CC(/C=C/[C](O[O])O)=C/C(O)=O
MEK	Methyl ethyl ketone	G	CCC(C)=O
MEKP	Peroxy radicals formed from MEK	G	[O]OCCC(=O)C
MGLY	Methylglyoxal and other α -carbonyl aldehydes	G	CC(=O)C=O
MO2	Methyl peroxy radical	G	CO[O]
MOH	Methanol	G	CO
MPAN	Peroxymethacryloynitrate and other higher peroxyacylnitrates from isoprene oxidation	G	O=N(=O)OOC(=O)C(=C)C
MVK	Methyl vinyl ketone	G	CC(=O)C=C
MVKP	Peroxy radicals formed from MVK	G	CC(=O)C(O)CO[O]
NALD	Nitrooxyacetaldehyde	G	O=CCON(=O)=O
NAPH	Naphthalene and other PAHs	G	C1=CC2=CC=CC=C2C=C1
NAPHP	Peroxy radicals from NAPH oxidation	G	C12=CC=CC=C1C3OOC(C3O[O])C2(O)



OLI	Internal alkenes	G	CC=C(C)C
OLIP	Peroxy radicals formed from OLI	G	[O]OC(C)(C)C(C)O
OLND	NO ₃ -alkene adduct reacting via decomposition	G	CC(O[O])CO[N+](=[O-])=O
OLNN	NO ₃ -alkene adduct reacting to form carbonitrates + HO ₂	G	CC(O[O])CO[N+](=[O-])=O
OLT	Terminal alkenes	G	CC=C
OLTP	Peroxy radicals formed from OLT	G	CC(CO)O[O]
ONIT	Organic nitrates	G	CCC(C)O[N+](=O)[O-]
OP1	Methyl hydrogen peroxide	G	COO
OP2	Higher organic peroxides	G	CCOO
OP3	Semivolatle organic peroxide	GP	CCC(=O)CC(OO)C(O)CC
OPB	Terpene-derived peroxides	G	OOC1(C)C(O)CC2CC1C2(C)C
ORA1	Formic acid	G	OC=O
ORA2	Acetic acid and higher acids	G	CC(O)=O
ORAP	Peroxy radical formed from ORA2 + HO reaction	G	[O]OCC(=O)O
PAA	Peroxyacetic acids and higher analogs	G	CC(=O)OO
PAN	Peroxyacetyl nitrate and higher saturated PANs	G	CC(=O)OON(=O)=O
PHEN	phenol and benzene diols	G	OC1=CC(O)=CC=C1
PINAL	Pinonaldehyde and similar APIN-derived aldehydes	G	O=CCC1CC(C(=O)C)C1(C)C
PINALP	Peroxy radicals from PINAL oxidation	G	O=CCC1(O[O])CC(C(=O)C)C1(C)C
PPN	Peroxypropionyl nitrate	G	CCC(=O)OO[N+](=O)[O-]
PROG	Propylene glycol and other 3 carbon dialcohols	G	CC(O)CO
RCO3	Higher saturated acyl peroxy radicals	G	CCC(=O)O[O]
ROCIOXY	Intermediate volatility oxygenated ROC species (directly emitted)	G	C[Si]1(C)O[Si](C)(C)O[Si](C)(C)O[Si](C)(C)O[Si](C)(C)O1
ROCNIALK	Alkane-like ROC, $C_i^* = 10^{-1} \mu\text{g m}^{-3}$	GP	CCCCCCCCCCCCCCCCCCCC(C)CCCC(C)CC CC
ROCNI0XY1	Oxygenated ROC, $C_i^* = 10^{-1} \mu\text{g m}^{-3}$ and $n_o:n_c$ of 0.1	GP	CCCCCCCCCCCCCCCCCCCC(=O)O
ROCNI0XY3	Oxygenated ROC, $C_i^* = 10^{-1} \mu\text{g m}^{-3}$ and $n_o:n_c$ of 0.3	GP	C(CCCCCC(=O)O)CCCC(=O)O
ROCNI0XY6	Oxygenated ROC, $C_i^* = 10^{-1} \mu\text{g m}^{-3}$ and $n_o:n_c$ of 0.6	GP	C(CCC(C(=O)O)O)CCC(=O)O
ROCNI2ALK	Alkane-like ROC, $C_i^* = 10^{-2} \mu\text{g m}^{-3}$	GP	CCCCCCCCCCCCCCCCCCCCCCCCCCCCCCCC C
ROCNI2OXY2	Oxygenated ROC, $C_i^* = 10^{-2} \mu\text{g m}^{-3}$ and $n_o:n_c$ of 0.2	GP	C#CCCC[C@H](CCCCCCCCCCCC(=O)O)O
ROCNI2OXY4	Oxygenated ROC, $C_i^* = 10^{-2} \mu\text{g m}^{-3}$ and $n_o:n_c$ of 0.4	GP	C(CCCCC(=O)O)CCCC(C(=O)O)O
ROCNI2OXY8	Oxygenated ROC, $C_i^* = 10^{-2} \mu\text{g m}^{-3}$ and $n_o:n_c$ of 0.8	GP	CC(=O)C(C(C(CO)O)O)O
ROCP0ALK	Alkane-like ROC, $C_i^* = 10^0 \mu\text{g m}^{-3}$	GP	CCCCCCCCCCCCCCCCCCCC(C)CCCCCCCC
ROCP0OXY2	Oxygenated ROC, $C_i^* = 10^0 \mu\text{g m}^{-3}$ and $n_o:n_c$ of 0.2	GP	CCCCCCCCCCCCCCCC(=O)CC(=O)O
ROCP0OXY4	Oxygenated ROC, $C_i^* = 10^0 \mu\text{g m}^{-3}$ and $n_o:n_c$ of 0.4	GP	C(CCCCC(=O)O)CCCC(=O)O
ROCP1ALK	Alkane-like ROC, $C_i^* = 10^1 \mu\text{g m}^{-3}$	GP	CCCCCCCCCCCCCCCCCCCCCCCCCCCC
ROCP1ALKP	Peroxy radicals from ROCP1ALK oxidation	G	CCCCCCCCCCCCCCCCCCCCCCCCCCCC(C)O [O]
ROCP1ALKP2	Hydroxy peroxy radicals from ROCP1ALK alkoxy product	G	CCCCCCCCCCCCCCCCCCCCCCCC(O[O])CCC (O)CC
ROCP1OXY1	Oxygenated ROC, $C_i^* = 10^1 \mu\text{g m}^{-3}$ and $n_o:n_c$ of 0.1	GP	CCCCCCCCCCCCCCCCCCCC(=O)O
ROCP1OXY3	Oxygenated ROC, $C_i^* = 10^1 \mu\text{g m}^{-3}$ and $n_o:n_c$ of 0.3	GP	C(CCCCCO)CCCC(=O)O
ROCP2ALK	Alkane-like ROC, $C_i^* = 10^2 \mu\text{g m}^{-3}$	GP	CCCCCCCCCCCCCCCCCCCCCCCC
ROCP2ALKP	Peroxy radicals from ROCP2ALK oxidation	G	CCCCCCCCCCCCCCCCCCCCCCCC(C)O[O]
ROCP2ALKP2	Hydroxy peroxy radicals from ROCP2ALK alkoxy product	G	CCCCCCCCCCCCCCCCCCCC(O[O])CCC(O)C C
ROCP2OXY2	Oxygenated ROC, $C_i^* = 10^2 \mu\text{g m}^{-3}$ and $n_o:n_c$ of 0.2	GP	CCCCCCCCCCCCCCCC(=O)O
ROCP3ALK	Alkane-like ROC, $C_i^* = 10^3 \mu\text{g m}^{-3}$	GP	CCCCCCCCCCCCCCCCCCCC
ROCP3ALKP	Peroxy radicals from ROCP3ALK oxidation	G	CCCCCCCCCCCCCCCCCCCC(C)O[O]
ROCP3ALKP2	Hydroxy peroxy radicals from ROCP3ALK alkoxy product	G	CCCCCCCCCCCCCCCC(O[O])CCC(O)CC
ROCP3OXY2	Oxygenated ROC, $C_i^* = 10^3 \mu\text{g m}^{-3}$ and $n_o:n_c$ of 0.2	GP	C(CCCCCO)CCCC=O



ROCP4ALK	Alkane-like ROC, $C_i^* = 10^4 \mu\text{g m}^{-3}$	G	CCCCCCCCCCCCCCCC
ROCP4ALKP	Peroxy radicals from ROCP4ALK oxidation	G	CCCCCCCCCCCCCCCC(CC)O[O]
ROCP4ALKP2	Hydroxy peroxy radicals from ROCP4ALK alkoxy product	G	CCCCCCCCCCCCCCCC(O[O])CCC(O)CC
ROCP4OXY2	Oxygenated ROC, $C_i^* = 10^4 \mu\text{g m}^{-3}$ and $n_o:n_c$ of 0.2	G	CCCCCC(CC)C(=O)O
ROCP5ALK	Alkane-like ROC, $C_i^* = 10^5 \mu\text{g m}^{-3}$	G	CCCCCCCCCCCCCCCC
ROCP5ALKP	Peroxy radicals from ROCP5ALK oxidation	G	CCCCCCCCCCCCCCCC(CC)O[O]
ROCP5ALKP2	Hydroxy peroxy radicals from ROCP5ALK alkoxy product	G	CCCCCCCCCCCC(O[O])CCC(O)CC
ROCP5ARO	Aromatic ROC, $C_i^* = 10^5 \mu\text{g m}^{-3}$	G	CCCCCCCCC1=CC=CC=C1
ROCP5AROP	Peroxy radicals from ROCP5ARO oxidation	G	CCCCCCCCC1(OO2)C=CC(O[O])C2C1O
ROCP5OXY1	Oxygenated ROC, $C_i^* = 10^5 \mu\text{g m}^{-3}$ and $n_o:n_c$ of 0.1	G	CCCCCCCCCCCC=O
ROCP6ALK	Alkane-like ROC, $C_i^* = 10^6 \mu\text{g m}^{-3}$	G	CCCCCCCCCCCCCCCC
ROCP6ALKP	Peroxy radicals from ROCP6ALK oxidation	G	CCCCCCCCCCCCCCCC(CC)O[O]
ROCP6ALKP2	Hydroxy peroxy radicals from ROCP6ALK alkoxy product	G	CCCCCCCCCCCC(O[O])CCC(O)CC
ROCP6ARO	Aromatic ROC, $C_i^* = 10^6 \mu\text{g m}^{-3}$	G	CCCCCCCCC1=CC=C(C)C=C1
ROCP6AROP	Peroxy radicals from ROCP6ARO oxidation	G	OC1C2C(CCCCCC(O[O]))C=CC1(C)OO2
ROCP6OXY1	Oxygenated ROC, $C_i^* = 10^6 \mu\text{g m}^{-3}$ and $n_o:n_c$ of 0.1	G	CCCCCCCCC=O
ROH	C3 and higher alcohols	G	CCCCO
SESQ	Sesquiterpenes	G	C/C1=C/CCC(=C)C2CC(C)(C)C2CC\1
SESQNRO2	Peroxy radicals from SESQ reaction with nitrate radicals	G	[O]OC1(C)CCC2C(CC2(C)C)C(=C)CCC1O[N+](=O)[O-]
SESQRO2	Peroxy radicals from SESQ reaction with OH	G	[O]OC1(C)CCC2C(CC2(C)C)C(=C)CCC1O
SLOWROC	Slowly reacting ROC with $k_{OH} < 3.5 \times 10^{-13} \text{ molec cm}^{-3} \text{ sec}^{-1}$	G	C#N
TOL	Toluene	G	CC1=CC=CC=C1
TOLP	Peroxy radicals formed from TOL	G	[O]OC1C=CC2(C)OOC1C2O
TRPN	Terpene nitrates	G	O=N(=O)OC1(C)C(O)CC2CC1C2(C)C
UALD	Unsaturated aldehydes	G	CC=C(C)C=O
UALP	Peroxy radicals formed from UALD	G	CC(O[O])C(C)(O)C=O
XYE	O- and p-xylene and other less reactive volatile aromatics with $k_{OH} < 1.46 \times 10^{-11} \text{ molec cm}^{-3} \text{ sec}^{-1}$	G	CCC1=CC=CC=C1
XYEP	Peroxy radicals formed from XYE	G	[O]OC1C=CC2(CC)OOC1C2O
XYM	M-xylene and other more reactive volatile aromatics with $k_{OH} > 1.46 \times 10^{-11} \text{ molec cm}^{-3} \text{ sec}^{-1}$	G	CC1=CC(C)=CC=C1
XYMP	Peroxy radicals formed from XYM	G	[O]OC1C=CC2(C)OOC1(C)C2O



1205 **Appendix B: Chemistry of CRACMM v1.0. For photolysis and heterogenous reactions (rate constant values not**
provided), rates depend on radiation, predicted concentrations, and/or other conditions, so a reference to the
underlying data and formulation is provided. Rate constant values (k), if provided, are specified at 298.15 K,
M=2.4615×10¹⁹ molecules cm⁻³, and 1.00 atm. This information is also available in the data archive as a mechanism text
 1210 **file (mech_cracmm1_aq.def) compatible with CMAQ. Partitioning of condensible organics is not listed here, and**
CMAQ assumes equilibrium partitioning calculated via operator splitting separate from the kinetic chemistry.

N	CMAQ Label	Reaction	Rate Constant Formula ^{a,b,c}	k (molec cm ⁻³ sec ⁻¹ or s ⁻¹)
1	R001	O ₃ → O ₃ P	σ from Sander et al. (2011); φ = 1.0 - φ of O ₃ (Reaction 2)	Not Applicable
2	R002	O ₃ → O ₁ D	σ and φ from Sander et al. (2011)	Not Applicable
3	R003	H ₂ O ₂ → 2.000*HO	σ from Sander et al. (2011); φ = 1.0	Not Applicable
4	R004	NO ₂ → O ₃ P + NO	σ and φ from Sander et al. (2011)	Not Applicable
5	R005	NO ₃ → NO	σ and φ from Sander et al. (2011)	Not Applicable
6	R006	NO ₃ → O ₃ P + NO ₂	σ and φ from Sander et al. (2011)	Not Applicable
7	R007	HONO → HO + NO	σ from Sander et al. (2011); φ = 1.0	Not Applicable
8	R008	HNO ₃ → HO + NO ₂	σ from Sander et al. (2011); φ = 1.0	Not Applicable
9	R009	HNO ₄ → 0.200*HO + 0.800*HO ₂ + 0.800*NO ₂ + 0.200*NO ₃	σ from Sander et al. (2011); φ = 1.0	Not Applicable
10	R010	HCHO → CO	σ and φ from Sander et al. (2011)	Not Applicable
11	R011	HCHO → 2.000*HO ₂ + CO	σ and φ from Sander et al. (2011)	Not Applicable
12	R012	ACD → HO ₂ + MO ₂ + CO	σ and φ from Sander et al. (2011)	Not Applicable
13	R013	ALD → HO ₂ + EHP + CO	σ from Burkholder et al. (2019); φ from Heicklen et al. (1986) and IUPAC datasheet P3 (updated 16th May 2002)	Not Applicable
14	R014	ACT → MO ₂ + ACO ₃	σ and φ from Burkholder et al. (2019)	Not Applicable
15	R014a	ACT → 2.000*MO ₂ + CO	σ and φ from Burkholder et al. (2019)	Not Applicable
16	R015	UALD → 1.220*HO ₂ + 0.784*ACO ₃ + 1.220*CO + 0.350*HCHO + 0.434*ALD + 0.216*KET	σ and φ from Magneron et al. (2002); uses crotonaldehyde	Not Applicable
17	TRP01	PINAL → HO ₂ + HC ₁₀ P + CO	Uses data for ALD (Reaction 13)	Not Applicable
18	TRP02	LIMAL → HO ₂ + HC ₁₀ P + CO	Uses data for ALD (Reaction 13)	Not Applicable
19	R016	MEK → 0.100*MO ₂ + EHP + 0.900*ACO ₃ + 0.100*CO	σ from Brewer et al. (2019); φ from IUPAC datasheet P8 (5th December 2005)	Not Applicable



N	CMAQ Label	Reaction	Rate Constant Formula ^{a,b,c}	k (molec cm ⁻³ sec ⁻¹ or s ⁻¹)
20	R017	KET → 1.500*ETHP + 0.500*ACO3 + 0.500*CO	σ from Brewer et al. (2019); φ from IUPAC datasheet P8 (5th December 2005)	Not Applicable
21	R018	HKET → HO2 + ACO3 + HCHO	σ from Yujing and Mellouki (2000); φ from IUPAC datasheet P8 (5th December 2005)	Not Applicable
22	R019	MACR → 0.340*HO + 0.660*HO2 + 0.670*ACO3 + 0.330*MACP + 0.340*XO2 + 0.670*CO + 0.670*HCHO	σ and φ from Sander et al. (2011)	Not Applicable
23	R020	MVK → 0.300*MO2 + 0.300*MACP + 0.700*CO + 0.700*UALD	σ and φ from Sander et al. (2011)	Not Applicable
24	R021	GLY → 2.000*CO	σ and φ from Sander et al. (2011)	Not Applicable
25	R022	GLY → HCHO + CO	σ and φ from Sander et al. (2011)	Not Applicable
26	R023	GLY → 2.000*HO2 + 2.000*CO	σ and φ from Sander et al. (2011)	Not Applicable
27	R024	MGLY → HO2 + ACO3 + CO	σ and φ from Sander et al. (2011)	Not Applicable
28	R025	DCB1 → 1.500*HO2 + 0.250*ACO3 + 0.200*XO2 + CO + 0.500*GLY + 0.500*MGLY	Uses data for MGLY (Reaction 27)	Not Applicable
29	R026	DCB2 → 1.500*HO2 + 0.250*ACO3 + 0.200*XO2 + CO + 0.500*GLY + 0.500*MGLY	Uses data for MGLY (Reaction 27)	Not Applicable
30	R027	BALD → CHO + HO2 + CO	σ and φ from SAPRC07 (Carter, 2010)	Not Applicable
31	R028	OP1 → HO + HO2 + HCHO	σ from Sander et al. (2011); φ = 1.0	Not Applicable
32	R029	OP2 → HO + HO2 + ALD	Uses data for OP1 (Reaction 31)	Not Applicable
33	TRP03	OPB → HO + HO2 + ALD	Uses data for OP1 (Reaction 31)	Not Applicable
34	R029a	OP3 → HO + HO2 + ALD	Uses data for OP1 (Reaction 31)	Not Applicable
35	R030	PAA → HO + MO2	σ from Sander et al. (2011); φ = 1.0	Not Applicable
36	R031	ONIT → HO2 + NO2 + 0.200*ALD + 0.800*KET	σ from Talukdar et al. (1997); φ = 1.0	Not Applicable
37	R032	PAN → ACO3 + NO2	σ and φ from Sander et al. (2011)	Not Applicable
38	R033	PAN → MO2 + NO3	σ from Sander et al. (2011); φ = 1.0 - φ of PAN in Reaction 36	Not Applicable
39	R034	O3 + HO → HO2	1.70×10 ⁻¹² exp(-940.00/T)	7.26×10 ⁻¹⁴
40	R035	O3 + HO2 → HO	1.00×10 ⁻¹⁴ exp(-490.00/T)	1.93×10 ⁻¹⁵
41	R036	O3 + NO → NO2	3.00×10 ⁻¹² exp(-1500.00/T)	1.96×10 ⁻¹⁴
42	R037	O3 + NO2 → NO3	1.20×10 ⁻¹³ exp(-2450.00/T)	3.24×10 ⁻¹⁷
43	R038	O3P + O2 + M → O3	6.10×10 ⁻³⁴ (T/300) ^{-2.40}	6.19×10 ⁻³⁴
44	R039	O3P + O3 →	8.00×10 ⁻¹² exp(-2060.00/T)	7.99×10 ⁻¹⁵
45	R040	O1D + O2 → O3P	3.30×10 ⁻¹¹ exp(55.00/T)	3.97×10 ⁻¹¹
46	R041	O1D + N2 → O3P	2.15×10 ⁻¹¹ exp(110.00/T)	3.11×10 ⁻¹¹
47	R042	O1D + H2O → 2.000*HO	1.63×10 ⁻¹⁰ exp(60.00/T)	1.99×10 ⁻¹⁰
48	R043	HO + H2 → HO2	2.80×10 ⁻¹² exp(-1800.00/T)	6.69×10 ⁻¹⁵



N	CMAQ Label	Reaction	Rate Constant Formula ^{a,b,c}	k (molec cm ⁻³ sec ⁻¹ or s ⁻¹)
49	R044	HO + HO ₂ →	$4.80 \times 10^{-11} \exp(250.00/T)$	1.11×10^{-10}
50	R045	HO ₂ + HO ₂ → H ₂ O ₂	$k_0 = 3.00 \times 10^{-13} \exp(460.0/T)$; $k_1 = 2.10 \times 10^{-33} \exp(920.0/T)$	2.53×10^{-12}
51	R046	HO ₂ + HO ₂ + H ₂ O → H ₂ O ₂	$k_0 = 4.20 \times 10^{-34} \exp(2660.0/T)$; $k_1 = 2.94 \times 10^{-54} \exp(3120.0/T)$	5.68E-30
52	R047	H ₂ O ₂ + HO → HO ₂	$1.80 \times 10^{-12} \exp(0.00/T)$	1.80×10^{-12}
53	R048	NO + O ₃ P → NO ₂	$k_0 = 9.10 \times 10^{-32} \exp(0.0/T)(T/300)^{-1.50}$; $k_i = 3.00 \times 10^{-11} \exp(0.0/T)(T/300)^{0.00}$; $n = 1.00$; $F = 0.60$	1.68×10^{-12}
54	R049	NO + HO → HONO	$k_0 = 7.10 \times 10^{-31} \exp(0.0/T)(T/300)^{-2.60}$; $k_i = 3.60 \times 10^{-11} \exp(0.0/T)(T/300)^{-0.10}$; $n = 1.00$; $F = 0.60$	7.46×10^{-12}
55	R050	NO + HO ₂ → NO ₂ + HO	$3.44 \times 10^{-12} \exp(260.00/T)$	8.23×10^{-12}
56	R051	NO + HO ₂ → HNO ₃	$k_0 = 6.0950 \times 10^{-14} \exp(270.0/T)(T/300)^{-1.00}$; $k_2 = 6.8570 \times 10^{-34} \exp(270.0/T)(T/300)^{1.00}$; $k_3 = -5.9680 \times 10^{-14} \exp(270.0/T)$	4.56×10^{-14}
57	R052	NO + NO + O ₂ → 2.000*NO ₂	$4.25 \times 10^{-39} \exp(663.50/T)$	3.93E-38
58	R053	HONO + HO → NO ₂	$3.00 \times 10^{-12} \exp(250.00/T)$	6.94×10^{-12}
59	R054	NO ₂ + O ₃ P → NO	$5.30 \times 10^{-12} \exp(200.00/T)$	1.04×10^{-11}
60	R055	NO ₂ + O ₃ P → NO ₃	$k_0 = 3.40 \times 10^{-31} \exp(0.0/T)(T/300)^{-1.60}$; $k_i = 2.30 \times 10^{-11} \exp(0.0/T)(T/300)^{-0.20}$; $n = 1.00$; $F = 0.60$	4.02×10^{-12}
61	R056	NO ₂ + HO → HNO ₃	$k_0 = 1.80 \times 10^{-30} \exp(0.0/T)(T/300)^{-3.00}$; $k_i = 2.80 \times 10^{-11} \exp(0.0/T)(T/300)^{0.00}$; $n = 1.00$; $F = 0.60$	1.06×10^{-11}
62	R057	HNO ₃ + HO → NO ₃	$k_0 = 2.40 \times 10^{-14} \exp(460.0/T)$; $k_1 = 2.70 \times 10^{-17} \exp(2199.0/T)$; $k_3 = 6.50 \times 10^{-34} \exp(1335.0/T)$	1.54×10^{-13}
63	R058	NO ₃ + HO → HO ₂ + NO ₂	2.00×10^{-11}	2.00×10^{-11}
64	R059	NO ₃ + HO ₂ → 0.700*HO + 0.700*NO ₂ + 0.300*HNO ₃	3.50×10^{-12}	3.50×10^{-12}
65	R060	NO ₃ + NO → 2.000*NO ₂	$1.70 \times 10^{-11} \exp(125.00/T)$	2.59×10^{-11}
66	R061	NO ₃ + NO ₂ → NO + NO ₂	$4.35 \times 10^{-14} \exp(-1335.00/T)$	4.94×10^{-16}
67	R062	NO ₃ + NO ₃ → 2.000*NO ₂	$8.50 \times 10^{-13} \exp(-2450.00/T)$	2.29×10^{-16}
68	R063	NO ₃ + NO ₂ → N ₂ O ₅	$k_0 = 2.40 \times 10^{-30} \exp(0.0/T)(T/300)^{-3.00}$; $k_i = 1.60 \times 10^{-12} \exp(0.0/T)(T/300)^{0.10}$; $n = 1.00$; $F = 0.60$	1.35×10^{-12}
69	R064	N ₂ O ₅ → NO ₂ + NO ₃	$1.72 \times 10^{26} \exp(-10840.00/T)$ *R063	3.76E-28



N	CMAQ Label	Reaction	Rate Constant Formula ^{a,b,c}	k (molec cm ⁻³ sec ⁻¹ or s ⁻¹)
70	R065	N ₂ O ₅ + H ₂ O → 2.000*HNO ₃	1.00E-22	1.00E-22
71	R066	NO ₂ + HO ₂ → HNO ₄	ko= 1.90E-31exp(0.0/T)(T/300) ^{-3.40} ; ki = 4.00×10 ⁻¹² exp(0.0/T)(T/300) ^{-0.30} ; n= 1.00;F= 0.60	1.31×10 ⁻¹²
	R067 ^d	HNO ₄ → HO ₂ + NO ₂	4.76×10 ²⁶ exp(-10900.00/T) *R066	8.28E-28
73	R068	HNO ₄ + HO → NO ₂	4.50×10 ⁻¹³ exp(610.00/T)	3.48×10 ⁻¹²
74	R069	SO ₂ + HO → HO ₂ + SULF + SULRXN	ko= 2.90E-31exp(0.0/T)(T/300) ^{-4.10} ; ki = 1.70×10 ⁻¹² exp(0.0/T)(T/300) ^{0.20} ; n= 1.00;F= 0.60	9.58×10 ⁻¹³
	R070	CO + HO → HO ₂	k ₀ = 1.44×10 ⁻¹³ exp(0.0/T); k ₁ = 2.74×10 ⁻³³ exp(0.0/T); 2.45×10 ⁻¹² exp(-1775.00/T)	2.11×10 ⁻¹³
76	R071	HO + CH ₄ → MO ₂	2.45×10 ⁻¹² exp(-1775.00/T)	6.36×10 ⁻¹⁵
77	R072	ETH + HO → ETHP	7.66×10 ⁻¹² exp(-1020.00/T)	2.50×10 ⁻¹³
78	R073	HC ₃ + HO → HC ₃ P + 0.000*ASOATJ	7.68×10 ⁻¹² exp(-370.00/T)	2.22×10 ⁻¹²
79	R074	HC ₅ + HO → HC ₅ P + 0.001*ASOATJ	1.01×10 ⁻¹¹ exp(-245.00/T)	4.44×10 ⁻¹²
80	R076	ETE + HO → ETEP	ko= 1.00E-28exp(0.0/T)(T/300) ^{-4.50} ; ki = 8.80×10 ⁻¹² exp(0.0/T)(T/300) ^{-0.85} ; n= 1.00;F= 0.60	8.20×10 ⁻¹²
	R077	OLT + HO → OLTP	5.72×10 ⁻¹² exp(500.00/T)	3.06×10 ⁻¹¹
82	R078	OLI + HO → OLIP	1.33×10 ⁻¹¹ exp(500.00/T)	7.11×10 ⁻¹¹
83	R080	ACE + HO → 0.650*HO + 0.350*HO ₂ + 0.350*CO + 0.650*GLY + 0.350*ORA1	ko= 5.50E-30exp(0.0/T)(T/300) ^{0.00} ; ki = 8.30×10 ⁻¹³ exp(0.0/T)(T/300) ^{2.00} ; n= 1.00;F= 0.60	7.47×10 ⁻¹³
	ROCARO31	BEN + HO → 0.470*BENP + 0.530*PHEN + 0.530*HO ₂	2.33×10 ⁻¹² exp(-193.00/T)	1.22×10 ⁻¹²
85	ROCARO41	TOL + HO → 0.820*TOLP + 0.180*CSL + 0.180*HO ₂	1.81×10 ⁻¹² exp(354.00/T)	5.93×10 ⁻¹²
86	ROCARO51	XYM + HO → 0.830*XYMP + 0.170*CSL + 0.170*HO ₂	2.33×10 ⁻¹¹	2.33×10 ⁻¹¹
87	ROCARO61	XYE + HO → 0.820*XYEP + 0.180*CSL + 0.180*HO ₂	7.16×10 ⁻¹²	7.16×10 ⁻¹²
88	R086	ISO + HO → ISOP	2.70×10 ⁻¹¹ exp(390.00/T)	9.99×10 ⁻¹¹
89	R087	API + HO → 0.975*APIP1 + 0.025*APIP2	1.21×10 ⁻¹¹ exp(440.00/T)	5.29×10 ⁻¹¹
90	R088	LIM + HO → 0.945*LIMP1 + 0.055*LIMP2	4.20×10 ⁻¹¹ exp(401.00/T)	1.61×10 ⁻¹⁰
91	TRP04	PINAL + HO → 0.230*PINALP + 0.770*RCO ₃	5.20×10 ⁻¹² exp(600.00/T)	3.89×10 ⁻¹¹
92	TRP05	LIMAL + HO → 0.700*LIMALP + 0.300*RCO ₃	1.00×10 ⁻¹⁰	1.00×10 ⁻¹⁰
93	R089	HCHO + HO → HO ₂ + CO	5.50×10 ⁻¹² exp(125.00/T)	8.36×10 ⁻¹²
94	R090	ACD + HO → ACO ₃	4.70×10 ⁻¹² exp(345.00/T)	1.50×10 ⁻¹¹
95	R091	ALD + HO → RCO ₃	4.90×10 ⁻¹² exp(405.00/T)	1.91×10 ⁻¹¹
96	R092	ACT + HO → ACTP	4.56×10 ⁻¹⁴ exp(-427.00/T)(T/300) ^{3.65}	1.06×10 ⁻¹⁴
97	R093	MEK + HO → MEKP	1.50×10 ⁻¹² exp(-90.00/T)	1.11×10 ⁻¹²
98	R094	KET + HO → KETP	2.80×10 ⁻¹² exp(10.00/T)	2.90×10 ⁻¹²
99	R095	HKET + HO → HO ₂ + MGLY	3.00×10 ⁻¹²	3.00×10 ⁻¹²
100	R096	MACR + HO → 0.570*MACP + 0.430*MCP	8.00×10 ⁻¹² exp(380.00/T)	2.86×10 ⁻¹¹
101	R097	MVK + HO → MVKP	2.60×10 ⁻¹² exp(610.00/T)	2.01×10 ⁻¹¹



N	CMAQ Label	Reaction	Rate Constant Formula ^{a,b,c}	k (molec cm ⁻³ sec ⁻¹ or s ⁻¹)
102	R098	UALD + HO → 0.313*ACO3 + 0.687*UALP	5.77×10 ⁻¹² exp(533.00/T)	3.45×10 ⁻¹¹
103	R099	GLY + HO → HO2 + 2.000*CO	1.10×10 ⁻¹¹	1.10×10 ⁻¹¹
104	R100	MGLY + HO → ACO3 + CO	9.26×10 ⁻¹³ exp(830.00/T)	1.50×10 ⁻¹¹
105	R101	DCB1 + HO → 0.520*HO2 + 0.330*CO + 0.400*ALD + 0.780*KET + 0.100*GLY + 0.010*MGLY	2.80×10 ⁻¹¹ exp(175.00/T)	5.04×10 ⁻¹¹
106	R102	DCB2 + HO → 0.520*HO2 + 0.330*CO + 0.130*MEK + 0.100*GLY + 0.010*MGLY + 0.780*OP2	2.80×10 ⁻¹¹ exp(175.00/T)	5.04×10 ⁻¹¹
107	R103	DCB3 + HO → 0.560*HO2 + 0.210*MACP + 0.110*CO + 0.270*GLY + 0.010*MGLY + 0.790*OP2	1.00×10 ⁻¹¹	1.00×10 ⁻¹¹
108	R104	BALD + HO → BALP	5.32×10 ⁻¹² exp(243.00/T)	1.20×10 ⁻¹¹
109	R105	PHEN + HO → 0.152*ASOATJ + 0.619*HO2 + 0.170*ADDC + 0.059*CHO + 0.619*MCT	6.75×10 ⁻¹² exp(405.00/T)	2.63×10 ⁻¹¹
110	R106	CSL + HO → 0.200*ASOATJ + 0.584*HO2 + 0.160*ADDC + 0.056*CHO + 0.584*MCT	4.65×10 ⁻¹¹ exp(0.00/T)	4.65×10 ⁻¹¹
111	R108	MCT + HO → MCTO	2.05×10 ⁻¹⁰ exp(0.00/T)	2.05×10 ⁻¹⁰
112	R109	MOH + HO → HO2 + HCHO	2.85×10 ⁻¹² exp(-345.00/T)	8.96×10 ⁻¹³
113	R110	EOH + HO → HO2 + ACD	3.00×10 ⁻¹² exp(20.00/T)	3.21×10 ⁻¹²
114	R111	ROH + HO → HO2 + 0.719*ALD + 0.184*ACD	2.60×10 ⁻¹² exp(200.00/T)	5.09×10 ⁻¹²
115	R112	ETEG + HO → HO2 + ALD	1.47×10 ⁻¹¹	1.47×10 ⁻¹¹
116	R113	OP1 + HO → 0.350*HO + 0.650*MO2 + 0.350*HCHO	2.90×10 ⁻¹² exp(190.00/T)	5.48×10 ⁻¹²
117	R114	OP2 + HO → 0.010*HO + 0.440*HC3P + 0.070*XO2 + 0.080*ALD + 0.410*KET	3.40×10 ⁻¹² exp(190.00/T)	6.43×10 ⁻¹²
118	TRP06	OPB + HO → 0.010*HO + 0.440*HC10P + 0.070*XO2 + 0.080*ALD + 0.410*KET	3.40×10 ⁻¹² exp(190.00/T)	6.43×10 ⁻¹²
119	R114a	OP3 + HO → 0.010*HO + 0.440*HC10P + 0.070*XO2 + 0.080*ALD + 0.410*KET	3.40×10 ⁻¹² exp(190.00/T)	6.43×10 ⁻¹²
120	R115	ISHP + HO → HO + MACR + 0.904*IEPOX	1.00×10 ⁻¹⁰	1.00×10 ⁻¹⁰
121	R116	MAHP + HO → MACP	3.00×10 ⁻¹¹	3.00×10 ⁻¹¹
122	R117	ORA1 + HO → HO2	4.50×10 ⁻¹³	4.50×10 ⁻¹³
123	R118	ORA2 + HO → 0.640*MO2 + 0.360*ORAP	4.00×10 ⁻¹⁴ exp(850.00/T)	6.92×10 ⁻¹³
124	R119	PAA + HO → 0.350*HO + 0.650*ACO3 + 0.350*XO2 + 0.350*HCHO	2.93×10 ⁻¹² exp(190.00/T)	5.54×10 ⁻¹²
125	R120	PAN + HO → XO2 + NO3 + HCHO	4.00×10 ⁻¹⁴	4.00×10 ⁻¹⁴
126	R121	PPN + HO → XO2 + NO3 + HCHO	4.00×10 ⁻¹⁴	4.00×10 ⁻¹⁴
127	R122	MPAN + HO → NO2 + HKET	3.20×10 ⁻¹¹	3.20×10 ⁻¹¹
128	R123	ONIT + HO → HC3P + NO2	5.31×10 ⁻¹² exp(-260.00/T)	2.22×10 ⁻¹²
129	TRP07	TRPN + HO → HOM	4.80×10 ⁻¹²	4.80×10 ⁻¹²
130	R124	NALD + HO → NO2 + XO2 + HKET	5.60×10 ⁻¹² exp(270.00/T)	1.39×10 ⁻¹¹
131	R125	ISON + HO → NALD + 0.070*HKET + 0.070*HCHO	1.30×10 ⁻¹¹	1.30×10 ⁻¹¹
132	R126	ETE + O3 → 0.080*HO + 0.150*HO2 + 0.430*CO + HCHO + 0.370*ORA1	9.14×10 ⁻¹⁵ exp(-2580.00/T)	1.60×10 ⁻¹⁸
133	R127	OLT + O3 → 0.220*HO + 0.320*HO2 + 0.080*MO2 + 0.060*ETHP + 0.040*HC3P + 0.020*HC5P + 0.068*H2O2 + 0.430*CO + 0.020*ETH + 0.015*HC3 + 0.006*HC5 + 0.032*BEN + 0.560*HCHO + 0.010*ACD + 0.440*ALD + 0.030*ACT + 0.020*BALD + 0.060*MEK + 0.010*HKET + 0.030*ORA1 + 0.060*ORA2	4.33×10 ⁻¹⁵ exp(-1800.00/T)	1.03×10 ⁻¹⁷
134	R128	OLI + O3 → 0.460*HO + 0.070*HO2 + 0.320*MO2 + 0.070*ETHP + 0.040*HC3P + 0.090*ACO3 + 0.370*CO + 0.026*H2O2 + 0.010*ETH + 0.010*HC3 + 0.090*HCHO + 0.457*ACD + 0.730*ALD + 0.110*ACT + 0.017*KET + 0.044*HKET + 0.017*ORA2	4.40×10 ⁻¹⁵ exp(-845.00/T)	2.59×10 ⁻¹⁶



N	CMAQ Label	Reaction	Rate Constant Formula ^{a,b,c}	k (molec cm ⁻³ sec ⁻¹ or s ⁻¹)
135	R130	ISO + O3 → 0.250*HO + 0.250*HO2 + 0.080*MO2 + 0.100*ACO3 + 0.100*MACP + 0.090*H2O2 + 0.140*CO + 0.580*HCHO + 0.461*MACR + 0.189*MVK + 0.280*ORA1 + 0.153*OLT	7.86×10 ⁻¹⁵ exp(-1913.00/T)	1.29×10 ⁻¹⁷
136	R131	API + O3 → 0.900*HO + 0.900*APIP1 + 0.050*APIP2 + 0.050*PINAL + 0.050*H2O2 + 0.140*CO	5.00×10 ⁻¹⁶ exp(-530.00/T)	8.45×10 ⁻¹⁷
137	R132	LIM + O3 → 0.840*HO + 0.840*LIMP1 + 0.110*LIMP2 + 0.050*LIMAL + 0.050*H2O2 + 0.140*CO	2.95×10 ⁻¹⁵ exp(-783.00/T)	2.13×10 ⁻¹⁶
138	TRP08	LIMAL + O3 → 0.040*HO + 0.670*HC10P + 0.790*HCHO + 0.330*KET + 0.040*HO2 + 0.200*CO	8.30×10 ⁻¹⁸	8.30×10 ⁻¹⁸
139	TRP09	TRPN + O3 → HOM	1.67×10 ⁻¹⁶	1.67×10 ⁻¹⁶
140	R132	MACR + O3 → 0.190*HO + 0.140*HO2 + 0.100*ACO3 + 0.220*CO + 0.500*MGLY + 0.450*ORA1	1.36×10 ⁻¹⁵ exp(-2112.00/T)	1.14×10 ⁻¹⁸
141	R134	MVK + O3 → 0.160*HO + 0.110*HO2 + 0.280*ACO3 + 0.010*XO2 + 0.560*CO + 0.100*HCHO + 0.540*MGLY + 0.070*ORA1 + 0.070*ORA2 + 0.100*ALD	8.50×10 ⁻¹⁶ exp(-1520.00/T)	5.19×10 ⁻¹⁸
142	R135	UALD + O3 → 0.100*HO + 0.072*HO2 + 0.008*MO2 + 0.002*ACO3 + 0.100*XO2 + 0.243*CO + 0.080*HCHO + 0.420*ACD + 0.028*KET + 0.491*GLY + 0.003*MGLY + 0.044*ORA1	1.66×10 ⁻¹⁸	1.66×10 ⁻¹⁸
143	R136	DCB1 + O3 → 0.050*HO + HO2 + 0.600*RCO3 + 0.600*XO2 + 1.500*CO + 0.050*HCHO + 0.050*GLY + 0.080*MGLY + 0.650*OP2	2.00×10 ⁻¹⁶	2.00×10 ⁻¹⁶
144	R137	DCB2 + O3 → 0.050*HO + HO2 + 0.600*RCO3 + 0.600*XO2 + 1.500*CO + 0.050*HCHO + 0.050*GLY + 0.080*MGLY + 0.700*DCB1 + 0.650*OP2	2.00×10 ⁻¹⁶	2.00×10 ⁻¹⁶
145	R138	DCB3 + O3 → 0.050*HO + HO2 + 1.500*CO + 0.480*GLY + 0.700*DCB1 + 0.250*ORA1 + 0.250*ORA2 + 0.110*PAA	9.00×10 ⁻¹⁷	9.00×10 ⁻¹⁷
146	R140	MCTO + O3 → MCTP	2.86×10 ⁻¹³	2.86×10 ⁻¹³
147	R141	ETE + NO3 → 0.800*OLNN + 0.200*OLND	4.39×10 ⁻¹³ exp(-2282.00/T)(T/300) ^{2.00}	2.06×10 ⁻¹⁶
148	R142	OLT + NO3 → 0.430*OLNN + 0.570*OLND	1.79×10 ⁻¹³ exp(-450.00/T)	3.96×10 ⁻¹⁴
149	R143	OLI + NO3 → 0.110*OLNN + 0.890*OLND	8.64×10 ⁻¹³ exp(450.00/T)	3.91×10 ⁻¹²
150	R145	ISO + NO3 → ISON	3.03×10 ⁻¹² exp(-446.00/T)	6.79×10 ⁻¹³
151	R146	API + NO3 → 0.975*APIP1 + 0.025*APIP2	1.19×10 ⁻¹² exp(490.00/T)	6.16×10 ⁻¹²
152	R147	LIM + NO3 → 0.945*LIMNP1 + 0.055*LIMNP2	1.22×10 ⁻¹¹	1.22×10 ⁻¹¹
153	TRP10	TRPN + NO3 → HOM	3.15×10 ⁻¹⁴ exp(-448.00/T)	7.01×10 ⁻¹⁵
154	R148	HCHO + NO3 → HO2 + CO + HNO3	2.00×10 ⁻¹² exp(-2440.00/T)	5.58×10 ⁻¹⁶
155	R149	ACD + NO3 → ACO3 + HNO3	1.40×10 ⁻¹² exp(-1900.00/T)	2.39×10 ⁻¹⁵
156	R150	ALD + NO3 → RCO3 + HNO3	3.76×10 ⁻¹² exp(-1900.00/T)	6.42×10 ⁻¹⁵
157	R151	MACR + NO3 → 0.680*HCHO + 0.320*MACP + 0.680*XO2 + 0.680*MGLY + 0.320*HNO3 + 0.680*NO2	3.40×10 ⁻¹⁵	3.40×10 ⁻¹⁵
158	R152	UALD + NO3 → HO2 + XO2 + 0.668*CO + 0.332*HCHO + 0.332*ALD + ONIT	5.02×10 ⁻¹³ exp(-1076.00/T)	1.36×10 ⁻¹⁴
159	R153	GLY + NO3 → HO2 + 2.000*CO + HNO3	2.90×10 ⁻¹² exp(-1900.00/T)	4.95×10 ⁻¹⁵
160	R154	MGLY + NO3 → ACO3 + CO + HNO3	3.76×10 ⁻¹² exp(-1900.00/T)	6.42×10 ⁻¹⁵
161	R155	PHEN + NO3 → 0.152*ASOATJ + 0.339*CHO + 0.850*ADDC + 0.424*ADCN + 0.424*HNO3	3.78×10 ⁻¹²	3.78×10 ⁻¹²
162	R156	CSL + NO3 → 0.200*ASOATJ + 0.320*CHO + 0.080*ADDC + 0.400*ADCN + 0.400*HNO3	1.06×10 ⁻¹²	1.06×10 ⁻¹²
163	R158	MCT + NO3 → MCTO + HNO3	2.01×10 ⁻¹⁰	2.01×10 ⁻¹⁰
164	R159	MPAN + NO3 → MACP + NO2	2.20×10 ⁻¹⁴ exp(-500.00/T)	4.11×10 ⁻¹⁵
165	TRP11	PINALP → HOM	1.00E+00	1.00E+00



N	CMAQ Label	Reaction	Rate Constant Formula ^{a,b,c}	k (molec cm ⁻³ sec ⁻¹ or s ⁻¹)
166	TRP12	LIMALP → HOM	1.00E+00	1.00E+00
167	R166	ACO3 + NO2 → PAN	ko= 9.70E-29exp(0.0/T)(T/300) ^{-5.60} ; ki = 9.30×10 ⁻¹² exp(0.0/T)(T/300) ^{-1.50} ; n=1.00;F= 0.60	8.68×10 ⁻¹²
	R167	PAN → ACO3 + NO2	1.11×10 ²⁸ e-14000.00/T) *R166	3.90×10 ⁻⁴⁸
169	R168	RCO3 + NO2 → PPN	ko= 9.70E-29exp(0.0/T)(T/300) ^{-5.60} ; ki = 9.30×10 ⁻¹² exp(0.0/T)(T/300) ^{-1.50} ; n= 1.00;F= 0.60	8.68×10 ⁻¹²
	R169	PPN → RCO3 + NO2	1.11×10 ²⁸ e-14000.00/T) *R168	3.90×10 ⁻⁴⁸
171	R170	MACP + NO2 → MPAN	2.80×10 ⁻¹² exp(181.00/T)	5.14×10 ⁻¹²
172	R171	MPAN → MACP + NO2	1.60×10 ¹⁶ exp(-13486.00/T)	3.63×10 ⁻⁰⁴
173	R172	MO2 + NO → HO2 + NO2 + HCHO	2.80×10 ⁻¹² exp(300.00/T)	7.66×10 ⁻¹²
174	R173	ETHP + NO → HO2 + NO2 + ACD	2.60×10 ⁻¹² exp(365.00/T)	8.84×10 ⁻¹²
175	R174	HC3P + NO → 0.660*HO2 + 0.131*MO2 + 0.048*ETHP + 0.089*XO2 + 0.935*NO2 + 0.504*ACD + 0.132*ALD + 0.165*ACT + 0.042*MEK + 0.065*ONIT	4.00×10 ⁻¹²	4.00×10 ⁻¹²
	R175	HC5P + NO → 0.200*HO2 + 0.051*MO2 + 0.231*ETHP + 0.235*XO2 + 0.864*NO2 + 0.018*HCHO + 0.045*ACD + 0.203*ALD + 0.033*MEK + 0.217*ACT + 0.033*KET + 0.272*HKET + 0.136*ONIT	4.00×10 ⁻¹²	4.00×10 ⁻¹²
177	R177	ETEP + NO → HO2 + NO2 + 1.600*HCHO + 0.200*ALD	9.00×10 ⁻¹²	9.00×10 ⁻¹²
178	R178	OLTP + NO → 0.780*HO2 + 0.970*NO2 + 0.780*HCHO + 0.012*ACD + 0.440*ALD + 0.060*ACT + 0.130*MEK + 0.030*ONIT	4.00×10 ⁻¹²	4.00×10 ⁻¹²
	R179	OLIP + NO → 0.830*HO2 + 0.950*NO2 + 0.810*ACD + 0.680*ALD + 0.200*ACT + 0.090*KET + 0.020*HKET + 0.050*ONIT	4.00×10 ⁻¹²	4.00×10 ⁻¹²
180	ROCARO33	BENP + NO → 0.000*ONIT + 0.001*VROCP4OXY2 + 0.001*VROCN1OXY6 + 0.998*NO2 + 0.998*HO2 + 0.000*BALD + 0.998*GLY + 0.499*FURANONE + 0.249*DCB2 + 0.249*DCB3	2.70×10 ⁻¹² exp(360.00/T)	9.03×10 ⁻¹²
181	ROCARO43	TOLP + NO → 0.000*ONIT + 0.001*VROCP4OXY2 + 0.001*VROCN1OXY6 + 0.998*NO2 + 0.998*HO2 + 0.085*BALD + 0.548*GLY + 0.365*MGLY + 0.365*FURANONE + 0.548*DCB1	2.70×10 ⁻¹² exp(360.00/T)	9.03×10 ⁻¹²
182	ROCARO53	XYMP + NO → 0.000*ONIT + 0.001*VROCP3OXY2 + 0.001*VROCP0OXY4 + 0.998*NO2 + 0.998*HO2 + 0.048*BALD + 0.703*GLY + 0.247*MGLY + 0.351*FURANONE + 0.598*DCB2	2.70×10 ⁻¹² exp(360.00/T)	9.03×10 ⁻¹²
183	ROCARO63	XYEP + NO → 0.000*ONIT + 0.001*VROCP3OXY2 + 0.001*VROCP0OXY4 + 0.998*NO2 + 0.998*HO2 + 0.085*BALD + 0.548*GLY + 0.365*MGLY + 0.456*FURANONE + 0.456*DCB2	2.70×10 ⁻¹² exp(360.00/T)	9.03×10 ⁻¹²
184	R188	ISOP + NO → 0.880*HO2 + 0.880*NO2 + 0.200*HCHO + 0.280*MACR + 0.440*MVK + 0.120*ISON + 0.021*GLY + 0.029*HKET + 0.027*ALD	2.43×10 ⁻¹² exp(360.00/T)	8.13×10 ⁻¹²
185	R189	APIP1 + NO → 0.820*HO2 + 0.820*NO2 + 0.820*PINAL + 0.180*TRPN	4.00×10 ⁻¹²	4.00×10 ⁻¹²
186	TRP13	APIP2 + NO → 0.820*HO + 0.820*NO2 + HOM	4.00×10 ⁻¹²	4.00×10 ⁻¹²



N	CMAQ Label	Reaction	Rate Constant Formula ^{a,b,c}	k (molec cm ⁻³ sec ⁻¹ or s ⁻¹)
187	TRP14	APINP1 + NO → 2.000*NO2 + PINAL	4.00×10 ⁻¹²	4.00×10 ⁻¹²
188	TRP15	APINP2 + NO → 0.820*NO2 + 0.820*HO + HOM	4.00×10 ⁻¹²	4.00×10 ⁻¹²
189	R190	LIMP1 + NO → 0.770*HO2 + 0.770*NO2 + 0.490*LIMAL + 0.280*HCHO + 0.280*UALD + 0.230*TRPN	4.00×10 ⁻¹²	4.00×10 ⁻¹²
190	TRP16	LIMP2 + NO → 0.770*HO + 0.770*NO2 + HOM	4.00×10 ⁻¹²	4.00×10 ⁻¹²
191	TRP17	LIMNP1 + NO → 2.000*NO2 + LIMAL	4.00×10 ⁻¹²	4.00×10 ⁻¹²
192	TRP18	LIMNP2 + NO → 0.770*NO2 + 0.770*HO + HOM	4.00×10 ⁻¹²	4.00×10 ⁻¹²
193	TRP19	PINALP + NO → 0.950*HO2 + 0.950*NO2 + 0.050*TRPN + 0.950*HCHO + 0.950*KET	2.70×10 ⁻¹² exp(360.00/T)	9.03×10 ⁻¹²
194	TRP20	LIMALP + NO → 0.940*HO2 + 0.940*NO2 + 0.060*TRPN + 0.940*HCHO + 0.940*KET	2.70×10 ⁻¹² exp(360.00/T)	9.03×10 ⁻¹²
195	R191	ACO3 + NO → MO2 + NO2	8.10×10 ⁻¹² exp(270.00/T)	2.00×10 ⁻¹¹
196	R192	RCO3 + NO → EHP + NO2	8.10×10 ⁻¹² exp(270.00/T)	2.00×10 ⁻¹¹
197	R193	ACTP + NO → ACO3 + NO2 + HCHO	2.90×10 ⁻¹² exp(300.00/T)	7.93×10 ⁻¹²
198	R194	MEKP + NO → 0.670*HO2 + NO2 + 0.330*HCHO + 0.670*DCB1	4.00×10 ⁻¹²	4.00×10 ⁻¹²
199	R195	KETP + NO → 0.770*HO2 + 0.230*ACO3 + 0.160*XO2 + NO2 + 0.460*ALD + 0.540*MGLY	4.00×10 ⁻¹²	4.00×10 ⁻¹²
200	R196	MACP + NO → 0.650*MO2 + 0.350*ACO3 + NO2 + 0.650*CO + 0.650*HCHO	2.54×10 ⁻¹² exp(360.00/T)	8.50×10 ⁻¹²
201	R197	MCP + NO → NO2 + 0.500*HO2 + 0.500*HCHO + HKET	2.54×10 ⁻¹² exp(360.00/T)	8.50×10 ⁻¹²
202	R198	MVKP + NO → 0.300*HO2 + 0.700*ACO3 + 0.700*XO2 + NO2 + 0.300*HCHO + 0.700*ALD + 0.300*MGLY	2.54×10 ⁻¹² exp(360.00/T)	8.50×10 ⁻¹²
203	R199	UALP + NO → HO2 + NO2 + 0.610*CO + 0.030*HCHO + 0.270*ALD + 0.180*GLY + 0.700*KET + 0.210*MGLY	2.54×10 ⁻¹² exp(360.00/T)	8.50×10 ⁻¹²
204	R200	BALP + NO → BAL1 + NO2	4.00×10 ⁻¹²	4.00×10 ⁻¹²
205	R201	BAL1 + NO → BAL2 + NO2	4.00×10 ⁻¹²	4.00×10 ⁻¹²
206	R202	ADDC + NO → HO2 + NO2 + 0.320*HKET + 0.680*GLY + 0.680*OP2	2.70×10 ⁻¹² exp(360.00/T)	9.03×10 ⁻¹²
207	R203	MCTP + NO → MCTO + NO2	2.70×10 ⁻¹² exp(360.00/T)	9.03×10 ⁻¹²
208	R204	ORAP + NO → NO2 + GLY + HO2	4.00×10 ⁻¹²	4.00×10 ⁻¹²
209	R205	OLNN + NO → NO2 + HO2 + ONIT	4.00×10 ⁻¹²	4.00×10 ⁻¹²
210	R206	OLND + NO → 2.000*NO2 + 0.287*HCHO + 1.240*ALD + 0.464*KET	4.00×10 ⁻¹²	4.00×10 ⁻¹²
211	R207	ADCN + NO → 2.000*NO2 + GLY + OP2	2.70×10 ⁻¹² exp(360.00/T)	9.03×10 ⁻¹²
212	R208	XO2 + NO → NO2	4.00×10 ⁻¹²	4.00×10 ⁻¹²
213	R209	BAL2 + NO2 → ONIT	2.00×10 ⁻¹¹	2.00×10 ⁻¹¹
214	R210	CHO + NO2 → ONIT	2.00×10 ⁻¹¹	2.00×10 ⁻¹¹
215	R211	MCTO + NO2 → ONIT	2.08×10 ⁻¹²	2.08×10 ⁻¹²
216	R212	MO2 + HO2 → OP1	4.10×10 ⁻¹³ exp(750.00/T)	5.07×10 ⁻¹²
217	R213	EHP + HO2 → OP2	7.50×10 ⁻¹³ exp(700.00/T)	7.85×10 ⁻¹²
218	R214	HC3P + HO2 → OP2	1.66×10 ⁻¹³ exp(1300.00/T)	1.30×10 ⁻¹¹
219	R215	HC5P + HO2 → OP2	1.66×10 ⁻¹³ exp(1300.00/T)	1.30×10 ⁻¹¹
220	R217	EHP + HO2 → OP2	1.90×10 ⁻¹³ exp(1300.00/T)	1.49×10 ⁻¹¹
221	R218	OLTP + HO2 → OP2	1.66×10 ⁻¹³ exp(1300.00/T)	1.30×10 ⁻¹¹
222	R219	OLIP + HO2 → OP2	1.66×10 ⁻¹³ exp(1300.00/T)	1.30×10 ⁻¹¹
223	ROCARO32	BENP + HO2 → 0.602*OP2 + 0.398*VROCN1OXY6	2.91×10 ⁻¹³ exp(1300.00/T)	2.28×10 ⁻¹¹
224	ROCARO42	TOLP + HO2 → 0.720*OP2 + 0.281*VROCN1OXY6	2.91×10 ⁻¹³ exp(1300.00/T)	2.28×10 ⁻¹¹
225	ROCARO52	XYMP + HO2 → 0.048*OP2 + 0.675*OP3 + 0.277*VROCP0OXY4	2.91×10 ⁻¹³ exp(1300.00/T)	2.28×10 ⁻¹¹
226	ROCARO62	XYEP + HO2 → 0.085*OP2 + 0.634*OP3 + 0.281*VROCP0OXY4	2.91×10 ⁻¹³ exp(1300.00/T)	2.28×10 ⁻¹¹
227	R228	ISOP + HO2 → ISHP	2.05×10 ⁻¹³ exp(1300.00/T)	1.60×10 ⁻¹¹
228	R229	APIP1 + HO2 → OPB	1.50×10 ⁻¹¹	1.50×10 ⁻¹¹



N	CMAQ Label	Reaction	Rate Constant Formula ^{a,b,c}	k (molec cm ⁻³ sec ⁻¹ or s ⁻¹)
229	TRP21	APIP2 + HO2 → HOM	1.50×10 ⁻¹¹	1.50×10 ⁻¹¹
230	TRP22	APINP1 + HO2 → TRPN	1.50×10 ⁻¹¹	1.50×10 ⁻¹¹
231	TRP23	APINP2 + HO2 → HOM	1.50×10 ⁻¹¹	1.50×10 ⁻¹¹
232	R230	LIMP1 + HO2 → OPB	1.50×10 ⁻¹¹	1.50×10 ⁻¹¹
233	TRP24	LIMP2 + HO2 → HOM	1.50×10 ⁻¹¹	1.50×10 ⁻¹¹
234	TRP25	LIMNP1 + HO2 → TRPN	1.50×10 ⁻¹¹	1.50×10 ⁻¹¹
235	TRP26	LIMNP2 + HO2 → HOM	1.50×10 ⁻¹¹	1.50×10 ⁻¹¹
236	TRP27	PINALP + HO2 → OPB	2.91×10 ⁻¹³ exp(1300.00/T)	2.28×10 ⁻¹¹
237	TRP28	LIMALP + HO2 → OPB	2.91×10 ⁻¹³ exp(1300.00/T)	2.28×10 ⁻¹¹
238	R231	ACO3 + HO2 → 0.440*HO + 0.440*MO2 + 0.150*ORA2 + 0.410*PAA	4.30×10 ⁻¹³ exp(1040.00/T)	1.41×10 ⁻¹¹
239	R232	RCO3 + HO2 → 0.440*HO + 0.440*ETHP + 0.150*ORA2 + 0.410*PAA	4.30×10 ⁻¹³ exp(1040.00/T)	1.41×10 ⁻¹¹
240	R233	ACTP + HO2 → 0.150*HO + 0.150*ACO3 + 0.150*HCHO + 0.850*OP2	1.15×10 ⁻¹³ exp(1300.00/T)	9.00×10 ⁻¹²
241	R234	MEKP + HO2 → OP2	1.15×10 ⁻¹³ exp(1300.00/T)	9.00×10 ⁻¹²
242	R235	KETP + HO2 → OP2	1.15×10 ⁻¹³ exp(1300.00/T)	9.00×10 ⁻¹²
243	R236	MACP + HO2 → MAHP	1.82×10 ⁻¹³ exp(1300.00/T)	1.42×10 ⁻¹¹
244	R237	MCP + HO2 → MAHP	1.82×10 ⁻¹³ exp(1300.00/T)	1.42×10 ⁻¹¹
245	R238	MVKP + HO2 → OP2	2.91×10 ⁻¹³ exp(1300.00/T)	2.28×10 ⁻¹¹
246	R239	UALP + HO2 → OP2	2.91×10 ⁻¹³ exp(1300.00/T)	2.28×10 ⁻¹¹
247	R240	ADDC + HO2 → OP2	3.75×10 ⁻¹³ exp(980.00/T)	1.00×10 ⁻¹¹
248	R241	CHO + HO2 → CSL	1.00×10 ⁻¹¹	1.00×10 ⁻¹¹
249	R242	MCTP + HO2 → OP2	3.75×10 ⁻¹³ exp(980.00/T)	1.00×10 ⁻¹¹
250	R243	ORAP + HO2 → OP2	1.15×10 ⁻¹³ exp(1300.00/T)	9.00×10 ⁻¹²
251	R244	OLNN + HO2 → ONIT	1.66×10 ⁻¹³ exp(1300.00/T)	1.30×10 ⁻¹¹
252	R245	OLND + HO2 → ONIT	1.66×10 ⁻¹³ exp(1300.00/T)	1.30×10 ⁻¹¹
253	R246	ADCN + HO2 → OP2	3.75×10 ⁻¹³ exp(980.00/T)	1.00×10 ⁻¹¹
254	R247	XO2 + HO2 → OP2	1.66×10 ⁻¹³ exp(1300.00/T)	1.30×10 ⁻¹¹
255	R248	MO2 + MO2 → 0.740*HO2 + 1.370*HCHO + 0.630*MOH	9.50×10 ⁻¹⁴ exp(390.00/T)	3.51×10 ⁻¹³
256	R249	ETHP + MO2 → HO2 + 0.750*HCHO + 0.750*ACD + 0.250*MOH + 0.250*EOH	1.18×10 ⁻¹³ exp(158.00/T)	2.00×10 ⁻¹³
257	R250	HC3P + MO2 → 0.894*HO2 + 0.080*MO2 + 0.026*ETHP + 0.026*XO2 + 0.827*HCHO + 0.198*ALD + 0.497*KET + 0.050*GLY + 0.250*MOH + 0.250*ROH	9.46×10 ⁻¹⁴ exp(431.00/T)	4.02×10 ⁻¹³
258	R251	HC5P + MO2 → 0.842*HO2 + 0.018*MO2 + 0.140*ETHP + 0.191*XO2 + 0.777*HCHO + 0.251*ALD + 0.618*KET + 0.250*MOH + 0.250*ROH	1.00×10 ⁻¹³ exp(467.00/T)	4.79×10 ⁻¹³
259	R253	ETEP + MO2 → HO2 + 1.950*HCHO + 0.150*ALD + 0.250*MOH + 0.250*ETEG	1.71×10 ⁻¹³ exp(708.00/T)	1.84×10 ⁻¹²
260	R254	OLTP + MO2 → HO2 + 1.500*HCHO + 0.705*ALD + 0.045*KET + 0.250*MOH + 0.250*ROH	1.46×10 ⁻¹³ exp(708.00/T)	1.57×10 ⁻¹²
261	R255	OLIP + MO2 → HO2 + 0.750*HCHO + 1.280*ALD + 0.218*KET + 0.250*MOH + 0.250*ROH	9.18×10 ⁻¹⁴ exp(708.00/T)	9.87×10 ⁻¹³
262	ROCARO35	BENP + MO2 → 0.680*HCHO + 1.370*HO2 + 0.320*MOH + 0.000*BALD + GLY + 0.500*FURANONE + 0.250*DCB2 + 0.250*DCB3	3.56×10 ⁻¹⁴ exp(708.00/T)	3.83×10 ⁻¹³
263	ROCARO45	TOLP + MO2 → 0.680*HCHO + 1.285*HO2 + 0.320*MOH + 0.085*BALD + 0.549*GLY + 0.366*MGLY + 0.366*FURANONE + 0.549*DCB1	3.56×10 ⁻¹⁴ exp(708.00/T)	3.83×10 ⁻¹³



N	CMAQ Label	Reaction	Rate Constant Formula ^{a,b,c}	k (molec cm ⁻³ sec ⁻¹ or s ⁻¹)
264	ROCARO55	XYMP + MO2 → 0.680*HCHO + 1.322*HO2 + 0.320*MOH + 0.048*BALD + 0.704*GLY + 0.247*MGLY + 0.352*FURANONE + 0.600*DCB2	3.56×10 ⁻¹⁴ exp(708.00/T)	3.83×10 ⁻¹³
265	ROCARO65	XYEP + MO2 → 0.680*HCHO + 1.285*HO2 + 0.320*MOH + 0.085*BALD + 0.549*GLY + 0.366*MGLY + 0.457*FURANONE + 0.457*DCB2	3.56×10 ⁻¹⁴ exp(708.00/T)	3.83×10 ⁻¹³
266	R264	ISOP + MO2 → HO2 + 1.310*HCHO + 0.159*MACR + 0.250*MVK + 0.250*MOH + 0.250*ROH + 0.023*ALD + 0.018*GLY + 0.016*HKET	3.40×10 ⁻¹⁴ exp(221.00/T)	7.14×10 ⁻¹⁴
267	R265	APIP1 + MO2 → HO2 + 0.680*HCHO + 0.600*PINAL + 0.070*KET + 0.320*MOH + 0.250*ROH	3.56×10 ⁻¹⁴ exp(708.00/T)	3.83×10 ⁻¹³
268	TRP29	APIP2 + MO2 → HO2 + 0.750*HCHO + 0.250*MOH + HOM	1.00×10 ⁻¹⁰	1.00×10 ⁻¹⁰
269	TRP30	APINP1 + MO2 → 0.370*HO2 + 0.860*NO2 + 0.680*HCHO + 0.860*PINAL + 0.320*MOH + 0.140*TRPN	3.56×10 ⁻¹⁴ exp(708.00/T)	3.83×10 ⁻¹³
270	TRP31	APINP2 + MO2 → 0.750*HO2 + 0.750*NO2 + 0.250*MOH + 0.750*HCHO + HOM	1.00×10 ⁻¹⁰	1.00×10 ⁻¹⁰
271	R266	LIMP1 + MO2 → HO2 + HCHO + 0.420*LIMAL + 0.300*KET + 0.320*MOH + 0.270*ROH	3.56×10 ⁻¹⁴ exp(708.00/T)	3.83×10 ⁻¹³
272	TRP32	LIMP2 + MO2 → HO2 + 0.750*HCHO + 0.250*MOH + HOM	1.00×10 ⁻¹⁰	1.00×10 ⁻¹⁰
273	TRP33	LIMNP1 + MO2 → 0.370*HO2 + 0.680*HCHO + 0.700*LIMAL + 0.700*NO2 + 0.320*MOH + 0.300*TRPN	3.56×10 ⁻¹⁴ exp(708.00/T)	3.83×10 ⁻¹³
274	TRP34	LIMNP2 + MO2 → 0.750*HO2 + 0.750*HCHO + 0.750*NO2 + 0.250*MOH + HOM	1.00×10 ⁻¹⁰	1.00×10 ⁻¹⁰
275	R267	ACO3 + MO2 → 0.900*HO2 + 0.900*MO2 + HCHO + 0.100*ORA2	2.00×10 ⁻¹¹ exp(500.00/T)	1.07×10 ⁻¹⁰
276	R268	RCO3 + MO2 → 0.900*HO2 + 0.900*MO2 + HCHO + 0.100*ORA2	2.00×10 ⁻¹¹ exp(500.00/T)	1.07×10 ⁻¹⁰
277	R269	ACTP + MO2 → 0.500*HO2 + 0.500*ACO3 + 1.500*HCHO + 0.250*MOH + 0.250*ROH + 0.125*ORA2	7.50×10 ⁻¹³ exp(500.00/T)	4.01×10 ⁻¹²
278	R270	MEKP + MO2 → 0.834*HO2 + HCHO + 0.334*DCB1 + 0.250*MOH + 0.250*ROH	6.91×10 ⁻¹³ exp(508.00/T)	3.80×10 ⁻¹²
279	R271	KETP + MO2 → HO2 + 0.750*HCHO + 0.500*DCB1 + 0.250*MOH + 0.250*ROH	6.91×10 ⁻¹³ exp(508.00/T)	3.80×10 ⁻¹²
280	R272	MACP + MO2 → 0.500*HO2 + 0.269*ACO3 + 0.500*CO + 1.660*HCHO + 0.067*ORA2 + 0.250*MO2 + 0.250*MOH + 0.250*ROH	3.40×10 ⁻¹⁴ exp(221.00/T)	7.14×10 ⁻¹⁴
281	R273	MCP + MO2 → NO2 + HO2 + 1.500*HCHO + 0.500*HKET + 0.250*MOH + 0.250*ROH	3.40×10 ⁻¹⁴ exp(221.00/T)	7.14×10 ⁻¹⁴
282	R274	MVKP + MO2 → HO2 + 1.160*ACO3 + 1.160*XO2 + 1.500*HCHO + 1.750*ALD + 0.500*MGLY + 0.250*MOH + 0.250*ROH + 0.292*ORA2	8.37×10 ⁻¹⁴	8.37×10 ⁻¹⁴
283	R275	UALP + MO2 → HO2 + 0.305*CO + 0.773*HCHO + 0.203*ALD + 0.525*KET + 0.135*GLY + 0.105*MGLY + 0.250*MOH + 0.250*ROH	3.40×10 ⁻¹⁴ exp(221.00/T)	7.14×10 ⁻¹⁴
284	R276	BALP + MO2 → HO2 + BAL1 + HCHO	3.56×10 ⁻¹⁴ exp(708.00/T)	3.83×10 ⁻¹³
285	R277	BAL1 + MO2 → HO2 + BAL2 + HCHO	3.56×10 ⁻¹⁴ exp(708.00/T)	3.83×10 ⁻¹³
286	R278	ADDC + MO2 → 2.000*HO2 + HCHO + 0.320*HKET + 0.680*GLY + 0.680*OP2	3.56×10 ⁻¹⁴ exp(708.00/T)	3.83×10 ⁻¹³
287	R279	MCTP + MO2 → HO2 + MCTO + HCHO	3.56×10 ⁻¹⁴ exp(708.00/T)	3.83×10 ⁻¹³
288	R280	ORAP + MO2 → HCHO + HO2 + GLY	7.50×10 ⁻¹³ exp(500.00/T)	4.01×10 ⁻¹²
289	R281	OLNN + MO2 → 2.000*HO2 + HCHO + ONIT	1.60×10 ⁻¹³ exp(708.00/T)	1.72×10 ⁻¹²



N	CMAQ Label	Reaction	Rate Constant Formula ^{a,b,c}	k (molec cm ⁻³ sec ⁻¹ or s ⁻¹)
290	R282	OLND + MO2 → 0.500*HO2 + 0.500*NO2 + 0.965*HCHO + 0.930*ALD + 0.348*KET + 0.250*MOH + 0.250*ROH + 0.500*ONIT	9.68×10 ⁻¹⁴ exp(708.00/T)	1.04×10 ⁻¹²
291	R283	ADCN + MO2 → HO2 + 0.700*NO2 + HCHO + 0.700*GLY + 0.700*OP2 + 0.300*ONIT	3.56×10 ⁻¹⁴	3.56×10 ⁻¹⁴
292	R284	XO2 + MO2 → HO2 + HCHO	5.99×10 ⁻¹⁵ exp(1510.00/T)	9.48×10 ⁻¹³
293	R285	ETHP + ACO3 → 0.500*HO2 + 0.500*MO2 + ACD + 0.500*ORA2	1.03×10 ⁻¹² exp(211.00/T)	2.09×10 ⁻¹²
294	R286	HC3P + ACO3 → 0.394*HO2 + 0.580*MO2 + 0.026*ETHP + 0.026*XO2 + 0.130*HCHO + 0.273*ALD + 0.662*KET + 0.067*GLY + 0.500*ORA2	6.90×10 ⁻¹³ exp(460.00/T)	3.23×10 ⁻¹²
295	R287	HC5P + ACO3 → 0.342*HO2 + 0.518*MO2 + 0.140*ETHP + 0.191*XO2 + 0.042*HCHO + 0.381*ALD + 0.824*KET + 0.500*ORA2	5.59×10 ⁻¹³ exp(522.00/T)	3.22×10 ⁻¹²
296	R289	ETEP + ACO3 → 0.500*HO2 + 0.500*MO2 + 1.600*HCHO + 0.200*ALD + 0.500*ORA2	9.48×10 ⁻¹³ exp(765.00/T)	1.23×10 ⁻¹¹
297	R290	OLTP + ACO3 → 0.500*HO2 + 0.500*MO2 + HCHO + 0.940*ALD + 0.060*KET + 0.500*ORA2	8.11×10 ⁻¹³ exp(765.00/T)	1.06×10 ⁻¹¹
298	R291	OLIP + ACO3 → 0.500*HO2 + 0.500*MO2 + 1.710*ALD + 0.290*KET + 0.500*ORA2	5.09×10 ⁻¹³ exp(765.00/T)	6.62×10 ⁻¹²
299	ROCARO36	BENP + ACO3 → 0.700*MO2 + HO2 + 0.300*ORA2 + 0.000*BALD + GLY + 0.500*FURANONE + 0.250*DCB2 + 0.250*DCB3	7.40×10 ⁻¹³ exp(765.00/T)	9.63×10 ⁻¹²
300	ROCARO46	TOLP + ACO3 → 0.700*MO2 + 0.915*HO2 + 0.300*ORA2 + 0.085*BALD + 0.549*GLY + 0.366*MGLY + 0.366*FURANONE + 0.549*DCB1	7.40×10 ⁻¹³ exp(765.00/T)	9.63×10 ⁻¹²
301	ROCARO56	XYMP + ACO3 → 0.700*MO2 + 0.952*HO2 + 0.300*ORA2 + 0.048*BALD + 0.704*GLY + 0.247*MGLY + 0.352*FURANONE + 0.600*DCB2	7.40×10 ⁻¹³ exp(765.00/T)	9.63×10 ⁻¹²
302	ROCARO66	XYEP + ACO3 → 0.700*MO2 + 0.915*HO2 + 0.300*ORA2 + 0.085*BALD + 0.549*GLY + 0.366*MGLY + 0.457*FURANONE + 0.457*DCB2	7.40×10 ⁻¹³ exp(765.00/T)	9.63×10 ⁻¹²
303	R300	ISOP + ACO3 → 0.500*HO2 + 0.500*MO2 + 1.048*HCHO + 0.219*MACR + 0.305*MVK + 0.500*ORA2	8.40×10 ⁻¹⁴ exp(221.00/T)	1.76×10 ⁻¹³
304	R301	APIP1 + ACO3 → 0.630*HO2 + 0.700*MO2 + 0.600*PINAL + 0.300*ORA2 + 0.070*KET + 0.250*ROH	7.40×10 ⁻¹³ exp(765.00/T)	9.63×10 ⁻¹²
305	TRP35	APIP2 + ACO3 → 0.500*HO2 + 0.500*MO2 + 0.500*ORA2 + HOM	1.00×10 ⁻¹⁰	1.00×10 ⁻¹⁰
306	TRP36	APINP1 + ACO3 → 0.860*NO2 + 0.140*TRPN + 0.860*PINAL + 0.700*MO2 + 0.300*ORA2	7.40×10 ⁻¹³ exp(765.00/T)	9.63×10 ⁻¹²
307	TRP37	APINP2 + ACO3 → 0.500*NO2 + 0.500*MO2 + 0.500*ORA2 + HOM	1.00×10 ⁻¹⁰	1.00×10 ⁻¹⁰
308	R302	LIMP1 + ACO3 → 0.630*HO2 + 0.700*MO2 + 0.420*LIMAL + 0.300*KET + 0.300*ORA2 + 0.320*HCHO + 0.270*ROH	7.40×10 ⁻¹³ exp(765.00/T)	9.63×10 ⁻¹²
309	TRP38	LIMP2 + ACO3 → 0.500*HO2 + 0.500*MO2 + 0.500*ORA2 + HOM	1.00×10 ⁻¹⁰	1.00×10 ⁻¹⁰
310	TRP39	LIMNP1 + ACO3 → 0.700*NO2 + 0.700*LIMAL + 0.300*TRPN + 0.700*MO2 + 0.300*ORA2	7.40×10 ⁻¹³ exp(765.00/T)	9.63×10 ⁻¹²
311	TRP40	LIMNP2 + ACO3 → 0.500*MO2 + 0.500*NO2 + 0.500*ORA2 + HOM	1.00×10 ⁻¹⁰	1.00×10 ⁻¹⁰
312	R303	ACO3 + ACO3 → 2.000*MO2	2.50×10 ⁻¹² exp(500.00/T)	1.34×10 ⁻¹¹
313	R304	RCO3 + ACO3 → MO2 + ETHP	2.50×10 ⁻¹² exp(500.00/T)	1.34×10 ⁻¹¹
314	R305	ACTP + ACO3 → 0.500*MO2 + 0.500*ACO3 + HCHO + 0.750*ORA2	7.51×10 ⁻¹³ exp(565.00/T)	5.00×10 ⁻¹²



N	CMAQ Label	Reaction	Rate Constant Formula ^{a,b,c}	k (molec cm ⁻³ sec ⁻¹ or s ⁻¹)
315	R306	MEKP + ACO3 → 0.330*HO2 + 0.500*MO2 + 0.330*HCHO + 0.334*DCB1 + 0.500*ORA2	7.51×10 ⁻¹³ exp(565.00/T)	5.00×10 ⁻¹²
316	R307	KETP + ACO3 → 0.500*HO2 + 0.500*MO2 + 0.500*DCB1 + 0.500*ORA2	7.51×10 ⁻¹³ exp(565.00/T)	5.00×10 ⁻¹²
317	R308	MACP + ACO3 → 0.635*ORA2 + 0.500*MO2 + 0.269*ACO3 + 0.500*CO + HCHO	8.40×10 ⁻¹⁴ exp(221.00/T)	1.76×10 ⁻¹³
318	R309	MCP + ACO3 → NO2 + 0.500*HO2 + HCHO + 0.500*HKET + 0.500*MO2 + 0.500*ORA2	8.40×10 ⁻¹⁴ exp(221.00/T)	1.76×10 ⁻¹³
319	R310	MVKP + ACO3 → 0.500*HO2 + 0.500*MO2 + 1.160*ACO3 + 1.160*XO2 + HCHO + 2.300*ALD + 0.500*MGLY + 1.083*ORA2	1.68×10 ⁻¹² exp(500.00/T)	8.99×10 ⁻¹²
320	R311	UALP + ACO3 → 0.500*HO2 + 0.500*MO2 + 0.500*CO + 0.030*HCHO + 0.270*ALD + 0.700*KET + 0.180*GLY + 0.105*MGLY + 0.500*ORA2	1.68×10 ⁻¹² exp(500.00/T)	8.99×10 ⁻¹²
321	R312	BALP + ACO3 → MO2 + BAL1	7.40×10 ⁻¹³ exp(765.00/T)	9.63×10 ⁻¹²
322	R313	BAL1 + ACO3 → MO2 + BAL2	7.40×10 ⁻¹³ exp(765.00/T)	9.63×10 ⁻¹²
323	R314	ADDC + ACO3 → 2.000*HO2 + MO2 + 0.320*HKET + 0.680*GLY + 0.680*OP2	7.40×10 ⁻¹³ exp(708.00/T)	7.95×10 ⁻¹²
324	R315	MCTP + ACO3 → HO2 + MO2 + MCTO	7.40×10 ⁻¹³ exp(708.00/T)	7.95×10 ⁻¹²
325	R316	ORAP + ACO3 → MO2 + GLY	7.51×10 ⁻¹³ exp(565.00/T)	5.00×10 ⁻¹²
326	R317	OLNN + ACO3 → HO2 + MO2 + ONIT	8.85×10 ⁻¹³ exp(765.00/T)	1.15×10 ⁻¹¹
327	R318	OLND + ACO3 → 0.500*MO2 + NO2 + 0.287*HCHO + 1.240*ALD + 0.464*KET + 0.500*ORA2	5.37×10 ⁻¹³ exp(765.00/T)	6.99×10 ⁻¹²
328	R319	ADCN + ACO3 → HO2 + MO2 + 0.700*NO2 + 0.700*GLY + 0.700*OP2 + 0.300*ONIT	7.40×10 ⁻¹³ exp(708.00/T)	7.95×10 ⁻¹²
329	R320	XO2 + ACO3 → MO2	3.40×10 ⁻¹⁴ exp(1560.00/T)	6.37×10 ⁻¹²
330	R321	RCO3 + RCO3 → 2.000*ETHP	2.50×10 ⁻¹² exp(500.00/T)	1.34×10 ⁻¹¹
331	R322	MO2 + NO3 → HO2 + HCHO + NO2	1.20×10 ⁻¹²	1.20×10 ⁻¹²
332	R323	ETHP + NO3 → HO2 + NO2 + ACD	1.20×10 ⁻¹²	1.20×10 ⁻¹²
333	R324	HC3P + NO3 → 0.254*HO2 + 0.140*MO2 + 0.092*XO2 + 0.503*ETHP + NO2 + 0.519*ACD + 0.147*ALD + 0.075*MEK + 0.095*ACT	1.20×10 ⁻¹²	1.20×10 ⁻¹²
334	R325	HC5P + NO3 → 0.488*HO2 + 0.055*MO2 + 0.280*ETHP + 0.485*XO2 + NO2 + 0.024*HCHO + 0.241*ALD + 0.060*KET + 0.063*MEK + 0.247*ACT + 0.048*ACD + 0.275*HKET	1.20×10 ⁻¹²	1.20×10 ⁻¹²
335	R327	ETEP + NO3 → HO2 + NO2 + 1.600*HCHO + 0.200*ALD	1.20×10 ⁻¹²	1.20×10 ⁻¹²
336	R328	OLTP + NO3 → 0.470*ALD + 0.790*HCHO + 0.790*HO2 + NO2 + 0.180*MEK + 0.020*ACD + 0.090*ACT	1.20×10 ⁻¹²	1.20×10 ⁻¹²
337	R329	OLIP + NO3 → 0.860*HO2 + 0.720*ALD + 0.110*KET + NO2 + 0.200*ACT + 0.850*ACD + 0.040*HKET	1.20×10 ⁻¹²	1.20×10 ⁻¹²
338	ROCARO34	BENP + NO3 → NO2 + HO2 + 0.000*BALD + GLY + 0.500*FURANONE + 0.250*DCB2 + 0.250*DCB3	2.30×10 ⁻¹²	2.30×10 ⁻¹²
339	ROCARO44	TOLP + NO3 → NO2 + 0.915*HO2 + 0.085*BALD + 0.549*GLY + 0.366*MGLY + 0.366*FURANONE + 0.549*DCB1	2.30×10 ⁻¹²	2.30×10 ⁻¹²
340	ROCARO54	XYMP + NO3 → NO2 + 0.952*HO2 + 0.048*BALD + 0.704*GLY + 0.247*MGLY + 0.352*FURANONE + 0.600*DCB2	2.30×10 ⁻¹²	2.30×10 ⁻¹²
341	ROCARO64	XYEP + NO3 → NO2 + 0.915*HO2 + 0.085*BALD + 0.549*GLY + 0.366*MGLY + 0.457*FURANONE + 0.457*DCB2	2.30×10 ⁻¹²	2.30×10 ⁻¹²
342	R338	ISOP + NO3 → HO2 + NO2 + 0.750*HCHO + 0.318*MACR + 0.500*MVK + 0.024*GLY + 0.033*HKET + 0.031*ALD	1.20×10 ⁻¹²	1.20×10 ⁻¹²
343	R339	APIP1 + NO3 → HO2 + NO2 + ALD + KET	1.20×10 ⁻¹²	1.20×10 ⁻¹²
344	R340	LIMP1 + NO3 → HO2 + NO2 + 0.385*OLI + 0.385*HCHO + 0.615*MACR	1.20×10 ⁻¹²	1.20×10 ⁻¹²



N	CMAQ Label	Reaction	Rate Constant Formula ^{a,b,c}	k (molec cm ⁻³ sec ⁻¹ or s ⁻¹)
345	R341	ACO3 + NO3 → MO2 + NO2	4.00×10 ⁻¹²	4.00×10 ⁻¹²
346	R342	RCO3 + NO3 → ETHP + NO2	4.00×10 ⁻¹²	4.00×10 ⁻¹²
347	R343	ACTP + NO3 → ACO3 + NO2 + HCHO	1.20×10 ⁻¹²	1.20×10 ⁻¹²
348	R344	MEKP + NO3 → 0.670*HO2 + NO2 + 0.330*HCHO + 0.670*DCB1	1.20×10 ⁻¹²	1.20×10 ⁻¹²
349	R345	KETP + NO3 → HO2 + NO2 + DCB1	1.20×10 ⁻¹²	1.20×10 ⁻¹²
350	R346	MACP + NO3 → HCHO + 0.538*ACO3 + CO + NO2	1.20×10 ⁻¹²	1.20×10 ⁻¹²
351	R347	MCP + NO3 → NO2 + HO2 + HCHO + HKET	1.20×10 ⁻¹²	1.20×10 ⁻¹²
352	R348	MVKP + NO3 → 0.300*HO2 + 0.700*ACO3 + 0.700*XO2 + NO2 + 0.300*HCHO + 0.700*ALD + 0.300*MGLY	2.50×10 ⁻¹²	2.50×10 ⁻¹²
353	R349	UALP + NO3 → HO2 + NO2 + 0.610*CO + 0.030*HCHO + 0.270*ALD + 0.700*KET + 0.180*GLY + 0.210*MGLY	2.50×10 ⁻¹²	2.50×10 ⁻¹²
354	R350	BALP + NO3 → BAL1 + NO2	2.50×10 ⁻¹²	2.50×10 ⁻¹²
355	R351	BAL1 + NO3 → BAL2 + NO2	2.50×10 ⁻¹²	2.50×10 ⁻¹²
356	R352	ADDC + NO3 → HO2 + NO2 + 0.320*HKET + 0.680*GLY + 0.680*OP2	1.20×10 ⁻¹²	1.20×10 ⁻¹²
357	R353	MCTP + NO3 → NO2 + MCTO	1.20×10 ⁻¹²	1.20×10 ⁻¹²
358	R354	ORAP + NO3 → NO2 + GLY + HO2	1.20×10 ⁻¹²	1.20×10 ⁻¹²
359	R355	OLNN + NO3 → HO2 + NO2 + ONIT	1.20×10 ⁻¹²	1.20×10 ⁻¹²
360	R356	OLND + NO3 → 2.000*NO2 + 0.287*HCHO + 1.240*ALD + 0.464*KET	1.20×10 ⁻¹²	1.20×10 ⁻¹²
361	R357	ADCN + NO3 → 2.000*NO2 + GLY + OP2	1.20×10 ⁻¹²	1.20×10 ⁻¹²
362	R358	OLNN + OLNN → HO2 + 2.000*ONIT	7.00×10 ⁻¹⁴ exp(1000.00/T)	2.00×10 ⁻¹²
363	R359	OLNN + OLND → 0.500*HO2 + 0.500*NO2 + 0.202*HCHO + 0.640*ALD + 0.149*KET + 1.500*ONIT	4.25×10 ⁻¹⁴ exp(1000.00/T)	1.22×10 ⁻¹²
364	R360	OLND + OLND → NO2 + 0.504*HCHO + 1.210*ALD + 0.285*KET + ONIT	2.96×10 ⁻¹⁴ exp(1000.00/T)	8.47×10 ⁻¹³
365	R361	XO2 + NO3 → NO2	1.20×10 ⁻¹²	1.20×10 ⁻¹²
366	R362	XO2 + RCO3 → ETHP	2.50×10 ⁻¹² exp(500.00/T)	1.34×10 ⁻¹¹
367	R363	XO2 + XO2 →	7.13×10 ⁻¹⁷ exp(2950.00/T)	1.41×10 ⁻¹²
368	TRP41	APIP2 + APIP1 → 0.960*HOM + 0.480*ROH + 0.480*PINAL + 0.480*HO + 0.480*HO2 + 0.040*ELHOM	1.00×10 ⁻¹⁰	1.00×10 ⁻¹⁰
369	TRP42	APIP2 + LIMP1 → 0.960*HOM + 0.480*ROH + 0.480*LIMAL + 0.480*HO + 0.480*HO2 + 0.040*ELHOM	1.00×10 ⁻¹⁰	1.00×10 ⁻¹⁰
370	TRP43	APIP2 + ISOP → 0.960*HOM + 0.480*ROH + 0.480*HCHO + 0.480*MVK + 0.480*HO + 0.480*HO2 + 0.040*ELHOM	1.00×10 ⁻¹⁰	1.00×10 ⁻¹⁰
371	TRP44	LIMP2 + APIP1 → 0.960*HOM + 0.480*ROH + 0.480*PINAL + 0.480*HO + 0.480*HO2 + 0.040*ELHOM	1.00×10 ⁻¹⁰	1.00×10 ⁻¹⁰
372	TRP45	LIMP2 + LIMP1 → 0.960*HOM + 0.480*ROH + 0.480*LIMAL + 0.480*HO + 0.480*HO2 + 0.040*ELHOM	1.00×10 ⁻¹⁰	1.00×10 ⁻¹⁰
373	TRP46	LIMP2 + ISOP → 0.960*HOM + 0.480*ROH + 0.480*HCHO + 0.480*MVK + 0.480*HO + 0.480*HO2 + 0.040*ELHOM	1.00×10 ⁻¹⁰	1.00×10 ⁻¹⁰
374	TRP47	APINP2 + APIP1 → 0.960*HOM + 0.480*ROH + 0.480*PINAL + 0.480*NO2 + 0.480*HO2 + 0.040*ELHOM	1.00×10 ⁻¹⁰	1.00×10 ⁻¹⁰
375	TRP48	APINP2 + LIMP1 → 0.960*HOM + 0.480*ROH + 0.480*LIMAL + 0.480*NO2 + 0.480*HO2 + 0.040*ELHOM	1.00×10 ⁻¹⁰	1.00×10 ⁻¹⁰
376	TRP49	APINP2 + ISOP → 0.960*HOM + 0.480*ROH + 0.480*HCHO + 0.480*MVK + 0.480*NO2 + 0.480*HO2 + 0.040*ELHOM	1.00×10 ⁻¹⁰	1.00×10 ⁻¹⁰
377	TRP50	LIMNP2 + APIP1 → 0.960*HOM + 0.480*ROH + 0.480*PINAL + 0.480*NO2 + 0.480*HO2 + 0.040*ELHOM	1.00×10 ⁻¹⁰	1.00×10 ⁻¹⁰
378	TRP51	LIMNP2 + LIMP1 → 0.960*HOM + 0.480*ROH + 0.480*LIMAL + 0.480*NO2 + 0.480*HO2 + 0.040*ELHOM	1.00×10 ⁻¹⁰	1.00×10 ⁻¹⁰



N	CMAQ Label	Reaction	Rate Constant Formula ^{a,b,c}	k (molec cm ⁻³ sec ⁻¹ or s ⁻¹)
379	TRP52	LIMNP2 + ISOP → 0.960*HOM + 0.480*ROH + 0.480*HCHO + 0.480*MVK + 0.480*NO2 + 0.480*HO2 + 0.040*ELHOM	1.00×10 ⁻¹⁰	1.00×10 ⁻¹⁰
380	SA14	IEPOX + HO → HO	5.78×10 ⁻¹¹ exp(-400.00/T)	1.51×10 ⁻¹¹
381	R001c	VROCIIOXY + HO → 0.852*ETHP + 0.149*ASOATJ	6.89×10 ⁻¹²	6.89×10 ⁻¹²
382	R002c	SLOWROC + HO → ETHP + 0.001*ASOATJ	6.55×10 ⁻¹⁴	6.55×10 ⁻¹⁴
383	T17	ACRO + HO → 0.570*MACP + 0.430*MCP	8.00×10 ⁻¹² exp(380.00/T)	2.86×10 ⁻¹¹
384	T18	ACRO + O3 → 0.840*CO + 0.560*HO2 + 0.280*HO + 0.720*HCHO + 0.620*GLY	2.90E-19	2.90E-19
385	T19	ACRO + NO3 → 0.680*HCHO + 0.320*MACP + 0.680*XO2 + 0.680*MGLY + 0.320*HNO3 + 0.680*NO2	3.40×10 ⁻¹⁵	3.40×10 ⁻¹⁵
386	T20	ACRO → CO + 0.477*HO2 + 0.250*ETE + 0.354*ACO3 + 0.204*HO + 0.150*HCHO + 0.027*MO2	φ from MVK (Atkinson et al., 2006; Gierczak et al., 1997), σ from Sander et al. (2006) as implemented by Hutzell et al. (2012)	Not Available
387	T10	BDE13 + HO → 0.667*BDE13P + 0.333*UALD + 0.333*HO2	1.48×10 ⁻¹¹ exp(448.00/T)	6.65×10 ⁻¹¹
388	T10a	BDE13P + NO → 0.968*HO2 + 0.968*NO2 + 0.895*ACRO + 0.895*HCHO + 0.072*FURAN + 0.032*ONIT	9.05×10 ⁻¹²	9.05×10 ⁻¹²
389	T10b	BDE13P + NO3 → HO2 + NO2 + 0.925*ACRO + 0.925*HCHO + 0.075*FURAN	2.30×10 ⁻¹²	2.30×10 ⁻¹²
390	T10c	BDE13P + HO2 → OP2	1.61×10 ⁻¹¹	1.61×10 ⁻¹¹
391	T10d	BDE13P + MO2 → 0.320*MOH + 1.143*HCHO + 0.870*HO2 + 0.463*ACRO + 0.250*OLT + 0.231*MVK + 0.037*FURAN + 0.019*UALD	2.39×10 ⁻¹²	2.39×10 ⁻¹²
392	T10e	BDE13P + ACO3 → 0.700*MO2 + 0.300*ORA2 + 0.800*HO2 + 0.740*ACRO + 0.740*HCHO + 0.185*MVK + 0.060*FURAN + 0.015*UALD	1.37×10 ⁻¹¹	1.37×10 ⁻¹¹
393	T11	BDE13 + O3 → 0.620*ACRO + 0.630*CO + 0.420*HO2 + 0.080*HO + 0.830*HCHO + 0.170*ETE	1.34×10 ⁻¹⁴ exp(-2283.00/T)	6.33×10 ⁻¹⁸
394	T12	BDE13 + NO3 → 0.900*OLNN + 0.100*OLND + 0.900*ACRO	1.00×10 ⁻¹³	1.00×10 ⁻¹³
395	R003c	FURAN + HO → 0.490*DCB1 + 0.490*HO2 + 0.510*FURANO2	5.01×10 ⁻¹¹	5.01×10 ⁻¹¹
396	R004c	FURANO2 + NO → 0.080*ONIT + 0.920*NO2 + 0.920*FURANONE + 0.750*HO2 + 0.170*MO2	2.70×10 ⁻¹² exp(360.00/T)	9.03×10 ⁻¹²
397	R005c	FURANO2 + HO2 → 0.600*OP2 + 0.400*FURANONE + 0.400*HO + 0.320*HO2 + 0.080*MO2	3.75×10 ⁻¹³ exp(980.00/T)	1.00×10 ⁻¹¹
398	R006c	FURANONE + HO → 0.650*KET + 0.310*GLY + 0.660*HO2 + 0.340*MO2 + 0.430*CO + 0.040*ASOATJ	4.40×10 ⁻¹¹	4.40×10 ⁻¹¹
399	R007c	FURAN + O3 → 0.020*HO + ALD	3.43×10 ⁻¹⁷	3.43×10 ⁻¹⁷
400	R008c	FURAN + NO3 → NO2 + 0.800*DCB1 + 0.200*DCB3	8.99×10 ⁻¹²	8.99×10 ⁻¹²
401	R010c	PROG + HO → 0.613*HKET + 0.387*ALD + HO2	1.20×10 ⁻¹¹	1.20×10 ⁻¹¹
402	R011c	SESQ + NO3 → SESQNRO2	1.90×10 ⁻¹¹	1.90×10 ⁻¹¹
403	R012c	SESQNRO2 + HO2 → VROCP0OXY4	2.84×10 ⁻¹³ exp(1300.00/T)	2.22×10 ⁻¹¹
404	R013c	SESQNRO2 + NO → VROCP3OXY2 + 2.000*NO2	2.70×10 ⁻¹² exp(360.00/T)	9.03×10 ⁻¹²
405	R014c	SESQNRO2 + NO3 → VROCP3OXY2 + 2.000*NO2	2.30×10 ⁻¹²	2.30×10 ⁻¹²
406	R015c	SESQ + O3 → 0.982*VROCP3OXY2 + 0.018*VROC2OXY2	1.20×10 ⁻¹⁴	1.20×10 ⁻¹⁴
407	R016c	SESQ + HO → SESQRO2	1.97×10 ⁻¹⁰	1.97×10 ⁻¹⁰
408	R017c	SESQRO2 + HO2 → VROCP0OXY2	2.84×10 ⁻¹³ exp(1300.00/T)	2.22×10 ⁻¹¹
409	R019c	SESQRO2 + NO3 → VROCP3OXY2	2.30×10 ⁻¹²	2.30×10 ⁻¹²
410	R020c	SESQRO2 + NO → 0.247*VROCP1OXY3 + 0.753*VROCP3OXY2 + 0.753*NO2	2.70×10 ⁻¹² exp(360.00/T)	9.03×10 ⁻¹²



N	CMAQ Label	Reaction	Rate Constant Formula ^{a,b,c}	k (molec cm ⁻³ sec ⁻¹ or s ⁻¹)
411	HET_GLY	GLY → AGLYJ	$\gamma=2.9 \times 10^{-3}$, based on Liggio et al. (2005) as implemented by Pye et al. (2015)	Not Available ^b
412	HET_MGLY	MGLY → AGLYJ	$\gamma=2.9 \times 10^{-3}$, based on Liggio et al. (2005) as implemented by Pye et al. (2015)	Not Available ^b
413	HET_N2O5	N2O5 → 2.000*HNO3	Davis et al. (2008) equation 15	Not Available ^b
414	HET_NO2	NO2 → 0.500*HONO + 0.500*HNO3	$\gamma\gamma=4 \times 10^{-4} \text{ m s}^{-1}$ (Vogel et al., 2003)	Not Available ^b
415	HAL_Ozone ^c	O3 →	$\min(6.701 \times 10^{-11} \exp(1.074 \times 10^{+1}P) + 3.415E-08 \exp(-6.713 \times 10^{-1}P), 2.000 \times 10^{-06})$	2.00×10^{-6}
416	HET_IEPOX	IEPOX → IEPOXP	Uptake coefficient calculated based on particle composition following Pye et al. (2013) with parameter updates of Pye et al. (2017)	Not Applicable ^b
417	HET_ISO3TE T	IEPOXP → AISO3NOSJ	Ratio of 2-methyltetrols+IEPOX-derived organonitrate formation rates to total condensed phase reaction rate	Not Applicable
418	HET_IEPOX OS	IEPOXP + ASO4J → AISO3OSJ	Ratio of Organosulfate formation rate to total IEPOX condensed phase reaction rate	Not Applicable
419	ROCALK1c	VROCP6ALK + HO → VROCP6ALKP	1.53×10^{-11}	1.53×10^{-11}
420	ROCALK2c	VROCP5ALK + HO → VROCP5ALKP	1.68×10^{-11}	1.68×10^{-11}
421	ROCALK3c	VROCP4ALK + HO → VROCP4ALKP	2.24×10^{-11}	2.24×10^{-11}
422	ROCALK4c	VROCP3ALK + HO → VROCP3ALKP	2.67×10^{-11}	2.67×10^{-11}
423	ROCALK5c	VROCP2ALK + HO → VROCP2ALKP	3.09×10^{-11}	3.09×10^{-11}
424	ROCALK6c	VROCP1ALK + HO → VROCP1ALKP	3.38×10^{-11}	3.38×10^{-11}
425	HC1001	HC10 + HO → HC10P	1.10×10^{-11}	1.10×10^{-11}
426	ROCALK7c	VROCP6ALKP + NO → 0.720*VROCP6ALKP2 + 0.280*VROCP4OXY2 + 0.720*NO2	$2.70 \times 10^{-12} \exp(360.00/T)$	9.03×10^{-12}
427	ROCALK8c	VROCP5ALKP + NO → 0.720*VROCP5ALKP2 + 0.280*VROCP3OXY2 + 0.720*NO2	$2.70 \times 10^{-12} \exp(360.00/T)$	9.03×10^{-12}
428	ROCALK9c	VROCP4ALKP + NO → 0.720*VROCP4ALKP2 + 0.280*VROCP2OXY2 + 0.720*NO2	$2.70 \times 10^{-12} \exp(360.00/T)$	9.03×10^{-12}
429	ROCALK10c	VROCP3ALKP + NO → 0.720*VROCP3ALKP2 + 0.280*VROCP1OXY1 + 0.720*NO2	$2.70 \times 10^{-12} \exp(360.00/T)$	9.03×10^{-12}
430	ROCALK11c	VROCP2ALKP + NO → 0.720*VROCP2ALKP2 + 0.280*VROCP0OXY2 + 0.720*NO2	$2.70 \times 10^{-12} \exp(360.00/T)$	9.03×10^{-12}
431	ROCALK12c	VROCP1ALKP + NO → 0.720*VROCP1ALKP2 + 0.280*VROCN1OXY1 + 0.720*NO2	$2.70 \times 10^{-12} \exp(360.00/T)$	9.03×10^{-12}
432	HC1002	HC10P + NO → 0.740*HC10P2 + 0.260*ONIT + 0.740*NO2	$2.70 \times 10^{-12} \exp(360.00/T)$	9.03×10^{-12}
433	ROCALK13c	VROCP6ALKP + NO3 → VROCP6ALKP2 + NO2	2.30×10^{-12}	2.30×10^{-12}
434	ROCALK14c	VROCP5ALKP + NO3 → VROCP5ALKP2 + NO2	2.30×10^{-12}	2.30×10^{-12}
435	ROCALK15c	VROCP4ALKP + NO3 → VROCP4ALKP2 + NO2	2.30×10^{-12}	2.30×10^{-12}
436	ROCALK16c	VROCP3ALKP + NO3 → VROCP3ALKP2 + NO2	2.30×10^{-12}	2.30×10^{-12}



N	CMAQ Label	Reaction	Rate Constant Formula ^{a,b,c}	k (molec cm ⁻³ sec ⁻¹ or s ⁻¹)
437	ROCALK17c	VROCP2ALKP + NO3 → VROCP2ALKP2 + NO2	2.30×10 ⁻¹²	2.30×10 ⁻¹²
438	ROCALK18c	VROCP1ALKP + NO3 → VROCP1ALKP2 + NO2	2.30×10 ⁻¹²	2.30×10 ⁻¹²
439	HC1003	HC10P + NO3 → HC10P2 + NO2	2.30×10 ⁻¹²	2.30×10 ⁻¹²
440	ROCALK19c	VROCP6ALKP + HO2 → VROCP3OXY2	2.17×10 ⁻¹¹	2.17×10 ⁻¹¹
441	ROCALK20c	VROCP5ALKP + HO2 → VROCP2OXY2	2.20×10 ⁻¹¹	2.20×10 ⁻¹¹
442	ROCALK21c	VROCP4ALKP + HO2 → VROCP1OXY1	2.25×10 ⁻¹¹	2.25×10 ⁻¹¹
443	ROCALK22c	VROCP3ALKP + HO2 → VROCP0OXY2	2.26×10 ⁻¹¹	2.26×10 ⁻¹¹
444	ROCALK23c	VROCP2ALKP + HO2 → VROCN1OXY1	2.27×10 ⁻¹¹	2.27×10 ⁻¹¹
445	ROCALK24c	VROCP1ALKP + HO2 → VROCN2OXY2	2.27×10 ⁻¹¹	2.27×10 ⁻¹¹
446	HC1004	HC10P + HO2 → OP2	2.66×10 ⁻¹³ exp(1300.00/T)	2.08×10 ⁻¹¹
447	ROCALK25c	VROCP6ALKP2 → HO2 + VROCP3OXY2	1.88E-01	1.88E-01
448	ROCALK26c	VROCP5ALKP2 → HO2 + VROCP2OXY2	1.88E-01	1.88E-01
449	ROCALK27c	VROCP4ALKP2 → HO2 + VROCP1OXY1	1.88E-01	1.88E-01
450	ROCALK28c	VROCP3ALKP2 → HO2 + VROCP0OXY2	1.88E-01	1.88E-01
451	ROCALK29c	VROCP2ALKP2 → HO2 + VROCN1OXY1	1.88E-01	1.88E-01
452	ROCALK30c	VROCP1ALKP2 → HO2 + VROCN2OXY2	1.88E-01	1.88E-01
453	HC1005	HC10P2 → HO2 + VROCP4OXY2	1.88E-01	1.88E-01
454	ROCALK31c	VROCP6ALKP2 + NO → 0.140*VROCP2OXY2 + 0.860*NO2 + 0.860*VROCP3OXY2 + 0.860*HO2	2.70×10 ⁻¹² exp(360.00/T)	9.03×10 ⁻¹²
455	ROCALK32c	VROCP5ALKP2 + NO → 0.140*VROCP1OXY3 + 0.860*NO2 + 0.860*VROCP2OXY2 + 0.860*HO2	2.70×10 ⁻¹² exp(360.00/T)	9.03×10 ⁻¹²
456	ROCALK33c	VROCP4ALKP2 + NO → 0.140*VROCP0OXY2 + 0.860*NO2 + 0.860*VROCP1OXY1 + 0.860*HO2	2.70×10 ⁻¹² exp(360.00/T)	9.03×10 ⁻¹²
457	ROCALK34c	VROCP3ALKP2 + NO → 0.140*VROCN1OXY1 + 0.860*NO2 + 0.860*VROCP0OXY2 + 0.860*HO2	2.70×10 ⁻¹² exp(360.00/T)	9.03×10 ⁻¹²
458	ROCALK35c	VROCP2ALKP2 + NO → 0.140*VROCN2OXY2 + 0.860*NO2 + 0.860*VROCN1OXY1 + 0.860*HO2	2.70×10 ⁻¹² exp(360.00/T)	9.03×10 ⁻¹²
459	ROCALK36c	VROCP1ALKP2 + NO → VROCN2OXY2 + 0.860*NO2 + 0.860*HO2	2.70×10 ⁻¹² exp(360.00/T)	9.03×10 ⁻¹²
460	HC1006	HC10P2 + NO → 0.120*ONIT + 0.880*NO2 + 0.880*KET + 0.880*HO2	2.70×10 ⁻¹² exp(360.00/T)	9.03×10 ⁻¹²
461	ROCALK37c	VROCP6ALKP2 + NO3 → NO2 + VROCP3OXY2 + HO2	2.30×10 ⁻¹²	2.30×10 ⁻¹²
462	ROCALK38c	VROCP5ALKP2 + NO3 → NO2 + VROCP2OXY2 + HO2	2.30×10 ⁻¹²	2.30×10 ⁻¹²
463	ROCALK39c	VROCP4ALKP2 + NO3 → NO2 + VROCP1OXY1 + HO2	2.30×10 ⁻¹²	2.30×10 ⁻¹²
464	ROCALK40c	VROCP3ALKP2 + NO3 → NO2 + VROCP0OXY2 + HO2	2.30×10 ⁻¹²	2.30×10 ⁻¹²
465	ROCALK41c	VROCP2ALKP2 + NO3 → NO2 + VROCN1OXY1 + HO2	2.30×10 ⁻¹²	2.30×10 ⁻¹²
466	ROCALK42c	VROCP1ALKP2 + NO3 → NO2 + VROCN2OXY2 + HO2	2.30×10 ⁻¹²	2.30×10 ⁻¹²
467	HC1007	HC10P2 + NO3 → NO2 + KET + HO2	2.30×10 ⁻¹²	2.30×10 ⁻¹²
468	ROCALK43c	VROCP6ALKP2 + HO2 → VROCP1OXY3	2.17×10 ⁻¹¹	2.17×10 ⁻¹¹
469	ROCALK44c	VROCP5ALKP2 + HO2 → VROCP0OXY2	2.20×10 ⁻¹¹	2.20×10 ⁻¹¹
470	ROCALK45c	VROCP4ALKP2 + HO2 → VROCN1OXY1	2.25×10 ⁻¹¹	2.25×10 ⁻¹¹
471	ROCALK46c	VROCP3ALKP2 + HO2 → VROCN2OXY2	2.26×10 ⁻¹¹	2.26×10 ⁻¹¹
472	ROCALK47c	VROCP2ALKP2 + HO2 → VROCN2OXY2	2.27×10 ⁻¹¹	2.27×10 ⁻¹¹
473	ROCALK48c	VROCP1ALKP2 + HO2 → VROCN2OXY2	2.27×10 ⁻¹¹	2.27×10 ⁻¹¹
474	HC1008	HC10P2 + HO2 → VROCP2OXY2	2.66×10 ⁻¹³ exp(1300.00/T)	2.08×10 ⁻¹¹
475	ROCARO01	VROCP6ARO + HO → 0.840*VROCP6AROP + 0.160*HO2 + 0.160*VROCP4OXY2	1.81×10 ⁻¹¹	1.81×10 ⁻¹¹
476	ROCARO02	VROCP6AROP + HO2 → 0.059*VROCP4OXY2 + 0.905*VROCP1OXY3 + 0.036*VROCN2OXY4	2.91×10 ⁻¹³ exp(1300.00/T)	2.28×10 ⁻¹¹
477	ROCARO03	VROCP6AROP + NO → 0.000*VROCP4OXY2 + 0.002*VROCP2OXY2 + 0.000*VROCN1OXY3 + 0.998*NO2 +	2.70×10 ⁻¹² exp(360.00/T)	9.03×10 ⁻¹²



N	CMAQ Label	Reaction	Rate Constant Formula ^{a,b,c}	k (molec cm ⁻³ sec ⁻¹ or s ⁻¹)
		0.998*HO2 + 0.059*BALD + 0.469*GLY + 0.469*MGLY + 0.469*FURANONE + 0.469*DCB2		
478	ROCARO04	VROCP6AROP + NO3 → NO2 + 0.941*HO2 + 0.059*BALD + 0.470*GLY + 0.470*MGLY + 0.470*FURANONE + 0.470*DCB2	2.30×10 ⁻¹²	2.30×10 ⁻¹²
479	ROCARO05	VROCP6AROP + MO2 → 0.680*HCHO + 1.310*HO2 + 0.320*MOH + 0.059*BALD + 0.470*GLY + 0.470*MGLY + 0.470*FURANONE + 0.470*DCB2	3.56×10 ⁻¹⁴ exp(708.00/T)	3.83×10 ⁻¹³
480	ROCARO06	VROCP6AROP + ACO3 → 0.700*MO2 + 0.941*HO2 + 0.300*ORA2 + 0.059*BALD + 0.470*GLY + 0.470*MGLY + 0.470*FURANONE + 0.470*DCB2	7.40×10 ⁻¹³ exp(765.00/T)	9.63×10 ⁻¹²
481	ROCARO11	VROCP5ARO + HO → 0.840*VROCP5AROP + 0.160*HO2 + 0.160*VROCP3OXY2	1.81×10 ⁻¹¹	1.81×10 ⁻¹¹
482	ROCARO12	VROCP5AROP + HO2 → 0.059*VROCP3OXY2 + 0.905*VROCP0OXY2 + 0.036*VROCN2OXY4	2.91×10 ⁻¹³ exp(1300.00/T)	2.28×10 ⁻¹¹
483	ROCARO13	VROCP5AROP + NO → 0.000*VROCP3OXY2 + 0.002*VROCP1OXY3 + 0.000*VROCN2OXY4 + 0.998*NO2 + 0.998*HO2 + 0.059*VROCP4OXY2 + 0.469*GLY + 0.469*MGLY + 0.469*FURANONE + 0.469*DCB2	2.70×10 ⁻¹² exp(360.00/T)	9.03×10 ⁻¹²
484	ROCARO14	VROCP5AROP + NO3 → NO2 + 0.941*HO2 + 0.059*VROCP4OXY2 + 0.470*GLY + 0.470*MGLY + 0.470*FURANONE + 0.470*DCB2	2.30×10 ⁻¹²	2.30×10 ⁻¹²
485	ROCARO15	VROCP5AROP + MO2 → 0.680*HCHO + 1.310*HO2 + 0.320*MOH + 0.059*VROCP4OXY2 + 0.470*GLY + 0.470*MGLY + 0.470*FURANONE + 0.470*DCB2	3.56×10 ⁻¹⁴ exp(708.00/T)	3.83×10 ⁻¹³
486	ROCARO16	VROCP5AROP + ACO3 → 0.700*MO2 + 0.941*HO2 + 0.300*ORA2 + 0.059*VROCP4OXY2 + 0.470*GLY + 0.470*MGLY + 0.470*FURANONE + 0.470*DCB2	7.40×10 ⁻¹³ exp(765.00/T)	9.63×10 ⁻¹²
487	ROCARO21	NAPH + HO → 0.840*NAPHP + 0.160*HO2 + 0.160*VROCP3OXY2	2.31×10 ⁻¹¹	2.31×10 ⁻¹¹
488	ROCARO22	NAPHP + HO2 → 0.059*VROCP3OXY2 + 0.905*VROCP1OXY3 + 0.036*VROCN2OXY8	2.91×10 ⁻¹³ exp(1300.00/T)	2.28×10 ⁻¹¹
489	ROCARO23	NAPHP + NO → 0.060*VROCP4OXY2 + 0.002*VROCP2OXY2 + 0.000*VROCN2OXY8 + 0.998*NO2 + 0.998*HO2 + 0.469*GLY + 0.469*MGLY + 0.469*FURANONE + 0.469*DCB2	2.70×10 ⁻¹² exp(360.00/T)	9.03×10 ⁻¹²
490	ROCARO24	NAPHP + NO3 → NO2 + 0.941*HO2 + 0.059*VROCP4OXY2 + 0.470*GLY + 0.470*MGLY + 0.470*FURANONE + 0.470*DCB2	2.30×10 ⁻¹²	2.30×10 ⁻¹²
491	ROCARO25	NAPHP + MO2 → 0.680*HCHO + 1.310*HO2 + 0.320*MOH + 0.059*VROCP4OXY2 + 0.470*GLY + 0.470*MGLY + 0.470*FURANONE + 0.470*DCB2	3.56×10 ⁻¹⁴ exp(708.00/T)	3.83×10 ⁻¹³
492	ROCARO26	NAPHP + ACO3 → 0.700*MO2 + 0.941*HO2 + 0.300*ORA2 + 0.059*VROCP4OXY2 + 0.470*GLY + 0.470*MGLY + 0.470*FURANONE + 0.470*DCB2	7.40×10 ⁻¹³ exp(765.00/T)	9.63×10 ⁻¹²
493	ROCOXY1c	VROCN2OXY8 + HO → HO + 0.085*VROCN2OXY8 + 0.258*DCB1 + 0.258*MEK + 0.258*ACD + 0.258*ALD + 0.258*MO2 + 0.258*ETHP + 0.258*HC3P + 0.258*MEKP	5.90×10 ⁻¹¹	5.90×10 ⁻¹¹
494	ROCOXY2c	VROCN2OXY4 + HO → HO + 0.464*VROCN2OXY8 + 0.198*VROCN2OXY4 + 0.012*VROCN1OXY6 + 0.015*VROCN1OXY3 + 0.062*VROCP0OXY4 + 0.039*VROCP1OXY3 + 0.049*VROCP2OXY2 + 0.040*VROCP3OXY2 + 0.018*VROCP4OXY2 + 0.031*OP3 + 0.004*OP2 + 0.079*DCB1 + 0.079*MEK + 0.079*KET + 0.079*ACD + 0.079*ALD + 0.079*MO2 + 0.079*ETHP + 0.079*HC3P + 0.079*MEKP + 0.079*HC5P + 0.079*KETP	6.07×10 ⁻¹¹	6.07×10 ⁻¹¹



N	CMAQ Label	Reaction	Rate Constant Formula ^{a,b,c}	k (molec cm ⁻³ sec ⁻¹ or s ⁻¹)
495	ROCOXY3c	VROCN2OXY2 + HO → HO + 0.104*VROCN2OXY8 + 0.564*VROCN2OXY4 + 0.214*VROCN2OXY2 + 0.015*VROCN1OXY6 + 0.030*VROCN1OXY3 + 0.010*VROCN1OXY1 + 0.019*VROCP0OXY4 + 0.046*VROCP0OXY2 + 0.031*VROCP1OXY3 + 0.020*VROCP1OXY1 + 0.046*VROCP2OXY2 + 0.045*VROCP3OXY2 + 0.045*VROCP4OXY2 + 0.033*VROCP5OXY1 + 0.037*VROCP6OXY1 + 0.003*OP3 + 0.039*DCB1 + 0.039*HKET + 0.039*MEK + 0.039*ACD + 0.039*ALD + 0.039*MO2 + 0.039*ETHP + 0.039*HC3P + 0.039*MEKP + 0.092*HC5P	5.54×10 ⁻¹¹	5.54×10 ⁻¹¹
496	ROCOXY4c	VROCN1OXY6 + HO → HO + 0.204*VROCN2OXY8 + 0.007*VROCN2OXY4 + 0.184*DCB1 + 0.184*MEK + 0.184*KET + 0.184*ACD + 0.184*ALD + 0.184*MO2 + 0.184*ETHP + 0.184*HC3P + 0.184*MEKP + 0.184*HC5P	5.63×10 ⁻¹¹	5.63×10 ⁻¹¹
497	ROCOXY5c	VROCN1OXY3 + HO → HO + 0.279*VROCN2OXY8 + 0.403*VROCN2OXY4 + 0.009*VROCN2OXY2 + 0.032*VROCN1OXY6 + 0.008*VROCN1OXY3 + 0.019*VROCP0OXY4 + 0.010*VROCP0OXY2 + 0.051*VROCP1OXY3 + 0.007*VROCP1OXY1 + 0.051*VROCP2OXY2 + 0.046*VROCP3OXY2 + 0.051*VROCP4OXY2 + 0.014*VROCP5OXY1 + 0.013*OP2 + 0.065*DCB1 + 0.065*HKET + 0.065*MEK + 0.065*ACD + 0.065*ALD + 0.065*MO2 + 0.065*ETHP + 0.065*HC3P + 0.065*MEKP + 0.175*HC5P	5.46×10 ⁻¹¹	5.46×10 ⁻¹¹
498	ROCOXY6c	VROCN1OXY1 + HO → HO + 0.007*VROCN2OXY8 + 0.119*VROCN2OXY4 + 0.726*VROCN2OXY2 + 0.012*VROCN1OXY6 + 0.030*VROCN1OXY3 + 0.007*VROCN1OXY1 + 0.029*VROCP0OXY4 + 0.045*VROCP0OXY2 + 0.023*VROCP1OXY3 + 0.035*VROCP1OXY1 + 0.062*VROCP2OXY2 + 0.052*VROCP3OXY2 + 0.051*VROCP4OXY2 + 0.035*VROCP5OXY1 + 0.075*VROCP6OXY1 + 0.016*OP3 + 0.006*OP2 + 0.024*DCB1 + 0.024*HKET + 0.024*MEK + 0.024*ACD + 0.024*ALD + 0.024*MO2 + 0.024*ETHP + 0.024*HC3P + 0.024*MEKP + 0.054*HC5P	4.50×10 ⁻¹¹	4.50×10 ⁻¹¹
499	ROCOXY7c	VROCP0OXY4 + HO → HO + 0.282*VROCN2OXY8 + 0.117*VROCN2OXY4 + 0.032*VROCN1OXY6 + 0.018*VROCN1OXY3 + 0.001*VROCP0OXY4 + 0.066*VROCP2OXY2 + 0.053*VROCP3OXY2 + 0.025*VROCP4OXY2 + 0.005*OP2 + 0.107*DCB1 + 0.107*MEK + 0.107*KET + 0.107*ACD + 0.107*ALD + 0.107*MO2 + 0.107*ETHP + 0.107*HC3P + 0.107*MEKP + 0.107*HC5P + 0.107*KETP	5.17×10 ⁻¹¹	5.17×10 ⁻¹¹
500	ROCOXY8c	VROCP0OXY2 + HO → HO + 0.066*VROCN2OXY8 + 0.458*VROCN2OXY4 + 0.116*VROCN2OXY2 + 0.033*VROCN1OXY6 + 0.066*VROCN1OXY3 + 0.005*VROCN1OXY1 + 0.031*VROCP0OXY4 + 0.002*VROCP0OXY2 + 0.040*VROCP1OXY3 + 0.021*VROCP1OXY1 + 0.054*VROCP2OXY2 + 0.052*VROCP3OXY2 + 0.052*VROCP4OXY2 + 0.037*VROCP5OXY1 + 0.042*VROCP6OXY1 + 0.011*OP3 + 0.044*DCB1 + 0.044*HKET + 0.044*MEK + 0.044*ACD +	4.73×10 ⁻¹¹	4.73×10 ⁻¹¹



N	CMAQ Label	Reaction	Rate Constant Formula ^{a,b,c}	k (molec cm ⁻³ sec ⁻¹ or s ⁻¹)
		0.044*ALD + 0.044*MO2 + 0.044*ETHP + 0.044*HC3P + 0.044*MEKP + 0.105*HC5P		
501	ROCOXY9c	VROCP1OXY3 + HO → HO + 0.178*VROCN2OXY8 + 0.192*VROCN2OXY4 + 0.000*VROCN2OXY2 + 0.074*VROCN1OXY6 + 0.045*VROCN1OXY3 + 0.063*VROCP0OXY4 + 0.001*VROCP0OXY2 + 0.001*VROCP1OXY3 + 0.023*VROCP2OXY2 + 0.059*VROCP3OXY2 + 0.065*VROCP4OXY2 + 0.017*VROCP5OXY1 + 0.015*OP3 + 0.017*OP2 + 0.082*DCB1 + 0.082*HKET + 0.082*MEK + 0.082*ACD + 0.082*ALD + 0.082*MO2 + 0.082*ETHP + 0.082*HC3P + 0.082*MEKP + 0.222*HC5P	4.60×10 ⁻¹¹	4.60×10 ⁻¹¹
502	ROCOXY10c	VROCP1OXY1 + HO → HO + 0.002*VROCN2OXY8 + 0.134*VROCN2OXY4 + 0.335*VROCN2OXY2 + 0.008*VROCN1OXY6 + 0.119*VROCN1OXY3 + 0.076*VROCN1OXY1 + 0.029*VROCP0OXY4 + 0.077*VROCP0OXY2 + 0.028*VROCP1OXY3 + 0.012*VROCP1OXY1 + 0.065*VROCP2OXY2 + 0.071*VROCP3OXY2 + 0.067*VROCP4OXY2 + 0.042*VROCP5OXY1 + 0.091*VROCP6OXY1 + 0.007*OP3 + 0.003*OP2 + 0.030*DCB1 + 0.030*HKET + 0.030*MEK + 0.030*ACD + 0.030*ALD + 0.030*MO2 + 0.030*ETHP + 0.030*HC3P + 0.030*MEKP + 0.065*HC5P	3.80×10 ⁻¹¹	3.80×10 ⁻¹¹
503	ROCOXY11c	VROCP2OXY2 + HO → HO + 0.044*VROCN2OXY8 + 0.173*VROCN2OXY4 + 0.010*VROCN2OXY2 + 0.051*VROCN1OXY6 + 0.112*VROCN1OXY3 + 0.001*VROCN1OXY1 + 0.134*VROCP0OXY4 + 0.040*VROCP0OXY2 + 0.051*VROCP1OXY3 + 0.007*VROCP1OXY1 + 0.024*VROCP2OXY2 + 0.029*VROCP3OXY2 + 0.073*VROCP4OXY2 + 0.052*VROCP5OXY1 + 0.059*VROCP6OXY1 + 0.004*OP3 + 0.002*OP2 + 0.063*DCB1 + 0.063*HKET + 0.063*MEK + 0.063*ACD + 0.063*ALD + 0.063*MO2 + 0.063*ETHP + 0.063*HC3P + 0.063*MEKP + 0.149*HC5P	3.93×10 ⁻¹¹	3.93×10 ⁻¹¹
504	ROCOXY12c	VROCP3OXY2 + HO → HO + 0.032*VROCN2OXY8 + 0.076*VROCN2OXY4 + 0.001*VROCN2OXY2 + 0.053*VROCN1OXY6 + 0.049*VROCN1OXY3 + 0.155*VROCP0OXY4 + 0.015*VROCP0OXY2 + 0.105*VROCP1OXY3 + 0.001*VROCP1OXY1 + 0.053*VROCP2OXY2 + 0.009*VROCP3OXY2 + 0.043*VROCP4OXY2 + 0.058*VROCP5OXY1 + 0.066*VROCP6OXY1 + 0.051*OP3 + 0.011*OP2 + 0.070*DCB1 + 0.070*HKET + 0.070*MEK + 0.070*ACD + 0.070*ALD + 0.070*MO2 + 0.070*ETHP + 0.070*HC3P + 0.070*MEKP + 0.166*HC5P	3.52×10 ⁻¹¹	3.52×10 ⁻¹¹
505	ROCOXY13c	VROCP4OXY2 + HO → HO + 0.012*VROCN2OXY8 + 0.017*VROCN2OXY4 + 0.048*VROCN1OXY6 + 0.025*VROCN1OXY3 + 0.088*VROCP0OXY4 + 0.092*VROCP1OXY3 + 0.007*VROCP1OXY1 + 0.097*VROCP2OXY2 + 0.046*VROCP3OXY2 + 0.002*VROCP4OXY2 + 0.048*VROCP5OXY1 + 0.074*VROCP6OXY1 + 0.061*OP3 + 0.015*OP2 + 0.079*DCB1 + 0.079*HKET + 0.079*MEK + 0.079*ACD + 0.079*ALD +	3.12×10 ⁻¹¹	3.12×10 ⁻¹¹



N	CMAQ Label	Reaction	Rate Constant Formula ^{a,b,c}	k (molec cm ⁻³ sec ⁻¹ or s ⁻¹)
		0.079*MO2 + 0.079*ETHP + 0.079*HC3P + 0.079*MEKP + 0.173*HC5P		
506	ROCOXY14c	VROCP5OXY1 + HO → HO + 0.010*VROCN2OXY4 + 0.001*VROCN2OXY2 + 0.009*VROCN1OXY6 + 0.015*VROCN1OXY3 + 0.070*VROCP0OXY4 + 0.015*VROCP0OXY2 + 0.104*VROCP1OXY3 + 0.003*VROCP1OXY1 + 0.165*VROCP2OXY2 + 0.157*VROCP3OXY2 + 0.072*VROCP4OXY2 + 0.006*VROCP5OXY1 + 0.140*VROCP6OXY1 + 0.022*OP3 + 0.038*OP2 + 0.053*DCB1 + 0.053*HKET + 0.053*MEK + 0.053*ACD + 0.053*ALD + 0.053*MO2 + 0.053*ETHP + 0.053*HC3P + 0.053*MEKP + 0.128*HC5P	2.40×10 ⁻¹¹	2.40×10 ⁻¹¹
507	ROCOXY15c	VROCP6OXY1 + HO → HO + 0.006*VROCN1OXY6 + 0.005*VROCN1OXY3 + 0.022*VROCP0OXY4 + 0.050*VROCP1OXY3 + 0.002*VROCP1OXY1 + 0.088*VROCP2OXY2 + 0.138*VROCP3OXY2 + 0.146*VROCP4OXY2 + 0.043*VROCP5OXY1 + 0.096*VROCP6OXY1 + 0.032*OP3 + 0.059*OP2 + 0.057*DCB1 + 0.057*HKET + 0.057*MEK + 0.057*ACD + 0.057*ALD + 0.057*MO2 + 0.057*ETHP + 0.057*HC3P + 0.057*MEKP + 0.154*HC5P	2.05×10 ⁻¹¹	2.05×10 ⁻¹¹
508	ROCOXY16c	OP3 + HO → HO + 0.119*VROCN2OXY8 + 0.001*VROCN2OXY4 + 0.039*VROCN1OXY6 + 0.011*VROCP0OXY4 + 0.227*DCB1 + 0.227*MEK + 0.227*ACD + 0.227*ALD + 0.227*MO2 + 0.227*ETHP + 0.227*HC3P + 0.227*MEKP	4.69×10 ⁻¹¹	4.69×10 ⁻¹¹

^aReaction rate constants following Arrhenius behavior are specified as $k = Ae^{-E_a/RT}$. Fall-off or pressure dependent reaction rate constants are specified as follows (M equals air number density):

for rate constants with k_0 , k_i , n, F values: $k = [k_0M/(1+k_0M/k_i)]F^G$, where $G=(1+(\log_{10}(k_0M/k_i)/n)^2)^{-1}$;

1215 for rate constants with k_1 , k_2 : $k = k_1 + k_2M$;

for rate constants with k_0 , k_2 , k_3 : $k = k_0 + k_3M/(1+k_3M/k_2)$;

for rate constants with k_1 , k_2 , k_3 : $k = k_1 + k_2M + k_3$.

^bHeterogeneous rates are specified as, $k_{HET} = \frac{S_A}{r_p/D_g + 4/\nu\gamma}$, where S_A is the fine aerosol surface area, r_p is the effective particle radius,

1220 D_g is the gas-phase diffusivity, ν is the mean molecular speed, and γ is the uptake coefficient. In the case of heterogeneous NO₂ reaction, the gas-phase diffusivity term in the denominator is neglected.

^cCMAQ calculates photolysis rate coefficients (J-values) as follows:

$$J_i = \int_{\lambda_1}^{\lambda_2} F(\lambda)\sigma_i(\lambda)\phi_i(\lambda)d\lambda$$

1225 where $F(\lambda)$ is the actinic flux (photons cm⁻² min⁻¹ nm⁻¹), $\sigma_i(\lambda)$ is the absorption cross section for the molecule undergoing photolytic reaction (cm² molecule⁻¹), $\phi_i(\lambda)$ is the quantum yield of the photolysis reaction (molecules photon⁻¹), and λ is the wavelength (nm). CMAQ uses 7-binned absorption cross-section and quantum yield data for calculating J-values. Sources of absorption cross-section and quantum yield data are provided in the table.



^dThe rate constant for R067 is scaled to the reverse equilibrium of R066.

^eThe HAL_Ozone reaction represents loss of ozone over ocean surfaces due to halogen chemistry. The rate is set to zero if the sun is below the horizon and if the surface does not include sea or surf zones (P = air pressure in atmospheres) (Sarwar et al., 2015).

1230



References

- 1235 Achten, C. and Andersson, J. T.: Overview of polycyclic aromatic compounds (PAC), *Polycyclic Aromat. Compd.*, **35**, 177-186, <https://doi.org/10.1080/10406638.2014.994071>, 2015.
- Agency for Toxic Substances and Disease Registry: Toxicological profile for 1,3-butadiene, <https://www.atsdr.cdc.gov/ToxProfiles/tp28.pdf>, last access: 17 May 2022, 2012.
- 1240 Ahmadov, R., McKeen, S. A., Robinson, A. L., Bahreini, R., Middlebrook, A. M., de Gouw, J. A., Meagher, J., Hsie, E.-Y., Edgerton, E., Shaw, S., and Trainer, M.: A volatility basis set model for summertime secondary organic aerosols over the eastern United States in 2006, *J. Geophys. Res.-Atmos.*, **117**, <https://doi.org/10.1029/2011JD016831>, 2012.
- Appel, K. W., Bash, J. O., Fahey, K. M., Foley, K. M., Gilliam, R. C., Hogrefe, C., Hutzell, W. T., Kang, D., Mathur, R., Murphy, B. N., Napelenok, S. L., Nolte, C. G., Pleim, J. E., Pouliot, G. A., Pye, H. O. T., Ran, L., Roselle, S. J., Sarwar, G., Schwede, D. B., Sidi, F. I., Spero, T. L., and Wong, D. C.: The Community Multiscale Air Quality (CMAQ) model versions 5.3 and 5.3.1: system updates and evaluation, *Geosci. Model Dev.*, **14**, 2867-2897, <https://doi.org/10.5194/gmd-14-2867-2021>, 2021.
- 1245 Atkinson, R., Baulch, D. L., Cox, R. A., Crowley, J. N., Hampson, R. F., Hynes, R. G., Jenkin, M. E., Rossi, M. J., and Troe, J.: Evaluated kinetic and photochemical data for atmospheric chemistry: Volume I - gas phase reactions of O_x, HO_x, NO_x and SO_x species, *Atmos. Chem. Phys.*, **4**, 1461-1738, <https://doi.org/10.5194/acp-4-1461-2004>, 2004.
- 1250 Atkinson, R., Baulch, D. L., Cox, R. A., Crowley, J. N., Hampson, R. F., Hynes, R. G., Jenkin, M. E., Rossi, M. J., Troe, J., and Subcommittee, I.: Evaluated kinetic and photochemical data for atmospheric chemistry: Volume II - gas phase reactions of organic species, *Atmos. Chem. Phys.*, **6**, 3625-4055, <https://doi.org/10.5194/acp-6-3625-2006>, 2006.
- Aumont, B., Szopa, S., and Madronich, S.: Modelling the evolution of organic carbon during its gas-phase tropospheric oxidation: development of an explicit model based on a self generating approach, *Atmos. Chem. Phys.*, **5**, 2497-2517, <https://doi.org/10.5194/acp-5-2497-2005>, 2005.
- 1255 Baboomian, V. J., Gu, Y., and Nizkorodov, S. A.: Photodegradation of Secondary Organic Aerosols by Long-Term Exposure to Solar Actinic Radiation, *ACS Earth Space Chem.*, **4**, 1078-1089, <https://doi.org/10.1021/acsearthspacechem.0c00088>, 2020.
- Bates, K. H., Jacob, D. J., Li, K., Ivatt, P. D., Evans, M. J., Yan, Y., and Lin, J.: Development and evaluation of a new compact mechanism for aromatic oxidation in atmospheric models, *Atmos. Chem. Phys.*, **21**, 18351-18374, <https://doi.org/10.5194/acp-21-18351-2021>, 2021.
- 1260 Berndt, T., Chen, J., Kjærgaard, E. R., Møller, K. H., Tilgner, A., Hoffmann, E. H., Herrmann, H., Crounse, J. D., Wennberg, P. O., and Kjærgaard, H. G.: Hydrotrioxide (ROOOH) formation in the atmosphere, *Science*, **376**, 979-982, <https://doi.org/10.1126/science.abn6012>, 2022.
- Berndt, T., Richters, S., Jokinen, T., Hyttinen, N., Kurtén, T., Otkjær, R. V., Kjærgaard, H. G., Stratmann, F., Herrmann, H., 1265 Sipilä, M., Kulmala, M., and Ehn, M.: Hydroxyl radical-induced formation of highly oxidized organic compounds, *Nat. Commun.*, **7**, 13677, <https://doi.org/10.1038/ncomms13677>, 2016.
- Bianchi, F., Kurtén, T., Riva, M., Mohr, C., Rissanen, M. P., Roldin, P., Berndt, T., Crounse, J. D., Wennberg, P. O., Mentel, T. F., Wildt, J., Junninen, H., Jokinen, T., Kulmala, M., Worsnop, D. R., Thornton, J. A., Donahue, N., Kjærgaard, H. G., and Ehn, M.: Highly Oxygenated Organic Molecules (HOM) from gas-phase autoxidation involving peroxy radicals: A key 1270 contributor to atmospheric aerosol, *Chem. Rev.*, **119**, 3472-3509, <https://doi.org/10.1021/acs.chemrev.8b00395>, 2019.



- Birdsall, A. W. and Elrod, M. J.: Comprehensive NO-dependent study of the products of the oxidation of atmospherically relevant aromatic compounds, *J. Phys. Chem. A*, 115, 5397-5407, <https://doi.org/10.1021/jp2010327>, 2011.
- Blitz, M. A., Heard, D. E., Pilling, M. J., Arnold, S. R., and Chipperfield, M. P.: Pressure and temperature-dependent quantum yields for the photodissociation of acetone between 279 and 327.5 nm, *Geophys. Res. Lett.*, 31, 1275 <https://doi.org/10.1029/2003GL018793>, 2004.
- Bloss, C., Wagner, V., Jenkin, M. E., Volkamer, R., Bloss, W. J., Lee, J. D., Heard, D. E., Wirtz, K., Martin-Reviejo, M., Rea, G., Wenger, J. C., and Pilling, M. J.: Development of a detailed chemical mechanism (MCMv3.1) for the atmospheric oxidation of aromatic hydrocarbons, *Atmos. Chem. Phys.*, 5, 641-664, <https://doi.org/10.5194/acp-5-641-2005>, 2005.
- Brewer, J. F., Papanastasiou, D. K., Burkholder, J. B., Fischer, E. V., Ren, Y., Mellouki, A., and Ravishankara, A. R.: Atmospheric photolysis of methyl ethyl, diethyl, and propyl ethyl ketones: Temperature-dependent UV absorption cross sections, *J. Geophys. Res.-Atmos.*, 124, 5906-5918, <https://doi.org/10.1029/2019JD030391>, 2019.
- Browne, E. C., Wooldridge, P. J., Min, K. E., and Cohen, R. C.: On the role of monoterpene chemistry in the remote continental boundary layer, *Atmos. Chem. Phys.*, 14, 1225-1238, <https://doi.org/10.5194/acp-14-1225-2014>, 2014.
- Bruns, E. A., El Haddad, I., Slowik, J. G., Kilic, D., Klein, F., Baltensperger, U., and Prévôt, A. S. H.: Identification of significant precursor gases of secondary organic aerosols from residential wood combustion, *Sci. Rep.*, 6, 27881, <https://doi.org/10.1038/srep27881>, 2016.
- Burkholder, J. B., Sander, S. P., Abbatt, J., Barker, J. R., Cappa, C., Crouse, J. D., Dibble, T. S., Huie, R. E., Kolb, C. E., Kurylo, M. J., Orkin, V. L., Percival, C. J., Wilmouth, D. M., and Wine, P. H.: Chemical Kinetics and Photochemical Data for Use in Atmospheric Studies, Evaluation No. 19 JPL Publication 19-5, <https://jpldataeval.jpl.nasa.gov/pdf/NASA-JPL%20Evaluation%2019-5.pdf>, last access: 16 May 2022, 2019.
- Canagaratna, M. R., Jimenez, J. L., Kroll, J. H., Chen, Q., Kessler, S. H., Massoli, P., Hildebrandt Ruiz, L., Fortner, E., Williams, L. R., Wilson, K. R., Surratt, J. D., Donahue, N. M., Jayne, J. T., and Worsnop, D. R.: Elemental ratio measurements of organic compounds using aerosol mass spectrometry: characterization, improved calibration, and implications, *Atmos. Chem. Phys.*, 15, 253-272, <https://doi.org/10.5194/acp-15-253-2015>, 2015.
- 1295 Carlton, A. G., Turpin, B. J., Altieri, K. E., Seitzinger, S. P., Mathur, R., Roselle, S. J., and Weber, R. J.: CMAQ Model Performance Enhanced When In-Cloud Secondary Organic Aerosol is Included: Comparisons of Organic Carbon Predictions with Measurements, *Environ. Sci. Technol.*, 42, 8798-8802, <https://doi.org/10.1021/es801192n>, 2008.
- 1300 Carlton, A. G., Bhave, P. V., Napelenok, S. L., Edney, E. O., Sarwar, G., Pinder, R. W., Pouliot, G. A., and Houyoux, M.: Model representation of secondary organic aerosol in CMAQv4.7, *Environ. Sci. Technol.*, 44, 8553-8560, <https://doi.org/10.1021/es100636q>, 2010.
- Carter, W. P. L.: Development of the SAPRC-07 chemical mechanism, *Atmos. Environ.*, 44, 5324-5335, <https://doi.org/10.1016/j.atmosenv.2010.01.026>, 2010.
- Carter, W. P. L.: Updated maximum incremental reactivity scale and hydrocarbon bin reactivities for regulatory applications and Reactivity values in an Excel File, <https://intra.engr.ucr.edu/~carter/SAPRC/>, last access: 10 May 2022, 2019.
- 1305 Carter, W. P. L.: Development of an Improved Chemical Speciation Database for Processing Emissions of Volatile Organic Compounds for Air Quality Models, <https://intra.engr.ucr.edu/~carter/emitdb/>, last access: 11 March 2021, 2020a.



- Carter, W. P. L.: Documentation of the SAPRC-18 mechanism, <https://intra.engr.ucr.edu/~carter/SAPRC/18/S18doc.pdf>, last access: 13 June 2022, 2020b.
- 1310 Chan, E. A. W., Gantt, B., and McDow, S.: The reduction of summer sulfate and switch from summertime to wintertime PM_{2.5} concentration maxima in the United States, *Atmos. Environ.*, 175, 25-32, <https://doi.org/10.1016/j.atmosenv.2017.11.055>, 2018.
- Chen, J., Møller, K. H., Wennberg, P. O., and Kjaergaard, H. G.: Unimolecular reactions following indoor and outdoor limonene ozonolysis, *J. Phys. Chem. A*, 125, 669-680, <https://doi.org/10.1021/acs.jpca.0c09882>, 2021a.
- 1315 Chen, Q., Heald, C. L., Jimenez, J. L., Canagaratna, M. R., Zhang, Q., He, L.-Y., Huang, X.-F., Campuzano-Jost, P., Palm, B. B., Poulain, L., Kuwata, M., Martin, S. T., Abbatt, J. P. D., Lee, A. K. Y., and Liggio, J.: Elemental composition of organic aerosol: The gap between ambient and laboratory measurements, *Geophys. Res. Lett.*, 42, 4182-4189, <https://doi.org/10.1002/2015GL063693>, 2015.
- 1320 Chen, Y., Guo, H., Nah, T., Tanner, D. J., Sullivan, A. P., Takeuchi, M., Gao, Z., Vasilakos, P., Russell, A. G., Baumann, K., Huey, L. G., Weber, R. J., and Ng, N. L.: Low-molecular-weight carboxylic acids in the Southeastern U.S.: Formation, partitioning, and implications for organic aerosol aging, *Environ. Sci. Technol.*, 55, 6688-6699, <https://doi.org/10.1021/acs.est.1c01413>, 2021b.
- Choi, H., Schmidbauer, N., Sundell, J., Hasselgren, M., Spengler, J., and Bornehag, C.-G.: Common household chemicals and the allergy risks in pre-school age children, *PLoS One*, 5, e13423, <https://doi.org/10.1371/journal.pone.0013423>, 2010.
- 1325 Code of Federal Regulations: Volatile organic compounds (VOC), <https://ecfr.federalregister.gov/current/title-40/chapter-1/subchapter-C/part-51>, last access: 17 June 2022, 1986.
- Coggon, M. M., Lim, C. Y., Koss, A. R., Sekimoto, K., Yuan, B., Gilman, J. B., Hagan, D. H., Selimovic, V., Zarzana, K. J., Brown, S. S., Roberts, J. M., Müller, M., Yokelson, R., Wisthaler, A., Krechmer, J. E., Jimenez, J. L., Cappa, C., Kroll, J. H., de Gouw, J., and Warneke, C.: OH chemistry of non-methane organic gases (NMOGs) emitted from laboratory and ambient biomass burning smoke: evaluating the influence of furans and oxygenated aromatics on ozone and secondary NMOG formation, *Atmos. Chem. Phys.*, 19, 14875-14899, <https://doi.org/10.5194/acp-19-14875-2019>, 2019.
- 1330 Coggon, M. M., Gkatzelis, G. I., McDonald, B. C., Gilman, J. B., Schwantes, R. H., Abuhassan, N., Aikin, K. C., Arend, M. F., Berkoff, T. A., Brown, S. S., Campos, T. L., Dickerson, R. R., Gronoff, G., Hurley, J. F., Isaacman-VanWertz, G., Koss, A. R., Li, M., McKeen, S. A., Moshary, F., Peischl, J., Pospisilova, V., Ren, X., Wilson, A., Wu, Y., Trainer, M., and Warneke, C.: Volatile chemical product emissions enhance ozone and modulate urban chemistry, *P. Natl. Acad. Sci. USA*, 118, e2026653118, <https://doi.org/10.1073/pnas.2026653118>, 2021.
- 1335 Crouse, J. D., Nielsen, L. B., Jørgensen, S., Kjaergaard, H. G., and Wennberg, P. O.: Autoxidation of Organic Compounds in the Atmosphere, *J. Phys. Chem. Lett.*, 4, 3513-3520, <https://doi.org/10.1021/jz4019207>, 2013.
- 1340 D'Ambro, E. L., Schobesberger, S., Gaston, C. J., Lopez-Hilfiker, F. D., Lee, B. H., Liu, J., Zelenyuk, A., Bell, D., Cappa, C. D., Helgestad, T., Li, Z., Guenther, A., Wang, J., Wise, M., Caylor, R., Surratt, J. D., Riedel, T., Hyttinen, N., Salo, V. T., Hasan, G., Kurtén, T., Shilling, J. E., and Thornton, J. A.: Chamber-based insights into the factors controlling epoxydiol (IEPOX) secondary organic aerosol (SOA) yield, composition, and volatility, *Atmos. Chem. Phys.*, 19, 11253-11265, <https://doi.org/10.5194/acp-19-11253-2019>, 2019.
- 1345 D'Ambro, E. L., Pye, H. O. T., Bash, J. O., Bowyer, J., Allen, C., Efstathiou, C., Gilliam, R. C., Reynolds, L., Talgo, K., and Murphy, B. N.: Characterizing the air emissions, transport, and deposition of per- and polyfluoroalkyl substances from a fluoropolymer manufacturing facility, *Environ. Sci. Technol.*, 55, 862-870, <https://doi.org/10.1021/acs.est.0c06580>, 2021.



- Davis, J. M., Bhave, P. V., and Foley, K. M.: Parameterization of N₂O₅ reaction probabilities on the surface of particles containing ammonium, sulfate, and nitrate, *Atmos. Chem. Phys.*, 8, 5295-5311, <https://doi.org/10.5194/acp-8-5295-2008>, 2008.
- Dlugokencky, E.: Trends in Atmospheric Methane, https://gml.noaa.gov/ccgg/trends_ch4/, last access: 29 June 2022, 2022.
- 1350 Donahue, N. M., Epstein, S. A., Pandis, S. N., and Robinson, A. L.: A two-dimensional volatility basis set: 1. organic-aerosol mixing thermodynamics, *Atmos. Chem. Phys.*, 11, 3303-3318, <https://doi.org/10.5194/acp-11-3303-2011>, 2011.
- Donahue, N. M., Kroll, J. H., Pandis, S. N., and Robinson, A. L.: A two-dimensional volatility basis set – Part 2: Diagnostics of organic-aerosol evolution, *Atmos. Chem. Phys.*, 12, 615-634, <https://doi.org/10.5194/acp-12-615-2012>, 2012.
- 1355 Donahue, N. M., Robinson, A. L., Stanier, C. O., and Pandis, S. N.: Coupled partitioning, dilution, and chemical aging of semivolatile organics, *Environ. Sci. Technol.*, 40, 2635-2643, <https://doi.org/10.1021/es052297c>, 2006.
- Donahue, N. M., Chuang, W., Epstein, S. A., Kroll, J. H., Worsnop, D. R., Robinson, A. L., Adams, P. J., and Pandis, S. N.: Why do organic aerosols exist? Understanding aerosol lifetimes using the two-dimensional volatility basis set, *Environ. Chem.*, 10, 151-157, <https://doi.org/10.1071/EN13022>, 2013.
- 1360 Dunne, J. P., Horowitz, L. W., Adcroft, A. J., Ginoux, P., Held, I. M., John, J. G., Krasting, J. P., Malyshev, S., Naik, V., Paulot, F., Shevliakova, E., Stock, C. A., Zadeh, N., Balaji, V., Blanton, C., Dunne, K. A., Dupuis, C., Durachta, J., Dussin, R., Gauthier, P. P. G., Griffies, S. M., Guo, H., Hallberg, R. W., Harrison, M., He, J., Hurlin, W., McHugh, C., Menzel, R., Milly, P. C. D., Nikonov, S., Paynter, D. J., Ploshay, J., Radhakrishnan, A., Rand, K., Reichl, B. G., Robinson, T., Schwarzkopf, D. M., Sentman, L. T., Underwood, S., Vahlenkamp, H., Winton, M., Wittenberg, A. T., Wyman, B., Zeng, Y., and Zhao, M.: The GFDL Earth System Model Version 4.1 (GFDL-ESM 4.1): Overall coupled model description and simulation characteristics, *J. Adv. Model. Earth Syst.*, 12, e2019MS002015, <https://doi.org/10.1029/2019MS002015>, 2020.
- 1365 Edwards, P. M., Brown, S. S., Roberts, J. M., Ahmadov, R., Banta, R. M., deGouw, J. A., Dubé, W. P., Field, R. A., Flynn, J. H., Gilman, J. B., Graus, M., Helmig, D., Koss, A., Langford, A. O., Lefer, B. L., Lerner, B. M., Li, R., Li, S.-M., McKeen, S. A., Murphy, S. M., Parrish, D. D., Senff, C. J., Soltis, J., Stutz, J., Sweeney, C., Thompson, C. R., Trainer, M. K., Tsai, C., Veres, P. R., Washenfelder, R. A., Warneke, C., Wild, R. J., Young, C. J., Yuan, B., and Zamora, R.: High winter ozone pollution from carbonyl photolysis in an oil and gas basin, *Nature*, 514, 351-354, <https://doi.org/10.1038/nature13767>, 2014.
- 1370 Ehn, M., Thornton, J. A., Kleist, E., Sipilä, M., Junninen, H., Pullinen, I., Springer, M., Rubach, F., Tillmann, R., Lee, B., Lopez-Hilfiker, F., Andres, S., Acir, I.-H., Rissanen, M., Jokinen, T., Schobesberger, S., Kangasluoma, J., Kontkanen, J., Nieminen, T., Kurtén, T., Nielsen, L. B., Jørgensen, S., Kjaergaard, H. G., Canagaratna, M., Maso, M. D., Berndt, T., Petäjä, T., Wahner, A., Kerminen, V.-M., Kulmala, M., Worsnop, D. R., Wildt, J., and Mentel, T. F.: A large source of low-volatility secondary organic aerosol, *Nature*, 506, 476-479, <https://doi.org/10.1038/nature13032>, 2014.
- 1375 Foley, K. M., Pouliot, G., Eyth, A., Aldridge, M., Allen, C., Appel, K. W., Bash, J. O., Beardsley, M., Beidler, J., Choi, D., Farkas, C., Gilliam, R., Godfrey, J., Henderson, B. H., Hogrefe, C., Koplitz, S., Mason, R., Mathur, R., Misenis, C., Possiel, N., Pye, H. O. T., Reynolds, L., Roark, M., Roberts, S., Schwede, D. B., Seltzer, K. M., Sonntag, D., Talgo, K., Toro, C., Vukovich, J., and Xing, J.: 2002-2017 Anthropogenic emissions data for air quality modeling over the United States, submitted to *Data in Brief*, 2022.
- 1380 Gierczak, T., Burkholder, J. B., Talukdar, R. K., Mellouki, A., Barone, S. B., and Ravishankara, A. R.: Atmospheric fate of methyl vinyl ketone and methacrolein, *J. Photchem. Photobiol. A*, 110, 1-10, [https://doi.org/10.1016/S1010-6030\(97\)00159-7](https://doi.org/10.1016/S1010-6030(97)00159-7), 1997.



- 1385 Goliff, W. S., Stockwell, W. R., and Lawson, C. V.: The regional atmospheric chemistry mechanism, version 2, *Atmos. Environ.*, 68, 174-185, <https://doi.org/10.1016/j.atmosenv.2012.11.038>, 2013.
- Gómez Alvarez, E., Borrás, E., Viidanoja, J., and Hjorth, J.: Unsaturated dicarbonyl products from the OH-initiated photo-oxidation of furan, 2-methylfuran and 3-methylfuran, *Atmos. Environ.*, 43, 1603-1612, <https://doi.org/10.1016/j.atmosenv.2008.12.019>, 2009.
- 1390 Gordon, H., Sengupta, K., Rap, A., Duplissy, J., Frege, C., Williamson, C., Heinritzi, M., Simon, M., Yan, C., Almeida, J., Tröstl, J., Nieminen, T., Ortega, I. K., Wagner, R., Dunne, E. M., Adamov, A., Amorim, A., Bernhammer, A.-K., Bianchi, F., Breitenlechner, M., Brilke, S., Chen, X., Craven, J. S., Dias, A., Ehrhart, S., Fischer, L., Flagan, R. C., Franchin, A., Fuchs, C., Guida, R., Hakala, J., Hoyle, C. R., Jokinen, T., Junninen, H., Kangasluoma, J., Kim, J., Kirkby, J., Krapf, M., Kürten, A., Laaksonen, A., Lehtipalo, K., Makhmutov, V., Mathot, S., Molteni, U., Monks, S. A., Onnela, A., Peräkylä, O., Piel, F., Petäjä, T., Praplan, A. P., Pringle, K. J., Richards, N. A. D., Rissanen, M. P., Rondo, L., Sarnela, N., Schobesberger, S., Scott, C. E.,
1395 Seinfeld, J. H., Sharma, S., Sipilä, M., Steiner, G., Stozhkov, Y., Stratmann, F., Tomé, A., Virtanen, A., Vogel, A. L., Wagner, A. C., Wagner, P. E., Weingartner, E., Wimmer, D., Winkler, P. M., Ye, P., Zhang, X., Hansel, A., Dommen, J., Donahue, N. M., Worsnop, D. R., Baltensperger, U., Kulmala, M., Curtius, J., and Carslaw, K. S.: Reduced anthropogenic aerosol radiative forcing caused by biogenic new particle formation, *P. Natl. Acad. Sci. USA*, 113, 12053-12058, <https://doi.org/10.1073/pnas.1602360113>, 2016.
- 1400 Griffin, R. J., Cocker III, D. R., Flagan, R. C., and Seinfeld, J. H.: Organic aerosol formation from the oxidation of biogenic hydrocarbons, *J. Geophys. Res.-Atmos.*, 104, 3555-3567, <https://doi.org/10.1029/1998JD100049>, 1999.
- Grulke, C. M., Williams, A. J., Thillanadarajah, I., and Richard, A. M.: EPA's DSSTox database: History of development of a curated chemistry resource supporting computational toxicology research, *Comput. Toxicol.*, 12, 100096, <https://doi.org/10.1016/j.comtox.2019.100096>, 2019.
- 1405 Haywood, J. and Boucher, O.: Estimates of the direct and indirect radiative forcing due to tropospheric aerosols: A review, *Rev. Geophys.*, 38, 513-543, <https://doi.org/10.1029/1999RG000078>, 2000.
- He, Y., Lambe, A. T., Seinfeld, J. H., Cappa, C. D., Pierce, J. R., and Jathar, S. H.: Process-level modeling can simultaneously explain secondary organic aerosol evolution in chambers and flow reactors, *Environ. Sci. Technol.*, 56, 6262-6273, <https://doi.org/10.1021/acs.est.1c08520>, 2022.
- 1410 Heald, C. L. and Kroll, J. H.: The fuel of atmospheric chemistry: Toward a complete description of reactive organic carbon, *Sci. Adv.*, 6, eaay8967, <https://doi.org/10.1126/sciadv.aay8967>, 2020.
- Heald, C. L., Kroll, J. H., Jimenez, J. L., Docherty, K. S., DeCarlo, P. F., Aiken, A. C., Chen, Q., Martin, S. T., Farmer, D. K., and Artaxo, P.: A simplified description of the evolution of organic aerosol composition in the atmosphere, *Geophys. Res. Lett.*, 37, <https://doi.org/10.1029/2010GL042737>, 2010.
- 1415 Heald, C. L., Gouw, J. d., Goldstein, A. H., Guenther, A. B., Hayes, P. L., Hu, W., Isaacman-VanWertz, G., Jimenez, J. L., Keutsch, F. N., Koss, A. R., Misztal, P. K., Rappenglück, B., Roberts, J. M., Stevens, P. S., Washenfelder, R. A., Warneke, C., and Young, C. J.: Contrasting reactive organic carbon observations in the Southeast United States (SOAS) and Southern California (CalNex), *Environ. Sci. Technol.*, 54, 14923-14935, <https://doi.org/10.1021/acs.est.0c05027>, 2020.
- 1420 Hecklen, J., Desai, J., Bahta, A., Harper, C., and Simonaitis, R.: The temperature and wavelength dependence of the photo-oxidation of propionaldehyde, *J. Photochem.*, 34, 117-135, [https://doi.org/10.1016/0047-2670\(86\)85014-6](https://doi.org/10.1016/0047-2670(86)85014-6), 1986.
- Hodzic, A. and Jimenez, J. L.: Modeling anthropogenically controlled secondary organic aerosols in a megacity: a simplified framework for global and climate models, *Geosci. Model Dev.*, 4, 901-917, <https://doi.org/10.5194/gmd-4-901-2011>, 2011.



- 1425 Hoffmann, T., Odum, J. R., Bowman, F., Collins, D., Klockow, D., Flagan, R. C., and Seinfeld, J. H.: Formation of organic aerosols from the oxidation of biogenic hydrocarbons, *J. Atmos. Chem.*, 26, 189-222, <https://doi.org/10.1023/A:1005734301837>, 1997.
- Hutzell, W. T., Luecken, D. J., Appel, K. W., and Carter, W. P. L.: Interpreting predictions from the SAPRC07 mechanism based on regional and continental simulations, *Atmos. Environ.*, 46, 417-429, <https://doi.org/10.1016/j.atmosenv.2011.09.030>, 2012.
- 1430 IUPAC: IUPAC subcommittee for gas kinetic data evaluation, <http://www.iupac-kinetic.ch.cam.ac.uk/>, last access: 13 May 2022, 2010.
- Ivatt, P. D., Evans, M. J., and Lewis, A. C.: Suppression of surface ozone by an aerosol-inhibited photochemical ozone regime, *Nature Geoscience*, 15, 536-540, <https://doi.org/10.1038/s41561-022-00972-9>, 2022.
- Jaffe, D. A. and Wigder, N. L.: Ozone production from wildfires: A critical review, *Atmos. Environ.*, 51, 1-10, <https://doi.org/10.1016/j.atmosenv.2011.11.063>, 2012.
- 1435 Jaoui, M., Kleindienst, T. E., Docherty, K. S., Lewandowski, M., and Offenberg, J. H.: Secondary organic aerosol formation from the oxidation of a series of sesquiterpenes: α -cedrene, β -caryophyllene, α -humulene and α -farnesene with O₃, OH and NO₃ radicals, *Environ. Chem.*, 10, 178-193, <https://doi.org/10.1071/EN13025>, 2013.
- Jathar, S. H., Gordon, T. D., Hennigan, C. J., Pye, H. O. T., Pouliot, G., Adams, P. J., Donahue, N. M., and Robinson, A. L.: Unspeciated organic emissions from combustion sources and their influence on the secondary organic aerosol budget in the United States, *P. Natl. Acad. Sci. USA*, 111, 10473, <https://doi.org/10.1073/pnas.1323740111>, 2014.
- 1440 Jenkin, M. E., Saunders, S. M., and Pilling, M. J.: The tropospheric degradation of volatile organic compounds: a protocol for mechanism development, *Atmos. Environ.*, 31, 81-104, [https://doi.org/10.1016/S1352-2310\(96\)00105-7](https://doi.org/10.1016/S1352-2310(96)00105-7), 1997.
- Jenkin, M. E., Saunders, S. M., Wagner, V., and Pilling, M. J.: Protocol for the development of the Master Chemical Mechanism, MCM v3 (Part B): tropospheric degradation of aromatic volatile organic compounds, *Atmos. Chem. Phys.*, 3, 181-193, <https://doi.org/10.5194/acp-3-181-2003>, 2003.
- 1445 Jenkin, M. E., Wyche, K. P., Evans, C. J., Carr, T., Monks, P. S., Alfarra, M. R., Barley, M. H., McFiggans, G. B., Young, J. C., and Rickard, A. R.: Development and chamber evaluation of the MCM v3.2 degradation scheme for β -caryophyllene, *Atmos. Chem. Phys.*, 12, 5275-5308, <https://doi.org/10.5194/acp-12-5275-2012>, 2012.
- 1450 Jokinen, T., Berndt, T., Makkonen, R., Kerminen, V.-M., Junninen, H., Paasonen, P., Stratmann, F., Herrmann, H., Guenther, A. B., Worsnop, D. R., Kulmala, M., Ehn, M., and Sipilä, M.: Production of extremely low volatile organic compounds from biogenic emissions: Measured yields and atmospheric implications, *P. Natl. Acad. Sci. USA*, 112, 7123-7128, <https://doi.org/10.1073/pnas.1423977112>, 2015.
- Kaduwela, A., Luecken, D., Carter, W., and Derwent, R.: New directions: Atmospheric chemical mechanisms for the future, *Atmos. Environ.*, 122, 609-610, <https://doi.org/10.1016/j.atmosenv.2015.10.031>, 2015.
- 1455 Kim, P. S., Jacob, D. J., Fisher, J. A., Travis, K., Yu, K., Zhu, L., Yantosca, R. M., Sulprizio, M. P., Jimenez, J. L., Campuzano-Jost, P., Froyd, K. D., Liao, J., Hair, J. W., Fenn, M. A., Butler, C. F., Wagner, N. L., Gordon, T. D., Welti, A., Wennberg, P. O., Crouse, J. D., St. Clair, J. M., Teng, A. P., Millet, D. B., Schwarz, J. P., Markovic, M. Z., and Perring, A. E.: Sources, seasonality, and trends of southeast US aerosol: an integrated analysis of surface, aircraft, and satellite observations with the GEOS-Chem chemical transport model, *Atmos. Chem. Phys.*, 15, 10411-10433, <https://doi.org/10.5194/acp-15-10411-2015>, 2015.
- 1460



- Knote, C., Tuccella, P., Curci, G., Emmons, L., Orlando, J. J., Madronich, S., Baró, R., Jiménez-Guerrero, P., Luecken, D., Hogrefe, C., Forkel, R., Werhahn, J., Hirtl, M., Pérez, J. L., San José, R., Giordano, L., Brunner, D., Yahya, K., and Zhang, Y.: Influence of the choice of gas-phase mechanism on predictions of key gaseous pollutants during the AQMEII phase-2 intercomparison, *Atmos. Environ.*, 115, 553-568, <https://doi.org/10.1016/j.atmosenv.2014.11.066>, 2015.
- 1465 Koo, B., Knipping, E., and Yarwood, G.: 1.5-Dimensional volatility basis set approach for modeling organic aerosol in CAMx and CMAQ, *Atmos. Environ.*, 95, 158-164, <https://doi.org/10.1016/j.atmosenv.2014.06.031>, 2014.
- Koss, A. R., Sekimoto, K., Gilman, J. B., Selimovic, V., Coggon, M. M., Zarzana, K. J., Yuan, B., Lerner, B. M., Brown, S. S., Jimenez, J. L., Krechmer, J., Roberts, J. M., Warneke, C., Yokelson, R. J., and de Gouw, J.: Non-methane organic gas emissions from biomass burning: identification, quantification, and emission factors from PTR-ToF during the FIREX 2016 laboratory experiment, *Atmos. Chem. Phys.*, 18, 3299-3319, <https://doi.org/10.5194/acp-18-3299-2018>, 2018.
- 1470 Kroll, J. H., Smith, J. D., Che, D. L., Kessler, S. H., Worsnop, D. R., and Wilson, K. R.: Measurement of fragmentation and functionalization pathways in the heterogeneous oxidation of oxidized organic aerosol, *Phys. Chem. Chem. Phys.*, 11, 8005-8014, <https://doi.org/10.1039/B905289E>, 2009.
- Kroll, J. H., Donahue, N. M., Jimenez, J. L., Kessler, S. H., Canagaratna, M. R., Wilson, K. R., Altieri, K. E., Mazzoleni, L. R., Wozniak, A. S., Bluhm, H., Mysak, E. R., Smith, J. D., Kolb, C. E., and Worsnop, D. R.: Carbon oxidation state as a metric for describing the chemistry of atmospheric organic aerosol, *Nat. Chem.*, 3, 133-139, <https://doi.org/10.1038/nchem.948>, 2011.
- Kurtén, T., Møller, K. H., Nguyen, T. B., Schwantes, R. H., Misztal, P. K., Su, L., Wennberg, P. O., Fry, J. L., and Kjaergaard, H. G.: Alkoxy radical bond scissions explain the anomalously low secondary organic aerosol and organonitrate yields from α -pinene + NO₃, *The Journal of Physical Chemistry Letters*, 8, 2826-2834, <https://doi.org/10.1021/acs.jpcclett.7b01038>, 2017.
- 1480 Lannuque, V., Camredon, M., Couvidat, F., Hodzic, A., Valorso, R., Madronich, S., Bessagnet, B., and Aumont, B.: Exploration of the influence of environmental conditions on secondary organic aerosol formation and organic species properties using explicit simulations: development of the VBS-GECKO parameterization, *Atmos. Chem. Phys.*, 18, 13411-13428, <https://doi.org/10.5194/acp-18-13411-2018>, 2018.
- Lawrence, C. E., Casson, P., Brandt, R., Schwab, J. J., Dukett, J. E., Snyder, P., Yerger, E., Kelting, D., VandenBoer, T. C., and Lance, S.: Long-term monitoring of cloud water chemistry at Whiteface Mountain: The emergence of a new chemical regime, *Atmos. Chem. Phys. Discuss.*, 2022, 1-31, <https://doi.org/10.5194/acp-2022-313>, 2022.
- Lee, B. H., D'Ambro, E. L., Lopez-Hilfiker, F. D., Schobesberger, S., Mohr, C., Zawadowicz, M. A., Liu, J., Shilling, J. E., Hu, W., Palm, B. B., Jimenez, J. L., Hao, L., Virtanen, A., Zhang, H., Goldstein, A. H., Pye, H. O. T., and Thornton, J. A.: Resolving ambient organic aerosol formation and aging pathways with simultaneous molecular composition and volatility observations, *ACS Earth Space Chem.*, 4, 391-402, <https://doi.org/10.1021/acsearthspacechem.9b00302>, 2020.
- 1490 Li, Y., Schichtel Bret, A., Walker John, T., Schwede Donna, B., Chen, X., Lehmann Christopher, M. B., Puchalski Melissa, A., Gay David, A., and Collett Jeffrey, L.: Increasing importance of deposition of reduced nitrogen in the United States, *P. Natl. Acad. Sci. USA*, 113, 5874-5879, <https://doi.org/10.1073/pnas.1525736113>, 2016.
- Liggio, J., Li, S.-M., and McLaren, R.: Reactive uptake of glyoxal by particulate matter, *J. Geophys. Res.-Atmos.*, 110, <https://doi.org/10.1029/2004JD005113>, 2005.
- Loeffler, K. W., Koehler, C. A., Paul, N. M., and De Haan, D. O.: Oligomer formation in evaporating aqueous glyoxal and methyl glyoxal solutions, *Environ. Sci. Technol.*, 40, 6318-6323, <https://doi.org/10.1021/es060810w>, 2006.



- Lowe, C. N. and Williams, A. J.: Enabling high-throughput searches for multiple chemical data using the U.S.-EPA CompTox Chemicals Dashboard, *J. Chem. Inf. Model*, 61, 565-570, <https://doi.org/10.1021/acs.jcim.0c01273>, 2021.
- 1500 Lu, Q., Zhao, Y., and Robinson, A. L.: Comprehensive organic emission profiles for gasoline, diesel, and gas-turbine engines including intermediate and semi-volatile organic compound emissions, *Atmos. Chem. Phys.*, 18, 17637-17654, <https://doi.org/10.5194/acp-18-17637-2018>, 2018.
- 1505 Lu, Q., Murphy, B. N., Qin, M., Adams, P. J., Zhao, Y., Pye, H. O. T., Efstathiou, C., Allen, C., and Robinson, A. L.: Simulation of organic aerosol formation during the CalNex study: updated mobile emissions and secondary organic aerosol parameterization for intermediate-volatility organic compounds, *Atmos. Chem. Phys.*, 20, 4313-4332, <https://doi.org/10.5194/acp-20-4313-2020>, 2020.
- Magneron, I., Thévenet, R., Mellouki, A., Le Bras, G., Moortgat, G. K., and Wirtz, K.: A study of the photolysis and OH-initiated oxidation of acrolein and trans-crotonaldehyde, *J. Phys. Chem. A*, 106, 2526-2537, <https://doi.org/10.1021/jp013413a>, 2002.
- 1510 Makar, M., Antonelli, J., Di, Q., Cutler, D., Schwartz, J., and Dominici, F.: Estimating the causal effect of low levels of fine particulate matter on hospitalization, *Epidemiol.*, 28, <https://doi.org/10.1097/ede.0000000000000690>, 2017.
- Mansouri, K., Grulke, C. M., Judson, R. S., and Williams, A. J.: OPERA models for predicting physicochemical properties and environmental fate endpoints, *J. Cheminformatics*, 10, 10, <https://doi.org/10.1186/s13321-018-0263-1>, 2018.
- 1515 McClure, C. D. and Jaffe, D. A.: US particulate matter air quality improves except in wildfire-prone areas, *P. Natl. Acad. Sci. USA*, 115, 7901-7906, <https://doi.org/10.1073/pnas.1804353115>, 2018.
- McDonald, B. C., de Gouw, J. A., Gilman, J. B., Jathar, S. H., Akherati, A., Cappa, C. D., Jimenez, J. L., Lee-Taylor, J., Hayes, P. L., McKeen, S. A., Cui, Y. Y., Kim, S.-W., Gentner, D. R., Isaacman-VanWertz, G., Goldstein, A. H., Harley, R. A., Frost, G. J., Roberts, J. M., Ryerson, T. B., and Trainer, M.: Volatile chemical products emerging as largest petrochemical source of urban organic emissions, *Science*, 359, 760, <https://doi.org/10.1126/science.aaq0524>, 2018.
- 1520 McFiggans, G., Mentel, T. F., Wildt, J., Pullinen, I., Kang, S., Kleist, E., Schmitt, S., Springer, M., Tillmann, R., Wu, C., Zhao, D., Hallquist, M., Faxon, C., Le Breton, M., Hallquist, Å. M., Simpson, D., Bergström, R., Jenkin, M. E., Ehn, M., Thornton, J. A., Alfarra, M. R., Bannan, T. J., Percival, C. J., Priestley, M., Topping, D., and Kiendler-Scharr, A.: Secondary organic aerosol reduced by mixture of atmospheric vapours, *Nature*, 565, 587-593, <https://doi.org/10.1038/s41586-018-0871-y>, 2019.
- 1525 Moch, J. M., Dovrou, E., Mickley, L. J., Keutsch, F. N., Cheng, Y., Jacob, D. J., Jiang, J., Li, M., Munger, J. W., Qiao, X., and Zhang, Q.: Contribution of hydroxymethane sulfonate to ambient particulate matter: A potential explanation for high particulate sulfur during severe winter haze in Beijing, *Geophys. Res. Lett.*, 45, 11,969-911,979, <https://doi.org/10.1029/2018GL079309>, 2018.
- 1530 Møller, K. H., Otkjær, R. V., Chen, J., and Kjaergaard, H. G.: Double bonds are key to fast unimolecular reactivity in first-generation monoterpene hydroxy peroxy radicals, *J. Phys. Chem. A*, 124, 2885-2896, <https://doi.org/10.1021/acs.jpca.0c01079>, 2020.
- Molteni, U., Bianchi, F., Klein, F., El Haddad, I., Frege, C., Rossi, M. J., Dommen, J., and Baltensperger, U.: Formation of highly oxygenated organic molecules from aromatic compounds, *Atmos. Chem. Phys.*, 18, 1909-1921, <https://doi.org/10.5194/acp-18-1909-2018>, 2018.
- 1535 Molteni, U., Simon, M., Heinritzi, M., Hoyle, C. R., Bernhammer, A.-K., Bianchi, F., Breitenlechner, M., Brilke, S., Dias, A., Duplissy, J., Frege, C., Gordon, H., Heyn, C., Jokinen, T., Kürten, A., Lehtipalo, K., Makhmutov, V., Petäjä, T., Pieber, S. M.,



- Praplan, A. P., Schobesberger, S., Steiner, G., Stozhkov, Y., Tomé, A., Tröstl, J., Wagner, A. C., Wagner, R., Williamson, C., Yan, C., Baltensperger, U., Curtius, J., Donahue, N. M., Hansel, A., Kirkby, J., Kulmala, M., Worsnop, D. R., and Dommen, J.: Formation of highly oxygenated organic molecules from α -pinene ozonolysis: Chemical characteristics, mechanism, and kinetic model development, *ACS Earth Space Chem.*, 3, 873-883, <https://doi.org/10.1021/acsearthspacechem.9b00035>, 2019.
- 1540 Murphy, B. N., Woody, M. C., Jimenez, J. L., Carlton, A. M. G., Hayes, P. L., Liu, S., Ng, N. L., Russell, L. M., Setyan, A., Xu, L., Young, J., Zaveri, R. A., Zhang, Q., and Pye, H. O. T.: Semivolatile POA and parameterized total combustion SOA in CMAQv5.2: impacts on source strength and partitioning, *Atmos. Chem. Phys.*, 17, 11107-11133, <https://doi.org/10.5194/acp-17-11107-2017>, 2017.
- 1545 Nakao, S., Clark, C., Tang, P., Sato, K., and Cocker Iii, D.: Secondary organic aerosol formation from phenolic compounds in the absence of NO_x, *Atmos. Chem. Phys.*, 11, 10649-10660, <https://doi.org/10.5194/acp-11-10649-2011>, 2011.
- Nannoolal, Y., Rarey, J., and Ramjugernath, D.: Estimation of pure component properties: Part 3. Estimation of the vapor pressure of non-electrolyte organic compounds via group contributions and group interactions, *Fluid Phase Equilib.*, 269, 117-133, <https://doi.org/10.1016/j.fluid.2008.04.020>, 2008.
- 1550 Nannoolal, Y., Rarey, J., Ramjugernath, D., and Cordes, W.: Estimation of pure component properties: Part 1. Estimation of the normal boiling point of non-electrolyte organic compounds via group contributions and group interactions, *Fluid Phase Equilib.*, 226, 45-63, <https://doi.org/10.1016/j.fluid.2004.09.001>, 2004.
- 1555 Nault, B. A., Campuzano-Jost, P., Day, D. A., Schroder, J. C., Anderson, B., Beyersdorf, A. J., Blake, D. R., Brune, W. H., Choi, Y., Corr, C. A., de Gouw, J. A., Dibb, J., DiGangi, J. P., Diskin, G. S., Fried, A., Huey, L. G., Kim, M. J., Knote, C. J., Lamb, K. D., Lee, T., Park, T., Pusede, S. E., Scheuer, E., Thornhill, K. L., Woo, J. H., and Jimenez, J. L.: Secondary organic aerosol production from local emissions dominates the organic aerosol budget over Seoul, South Korea, during KORUS-AQ, *Atmos. Chem. Phys.*, 18, 17769-17800, <https://doi.org/10.5194/acp-18-17769-2018>, 2018.
- Ng, N. L., Canagaratna, M. R., Jimenez, J. L., Chhabra, P. S., Seinfeld, J. H., and Worsnop, D. R.: Changes in organic aerosol composition with aging inferred from aerosol mass spectra, *Atmos. Chem. Phys.*, 11, 6465-6474, <https://doi.org/10.5194/acp-11-6465-2011>, 2011.
- 1560 Ng, N. L., Kroll, J. H., Chan, A. W. H., Chhabra, P. S., Flagan, R. C., and Seinfeld, J. H.: Secondary organic aerosol formation from *m*-xylene, toluene, and benzene, *Atmos. Chem. Phys.*, 7, 3909-3922, <https://doi.org/10.5194/acp-7-3909-2007>, 2007.
- Nozière, B., Barnes, I., and Becker, K.-H.: Product study and mechanisms of the reactions of α -pinene and of pinonaldehyde with OH radicals, *J. Geophys. Res.-Atmos.*, 104, 23645-23656, <https://doi.org/10.1029/1999JD900778>, 1999.
- 1565 Pai, S. J., Carter, T. S., Heald, C. L., and Kroll, J. H.: Updated World Health Organization Air Quality Guidelines highlight the importance of non-anthropogenic PM_{2.5}, *Environ. Sci. Tech. Lett.*, 9, 501-506, <https://doi.org/10.1021/acs.estlett.2c00203>, 2022.
- Pankow, J. F.: An absorption model of the gas/aerosol partitioning involved in the formation of secondary organic aerosol, *Atmos. Environ.*, 28, 189-193, [https://doi.org/10.1016/1352-2310\(94\)90094-9](https://doi.org/10.1016/1352-2310(94)90094-9), 1994.
- 1570 Pankow, J. F. and Asher, W. E.: SIMPOL.1: a simple group contribution method for predicting vapor pressures and enthalpies of vaporization of multifunctional organic compounds, *Atmos. Chem. Phys.*, 8, 2773-2796, <https://doi.org/10.5194/acp-8-2773-2008>, 2008.



- Pennington, E. A., Seltzer, K. M., Murphy, B. N., Qin, M., Seinfeld, J. H., and Pye, H. O. T.: Modeling secondary organic aerosol formation from volatile chemical products, *Atmos. Chem. Phys.*, 21, 18247-18261, <https://doi.org/10.5194/acp-21-18247-2021>, 2021.
- 1575 Piletic, I. R. and Kleindienst, T. E.: Rates and yields of unimolecular reactions producing highly oxidized peroxy radicals in the OH-induced autoxidation of α -pinene, β -pinene, and limonene, *J. Phys. Chem. A*, 126, 88-100, <https://doi.org/10.1021/acs.jpca.1c07961>, 2022.
- Pond, Z. A., Hernandez, C. S., Adams, P. J., Pandis, S. N., Garcia, G. R., Robinson, A. L., Marshall, J. D., Burnett, R., Skyllakou, K., Garcia Rivera, P., Karnezi, E., Coleman, C. J., and Pope, C. A.: Cardiopulmonary mortality and fine particulate air pollution by species and source in a national U.S. cohort, *Environ. Sci. Technol.*, 56, 7214-7223, <https://doi.org/10.1021/acs.est.1c04176>, 2022.
- 1580 Porter, W. C., Jimenez, J. L., and Barsanti, K. C.: Quantifying atmospheric parameter ranges for ambient secondary organic aerosol formation, *ACS Earth Space Chem.*, 5, 2380-2397, <https://doi.org/10.1021/acsearthspacechem.1c00090>, 2021.
- Praske, E., Otkjær, R. V., Crouse, J. D., Hethcox, J. C., Stoltz, B. M., Kjaergaard, H. G., and Wennberg, P. O.: Atmospheric autoxidation is increasingly important in urban and suburban North America, *P. Natl. Acad. Sci. USA*, 115, 64-69, <https://doi.org/10.1073/pnas.1715540115>, 2018.
- Pye, H. O. T. and Pouliot, G. A.: Modeling the role of alkanes, polycyclic aromatic hydrocarbons, and their oligomers in secondary organic aerosol formation, *Environ. Sci. Technol.*, 46, 6041-6047, <https://doi.org/10.1021/es300409w>, 2012.
- Pye, H. O. T., Chan, A. W. H., Barkley, M. P., and Seinfeld, J. H.: Global modeling of organic aerosol: the importance of reactive nitrogen (NO_x and NO_3), *Atmos. Chem. Phys.*, 10, 11261-11276, <https://doi.org/10.5194/acp-10-11261-2010>, 2010.
- 1590 Pye, H. O. T., Appel, K. W., Seltzer, K. M., Ward-Caviness, C. K., and Murphy, B. N.: Human-health impacts of controlling secondary air pollution precursors, *Environ. Sci. Tech. Lett.*, 9, 96-101, <https://doi.org/10.1021/acs.estlett.1c00798>, 2022.
- Pye, H. O. T., Ward-Caviness, C. K., Murphy, B. N., Appel, K. W., and Seltzer, K. M.: Secondary organic aerosol association with cardiorespiratory disease mortality in the United States, *Nat. Commun.*, 12, 7215, <https://doi.org/10.1038/s41467-021-27484-1>, 2021.
- 1595 Pye, H. O. T., Luecken, D. J., Xu, L., Boyd, C. M., Ng, N. L., Baker, K. R., Ayres, B. R., Bash, J. O., Baumann, K., Carter, W. P. L., Edgerton, E., Fry, J. L., Hutzell, W. T., Schwede, D. B., and Shepson, P. B.: Modeling the current and future roles of particulate organic nitrates in the southeastern United States, *Environ. Sci. Technol.*, 49, 14195-14203, <https://doi.org/10.1021/acs.est.5b03738>, 2015.
- 1600 Pye, H. O. T., Pinder, R. W., Piletic, I. R., Xie, Y., Capps, S. L., Lin, Y.-H., Surratt, J. D., Zhang, Z., Gold, A., Luecken, D. J., Hutzell, W. T., Jaoui, M., Offenberg, J. H., Kleindienst, T. E., Lewandowski, M., and Edney, E. O.: Epoxide pathways improve model predictions of isoprene markers and reveal key role of acidity in aerosol formation, *Environ. Sci. Technol.*, 47, 11056-11064, <https://doi.org/10.1021/es402106h>, 2013.
- 1605 Pye, H. O. T., Murphy, B. N., Xu, L., Ng, N. L., Carlton, A. G., Guo, H., Weber, R., Vasilakos, P., Appel, K. W., Budisulistiorini, S. H., Surratt, J. D., Nenes, A., Hu, W., Jimenez, J. L., Isaacman-VanWertz, G., Misztal, P. K., and Goldstein, A. H.: On the implications of aerosol liquid water and phase separation for organic aerosol mass, *Atmos. Chem. Phys.*, 17, 343-369, <https://doi.org/10.5194/acp-17-343-2017>, 2017.



- 1610 Qin, M., Murphy, B. N., Isaacs, K. K., McDonald, B. C., Lu, Q., McKeen, S. A., Koval, L., Robinson, A. L., Efstathiou, C., Allen, C., and Pye, H. O. T.: Criteria pollutant impacts of volatile chemical products informed by near-field modelling, *Nat. Sustain.*, 4, 129-137, <https://doi.org/10.1038/s41893-020-00614-1>, 2021.
- Raber, W. H. and Moortgat, G. K.: *Progress and Problems in Atmospheric Chemistry*, World Scientific, Singapore 1996.
- RDKit: rdkit/rdkit: 2020_09_1 (Q3 2020) Release, <https://doi.org/10.5281/zenodo.4107869>, last access: 2 September 2022, 2020.
- RDKit: Open-source cheminformatics, <https://www.rdkit.org>, last access: 2 September 2022, 2022.
- 1615 Richters, S., Herrmann, H., and Berndt, T.: Highly oxidized RO₂ radicals and consecutive products from the ozonolysis of three sesquiterpenes, *Environ. Sci. Technol.*, 50, 2354-2362, <https://doi.org/10.1021/acs.est.5b05321>, 2016.
- Riedel, T. P., Lin, Y.-H., Budisulistiorini, S. H., Gaston, C. J., Thornton, J. A., Zhang, Z., Vizuete, W., Gold, A., and Surratt, J. D.: Heterogeneous reactions of isoprene-derived epoxides: Reaction probabilities and molar secondary organic aerosol yield estimates, *Environ. Sci. Tech. Lett.*, 2, 38-42, <https://doi.org/10.1021/ez500406f>, 2015.
- 1620 Riva, M., Chen, Y., Zhang, Y., Lei, Z., Olson, N. E., Boyer, H. C., Narayan, S., Yee, L. D., Green, H. S., Cui, T., Zhang, Z., Baumann, K., Fort, M., Edgerton, E., Budisulistiorini, S. H., Rose, C. A., Ribeiro, I. O., e Oliveira, R. L., dos Santos, E. O., Machado, C. M. D., Szopa, S., Zhao, Y., Alves, E. G., de Sá, S. S., Hu, W., Knipping, E. M., Shaw, S. L., Duvoisin Junior, S., de Souza, R. A. F., Palm, B. B., Jimenez, J.-L., Glasius, M., Goldstein, A. H., Pye, H. O. T., Gold, A., Turpin, B. J., Vizuete, W., Martin, S. T., Thornton, J. A., Dutcher, C. S., Ault, A. P., and Surratt, J. D.: Increasing isoprene epoxydiol-to-inorganic sulfate aerosol ratio results in extensive conversion of inorganic sulfate to organosulfur forms: Implications for aerosol physicochemical properties, *Environ. Sci. Technol.*, 53, 8682-8694, <https://doi.org/10.1021/acs.est.9b01019>, 2019.
- 1625 Robinson, A. L., Donahue, N. M., Shrivastava, M. K., Weitkamp, E. A., Sage, A. M., Grieshop, A. P., Lane, T. E., Pierce, J. R., and Pandis, S. N.: Rethinking organic aerosols: Semivolatile emissions and photochemical aging, *Science*, 315, 1259, <https://doi.org/10.1126/science.1133061>, 2007.
- 1630 Roldin, P., Ehn, M., Kurtén, T., Olenius, T., Rissanen, M. P., Sarnela, N., Elm, J., Rantala, P., Hao, L., Hyttinen, N., Heikkinen, L., Worsnop, D. R., Pichelstorfer, L., Xavier, C., Clusius, P., Öström, E., Petäjä, T., Kulmala, M., Vehkamäki, H., Virtanen, A., Riipinen, I., and Boy, M.: The role of highly oxygenated organic molecules in the Boreal aerosol-cloud-climate system, *Nat. Commun.*, 10, 4370, <https://doi.org/10.1038/s41467-019-12338-8>, 2019.
- 1635 Rolletter, M., Blocquet, M., Kaminski, M., Bohn, B., Dorn, H. P., Hofzumahaus, A., Holland, F., Li, X., Rohrer, F., Tillmann, R., Wegener, R., Kiendler-Scharr, A., Wahner, A., and Fuchs, H.: Photooxidation of pinonaldehyde at ambient conditions investigated in the atmospheric simulation chamber SAPHIR, *Atmos. Chem. Phys.*, 20, 13701-13719, <https://doi.org/10.5194/acp-20-13701-2020>, 2020.
- Safieddine, S. A., Heald, C. L., and Henderson, B. H.: The global nonmethane reactive organic carbon budget: A modeling perspective, *Geophys. Res. Lett.*, 44, 3897-3906, <https://doi.org/10.1002/2017GL072602>, 2017.
- 1640 Sander, S. P., Golden, D. M., Kurylo, M. J., Moortgat, G. K., Wine, P. H., Ravishankara, A. R., Kolb, C. E., Molina, M. J., Finlayson-Pitts, B. J., Huie, R. E., and Orkin, V. L.: Chemical kinetics and photochemical data for use in Atmospheric Studies Evaluation Number 15, <http://hdl.handle.net/2014/41648>, last 2006.
- 1645 Sander, S. P., Abbatt, J. P. D., Barker, J. R., Burkholder, J. B., Friedl, R. R., Golden, D. M., Huie, R. E., Kolb, C. E., Kurylo, M. J., Moortgat, G. K., Orkin, V. L., and Wine, P. H.: Chemical Kinetics and Photochemical Data for Use in Atmospheric Studies, Evaluation No. 17, last access: 16 May 2022, 2011.



- Sarwar, G., Gantt, B., Schwede, D., Foley, K., Mathur, R., and Saiz-Lopez, A.: Impact of enhanced ozone deposition and halogen chemistry on tropospheric ozone over the Northern Hemisphere, *Environ. Sci. Technol.*, 49, 9203-9211, <https://doi.org/10.1021/acs.est.5b01657>, 2015.
- 1650 Sarwar, G., Godowitch, J., Henderson, B. H., Fahey, K., Pouliot, G., Hutzell, W. T., Mathur, R., Kang, D., Goliff, W. S., and Stockwell, W. R.: A comparison of atmospheric composition using the Carbon Bond and Regional Atmospheric Chemistry Mechanisms, *Atmos. Chem. Phys.*, 13, 9695-9712, <https://doi.org/10.5194/acp-13-9695-2013>, 2013.
- Saunders, S. M., Jenkin, M. E., Derwent, R. G., and Pilling, M. J.: Protocol for the development of the Master Chemical Mechanism, MCM v3 (Part A): tropospheric degradation of non-aromatic volatile organic compounds, *Atmos. Chem. Phys.*, 3, 161-180, <https://doi.org/10.5194/acp-3-161-2003>, 2003.
- 1655 Scheffe, R. D., Strum, M., Phillips, S. B., Thurman, J., Eyth, A., Fudge, S., Morris, M., Palma, T., and Cook, R.: Hybrid modeling approach to estimate exposures of Hazardous Air Pollutants (HAPs) for the National Air Toxics Assessment (NATA), *Environ. Sci. Technol.*, 50, 12356-12364, <https://doi.org/10.1021/acs.est.6b04752>, 2016.
- Schervish, M. and Donahue, N. M.: Peroxy radical chemistry and the volatility basis set, *Atmos. Chem. Phys.*, 20, 1183-1199, <https://doi.org/10.5194/acp-20-1183-2020>, 2020.
- 1660 Schwantes, R. H., Schilling, K. A., McVay, R. C., Lignell, H., Coggon, M. M., Zhang, X., Wennberg, P. O., and Seinfeld, J. H.: Formation of highly oxygenated low-volatility products from cresol oxidation, *Atmos. Chem. Phys.*, 17, 3453-3474, <https://doi.org/10.5194/acp-17-3453-2017>, 2017.
- Seltzer, K. M., Murphy, B. N., Pennington, E. A., Allen, C., Talgo, K., and Pye, H. O. T.: Volatile Chemical Product Enhancements to Criteria Pollutants in the United States, *Environ. Sci. Technol.*, 56, 6905-6913, <https://doi.org/10.1021/acs.est.1c04298>, 2022.
- 1665 Seltzer, K. M., Pennington, E., Rao, V., Murphy, B. N., Strum, M., Isaacs, K. K., and Pye, H. O. T.: Reactive organic carbon emissions from volatile chemical products, *Atmos. Chem. Phys.*, 21, 5079-5100, <https://doi.org/10.5194/acp-21-5079-2021>, 2021.
- Shah, T., Shi, Y., Beardsley, R., and Yarwood, G.: Speciation Tool User's Guide Version 5.0, https://www.cmascenter.org/speciation_tool/documentation/5.0/Ramboll_sptool_users_guide_V5.pdf, last access: 2 August 2022, 2020.
- 1670 Simon, H., Baker, K. R., and Phillips, S.: Compilation and interpretation of photochemical model performance statistics published between 2006 and 2012, *Atmos. Environ.*, 61, 124-139, <https://doi.org/10.1016/j.atmosenv.2012.07.012>, 2012.
- Simon, H., Beck, L., Bhave, P. V., Divita, F., Hsu, Y., Luecken, D., Mobley, J. D., Pouliot, G. A., Reff, A., Sarwar, G., and Strum, M.: The development and uses of EPA's SPECIATE database, *Atmos. Pollut. Res.*, 1, 196-206, <https://doi.org/10.5094/APR.2010.026>, 2010.
- 1675 Srivastava, D., Vu, T. V., Tong, S., Shi, Z., and Harrison, R. M.: Formation of secondary organic aerosols from anthropogenic precursors in laboratory studies, *NPJ Clim. Atmos.*, 5, 22, <https://doi.org/10.1038/s41612-022-00238-6>, 2022.
- 1680 Stanfield, Z., Addington, C. K., Dionisio, K. L., Lyons, D., Tornero-Velez, R., Phillips, K. A., Buckley, T. J., and Isaacs, K. K.: Mining of Consumer Product Ingredient and Purchasing Data to Identify Potential Chemical Coexposures, *Environ. Health Perspect.*, 129, 067006, <https://doi.org/10.1289/EHP8610>, 2021.



- Stockwell, W. R., Kirchner, F., Kuhn, M., and Seefeld, S.: A new mechanism for regional atmospheric chemistry modeling, *J. Geophys. Res.-Atmos.*, 102, 25847-25879, <https://doi.org/10.1029/97JD00849>, 1997.
- 1685 Stockwell, W. R., Middleton, P., Chang, J. S., and Tang, X.: The second generation regional acid deposition model chemical mechanism for regional air quality modeling, *J. Geophys. Res.-Atmos.*, 95, 16343-16367, <https://doi.org/10.1029/JD095iD10p16343>, 1990.
- Surratt, J. D., Chan, A., W. H., Eddingsaas, N., C., Chan, M., Loza, C., L., Kwan, A., J., Hersey, S., P., Flagan, R., C., Wennberg, P., O., and Seinfeld, J., H.: Reactive intermediates revealed in secondary organic aerosol formation from isoprene, *P. Natl. Acad. Sci. USA*, 107, 6640-6645, <https://doi.org/10.1073/pnas.0911114107>, 2010.
- 1690 Talukdar, R. K., Burkholder, J. B., Hunter, M., Gilles, M. K., Roberts, J. M., and Ravishankara, A. R.: Atmospheric fate of several alkyl nitrates Part 2UV absorption cross-sections and photodissociation quantum yields, *J. Chem. Soc., Faraday Trans.*, 93, 2797-2805, <https://doi.org/10.1039/A701781B>, 1997.
- Tilmes, S., Lamarque, J. F., Emmons, L. K., Kinnison, D. E., Ma, P. L., Liu, X., Ghan, S., Bardeen, C., Arnold, S., Deeter, M., Vitt, F., Ryerson, T., Elkins, J. W., Moore, F., Spackman, J. R., and Val Martin, M.: Description and evaluation of tropospheric chemistry and aerosols in the Community Earth System Model (CESM1.2), *Geosci. Model Dev.*, 8, 1395-1426, <https://doi.org/10.5194/gmd-8-1395-2015>, 2015.
- 1695 Tuazon, E. C., Alvarado, A., Aschmann, S. M., Atkinson, R., and Arey, J.: Products of the gas-phase reactions of 1,3-Butadiene with OH and NO₃ Radicals, *Environ. Sci. Technol.*, 33, 3586-3595, <https://doi.org/10.1021/es990193u>, 1999.
- 1700 U.S. Environmental Protection Agency: Motor Vehicle Emission Simulator: MOVES3.0.0, <https://www.epa.gov/moves>, last access: 1 July 2022, 2020.
- U.S. Environmental Protection Agency: Human Exposure Model, <https://www.epa.gov/fera/download-human-exposure-model-hem>, last access: 19 April 2022, 2021a.
- U.S. Environmental Protection Agency: Dose-Response Assessment for Assessing Health Risks Associated With Exposure to Hazardous Air Pollutants, <https://www.epa.gov/fera/dose-response-assessment-assessing-health-risks-associated-exposure-hazardous-air-pollutants>, last access: 29 September 2021, 2021b.
- 1705 U.S. Environmental Protection Agency: CompTox Chemicals Dashboard, <https://comptox.epa.gov/dashboard/>, last access: 19 August 2021, 2021c.
- U.S. Environmental Protection Agency: SPECIATE Version 5.2 Database Development Documentation, 2022a.
- U.S. Environmental Protection Agency: CTS: Chemical Transformation Simulator, <https://qed.epa.gov/cts/>, last access: 5 August 2022, 2022b.
- 1710 U.S. Environmental Protection Agency: Federal Register, 40 CFR Part 63, [EPA-HQ-OAR-2014-0471; FRL-5562-08-OAR], RIN 2060-AS26, Clean Air Act Section 112 List of Hazardous Air Pollutant: Amendments to the List of Hazardous Air Pollutants (HAP) <https://www.govinfo.gov/content/pkg/FR-2022-01-05/pdf/2021-28315.pdf>, last access: 13 July 2022, 2022c.
- 1715 U.S. Environmental Protection Agency: List of chemicals within the certain glycol ethers category, https://ordspub.epa.gov/ords/guideme_ext/f?p=GUIDEME:GD:::RP:gd:glycol_ethers, last access: 19 April 2022, 2022d.



- U.S. Environmental Protection Agency: Nonattainment Areas for Criteria Pollutants (Green Book), <https://www.epa.gov/green-book>, last access: 13 May 2022, 2022e.
- 1720 U.S. Environmental Protection Agency Office of Research and Development: CMAQ (Version 5.3.3), <http://doi.org/10.5281/zenodo.3585898>, last 2019.
- Vannucci, P. F. and Cohen, R. C.: Decadal trends in the temperature dependence of summertime urban PM_{2.5} in the Northeast United States, *ACS Earth Space Chem.*, <https://doi.org/10.1021/acsearthspacechem.2c00077>, 2022.
- 1725 Vasquez, K. T., Crounse, J. D., Schulze, B. C., Bates, K. H., Teng, A. P., Xu, L., Allen, H. M., and Wennberg, P. O.: Rapid hydrolysis of tertiary isoprene nitrate efficiently removes NO_x from the atmosphere, *P. Natl. Acad. Sci. USA*, 117, 33011-33016, <https://doi.org/10.1073/pnas.2017442117>, 2020.
- Venecek, M. A., Carter, W. P. L., and Kleeman, M. J.: Updating the SAPRC Maximum Incremental Reactivity (MIR) scale for the United States from 1988 to 2010, *J. Air Waste Manage. Assoc.*, 68, 1301-1316, <https://doi.org/10.1080/10962247.2018.1498410>, 2018.
- 1730 Vereecken, L. and Nozière, B.: H migration in peroxy radicals under atmospheric conditions, *Atmos. Chem. Phys.*, 20, 7429-7458, <https://doi.org/10.5194/acp-20-7429-2020>, 2020.
- Vogel, B., Vogel, H., Kleffmann, J., and Kurtenbach, R.: Measured and simulated vertical profiles of nitrous acid—Part II. Model simulations and indications for a photolytic source, *Atmos. Environ.*, 37, 2957-2966, [https://doi.org/10.1016/S1352-2310\(03\)00243-7](https://doi.org/10.1016/S1352-2310(03)00243-7), 2003.
- 1735 Wang, S., Wu, R., Berndt, T., Ehn, M., and Wang, L.: Formation of highly oxidized radicals and multifunctional products from the atmospheric oxidation of alkylbenzenes, *Environ. Sci. Technol.*, 51, 8442-8449, <https://doi.org/10.1021/acs.est.7b02374>, 2017.
- 1740 Wang, S., Coggon, M. M., Gkatzelis, G. I., Warneke, C., Bourgeois, I., Ryerson, T., Peischl, J., Veres, P. R., Neuman, J. A., Hair, J., Shingler, T., Fenn, M., Diskin, G., Huey, L. G., Lee, Y. R., Apel, E. C., Hornbrook, R. S., Hills, A. J., Hall, S. R., Ullmann, K., Bela, M. M., Trainer, M. K., Kumar, R., Orlando, J. J., Flocke, F. M., and Emmons, L. K.: Chemical tomography in a fresh wildland fire plume: A Large Eddy Simulation (LES) Study, *J. Geophys. Res.-Atmos.*, 126, e2021JD035203, <https://doi.org/10.1029/2021JD035203>, 2021.
- Weber, J., Archer-Nicholls, S., Griffiths, P., Berndt, T., Jenkin, M., Gordon, H., Knote, C., and Archibald, A. T.: CRI-HOM: A novel chemical mechanism for simulating highly oxygenated organic molecules (HOMs) in global chemistry–aerosol–climate models, *Atmos. Chem. Phys.*, 20, 10889-10910, <https://doi.org/10.5194/acp-20-10889-2020>, 2020.
- 1745 Wennberg, P. O., Bates, K. H., Crounse, J. D., Dodson, L. G., McVay, R. C., Mertens, L. A., Nguyen, T. B., Praske, E., Schwantes, R. H., Smarte, M. D., St Clair, J. M., Teng, A. P., Zhang, X., and Seinfeld, J. H.: Gas-Phase reactions of isoprene and its major oxidation products, *Chem. Rev.*, 118, 3337-3390, <https://doi.org/10.1021/acs.chemrev.7b00439>, 2018.
- 1750 Williams, A. J., Grulke, C. M., Edwards, J., McEachran, A. D., Mansouri, K., Baker, N. C., Patlewicz, G., Shah, I., Wambaugh, J. F., Judson, R. S., and Richard, A. M.: The CompTox Chemistry Dashboard: a community data resource for environmental chemistry, *J. Cheminformatics*, 9, 61, <https://doi.org/10.1186/s13321-017-0247-6>, 2017.
- Wiser, F. W., Place, B. K., Siddhartha, S., Pye, H. O. T., Westervelt, D. M., Henze, D. K., Fiore, A. M., and McNeill, V. F.: AMORE-Isoprene v1.0: A new reduced mechanism for gas-phase isoprene oxidation, in prep.



- 1755 Womack, C. C., McDuffie, E. E., Edwards, P. M., Bares, R., de Gouw, J. A., Docherty, K. S., Dubé, W. P., Fibiger, D. L., Franchin, A., Gilman, J. B., Goldberger, L., Lee, B. H., Lin, J. C., Long, R., Middlebrook, A. M., Millet, D. B., Moravek, A., Murphy, J. G., Quinn, P. K., Riedel, T. P., Roberts, J. M., Thornton, J. A., Valin, L. C., Veres, P. R., Whitehill, A. R., Wild, R. J., Warneke, C., Yuan, B., Baasandorj, M., and Brown, S. S.: An Odd Oxygen Framework for Wintertime Ammonium Nitrate Aerosol Pollution in Urban Areas: NO_x and VOC Control as Mitigation Strategies, *Geophys. Res. Lett.*, 46, 4971-4979, <https://doi.org/10.1029/2019GL082028>, 2019.
- 1760 Woody, M. C., Baker, K. R., Hayes, P. L., Jimenez, J. L., Koo, B., and Pye, H. O. T.: Understanding sources of organic aerosol during CalNex-2010 using the CMAQ-VBS, *Atmos. Chem. Phys.*, 16, 4081-4100, <https://doi.org/10.5194/acp-16-4081-2016>, 2016.
- Xu, L., Møller, K. H., Crounse, J. D., Kjaergaard, H. G., and Wennberg, P. O.: New Insights into the Radical Chemistry and Product Distribution in the OH-Initiated Oxidation of Benzene, *Environ. Sci. Technol.*, 54, 13467-13477, <https://doi.org/10.1021/acs.est.0c04780>, 2020.
- 1765 Xu, L., Møller, K. H., Crounse, J. D., Otkjær, R. V., Kjaergaard, H. G., and Wennberg, P. O.: Unimolecular Reactions of Peroxy Radicals Formed in the Oxidation of α -Pinene and β -Pinene by Hydroxyl Radicals, *J. Phys. Chem. A*, 123, 1661-1674, <https://doi.org/10.1021/acs.jpca.8b11726>, 2019.
- 1770 Xu, L., Pye, H. O. T., He, J., Chen, Y., Murphy, B. N., and Ng, N. L.: Experimental and model estimates of the contributions from biogenic monoterpenes and sesquiterpenes to secondary organic aerosol in the southeastern United States, *Atmos. Chem. Phys.*, 18, 12613-12637, <https://doi.org/10.5194/acp-18-12613-2018>, 2018.
- Xu, W., Han, T., Du, W., Wang, Q., Chen, C., Zhao, J., Zhang, Y., Li, J., Fu, P., Wang, Z., Worsnop, D. R., and Sun, Y.: Effects of aqueous-phase and photochemical processing on secondary organic aerosol formation and evolution in Beijing, China, *Environ. Sci. Technol.*, 51, 762-770, <https://doi.org/10.1021/acs.est.6b04498>, 2017.
- 1775 Yee, L. D., Isaacman-VanWertz, G., Wernis, R. A., Meng, M., Rivera, V., Kreisberg, N. M., Hering, S. V., Bering, M. S., Glasius, M., Upshur, M. A., Gray Bé, A., Thomson, R. J., Geiger, F. M., Offenberg, J. H., Lewandowski, M., Kourtchev, I., Kalberer, M., de Sá, S., Martin, S. T., Alexander, M. L., Palm, B. B., Hu, W., Campuzano-Jost, P., Day, D. A., Jimenez, J. L., Liu, Y., McKinney, K. A., Artaxo, P., Viegas, J., Manzi, A., Oliveira, M. B., de Souza, R., Machado, L. A. T., Longo, K., and Goldstein, A. H.: Observations of sesquiterpenes and their oxidation products in central Amazonia during the wet and dry seasons, *Atmos. Chem. Phys.*, 18, 10433-10457, <https://doi.org/10.5194/acp-18-10433-2018>, 2018.
- 1780 Yeh, G. K. and Ziemann, P. J.: Alkyl nitrate formation from the reactions of C₈–C₁₄ n-alkanes with OH radicals in the presence of NO_x: Measured yields with essential corrections for gas–wall partitioning, *J. Phys. Chem. A*, 118, 8147-8157, <https://doi.org/10.1021/jp500631v>, 2014.
- Yujing, M. and Mellouki, A.: The near-UV absorption cross sections for several ketones, *J. Photchem. Photobiol. A*, 134, 31-36, [https://doi.org/10.1016/S1010-6030\(00\)00243-4](https://doi.org/10.1016/S1010-6030(00)00243-4), 2000.
- 1785 Zare, A., Fahey, K. M., Sarwar, G., Cohen, R. C., and Pye, H. O. T.: Vapor-Pressure pathways initiate but hydrolysis products dominate the aerosol estimated from organic nitrates, *ACS Earth Space Chem.*, 3, 1426-1437, <https://doi.org/10.1021/acsearthspacechem.9b00067>, 2019.
- 1790 Zhang, Q., Jimenez, J. L., Canagaratna, M. R., Ulbrich, I. M., Ng, N. L., Worsnop, D. R., and Sun, Y.: Understanding atmospheric organic aerosols via factor analysis of aerosol mass spectrometry: a review, *Anal. Bioanal. Chem.*, 401, 3045-3067, <https://doi.org/10.1007/s00216-011-5355-y>, 2011.



- Zhang, X., Cappa, C. D., Jathar, S. H., McVay, R. C., Ensberg, J. J., Kleeman, M. J., and Seinfeld, J. H.: Influence of vapor wall loss in laboratory chambers on yields of secondary organic aerosol, *P. Natl. Acad. Sci. USA*, 111, 5802, <https://doi.org/10.1073/pnas.1404727111>, 2014.
- 1795 Zhao, B., Wang, S., Donahue, N. M., Jathar, S. H., Huang, X., Wu, W., Hao, J., and Robinson, A. L.: Quantifying the effect of organic aerosol aging and intermediate-volatility emissions on regional-scale aerosol pollution in China, *Sci. Rep.*, 6, 28815-28815, <https://doi.org/10.1038/srep28815>, 2016.
- Zhao, Y., Thornton Joel, A., and Pye Havala, O. T.: Quantitative constraints on autoxidation and dimer formation from direct probing of monoterpene-derived peroxy radical chemistry, *P. Natl. Acad. Sci. USA*, 115, 12142-12147, <https://doi.org/10.1073/pnas.1812147115>, 2018.
- 1800 Zhu, S., Kinnon, M. M., Shaffer, B. P., Samuelson, G. S., Brouwer, J., and Dabdub, D.: An uncertainty for clean air: Air quality modeling implications of underestimating VOC emissions in urban inventories, *Atmos. Environ.*, 211, 256-267, <https://doi.org/10.1016/j.atmosenv.2019.05.019>, 2019.